BOUNDARY LAYER FLOW FIELDS AROUND

ROTATING SPHERES

By

XIJIA ZHU, B.Eng., M.Eng

A Thesis

Submitted to the School of Graduate Studies

in Partial Fulfillment of the Requirements

for the Degree

Doctor of Philosophy

McMaster University

BOUNDARY LAYER FLOW FIELDS

AROUND ROTATING SPHERES

DOCTOR OF PHILOSOPHY (1995)
(Mechanical Engineering)

McMASTER UNIVERSITY
Hamilton, Ontario

TITLE: Boundary Layer Flow Fields around Rotating Spheres

AUTHOR: Xijia Zhu,   B.Eng.   (Chongqing University)
                                  M.Eng.   (Chongqing University)

SUPERVISOR: Professor G. F. Round

NUMBER OF PAGES: xviii, 155

ABSTRACT

The boundary layer equations governing the conservation of mass and momentum and the corresponding boundary conditions are derived, using spherical coordinates for flow past a rotating sphere. A finite-volume-based numerical scheme using structured orthogonal body-fitted grids was used to examine potential and vortex flow around a stationary sphere and flow fields around rotating spheres whose axes are parallel and perpendicular to the free stream direction. Some parametric studies were conducted. The results are presented in graphical form for flow visualization. Experiments for the case of the rotational axis being perpendicular to the free stream were designed and data generated using a triple-sensor probe. It has found that the numerical results agreed reasonably well with experimental results within experimental uncertainty. The comparisons were not completed over whole flow field due to the limitations in the experimental conditions.

ACKNOWLEDGEMENTS

TABLE OF CONTENTS

LIST OF FIGURES

NOMENCLATURE

a	sphere radius
$a_N - a_L$	coefficients accounting for convection and diffusion
a_T	accounts for time change
a_P	contains influences of all the above a's
A_i	constant for wire i
b	accounts for the source term and contains contributions from boundary conditions and additional terms in the equations that do not fit general form
B_i	constant for wire i
d	sphere diameter
D	shaft diameter
e_i	unit vector in the i - direction
F	coefficient used to convert tangentially to normal resolute
F_i	force per unit volume in the i - direction
G	coefficient used to convert tangentially to normal resolute
H	coefficient used to convert tangentially to normal resolute
J	total flux

k_t	yaw factor
k_k	pitch factor
m	convection coefficient
n_i	constant for wire i
p	velocity component in local grid direction 1
P	pressure
$\vec{Q}$	total velocity vector
q	velocity component in local grid direction 2
r	radius of a circular cross section which is parallel to the equatorial plane
r	velocity component in local grid direction 3
R	dimensionless radius of a circular cross section which is parallel to the equatorial plane, $2r/aRe$
R	dimensionless distance in the radial direction of the measurement sphere
$\vec{R}$	radius vector
Re	Reynolds number, $2U_\infty a/\upsilon$
S	source per unit volume per unit time
t	time
Ta	Taylor number, $4\omega^2 a^4/\upsilon^2$
Ta/Re^2	spin parameter, $\omega^2 a^2/U_\infty^2$
u	meridional (x - direction) component of velocity

u^*	potential velocity component in the x - direction for the case of rotating axis is parallel to the free stream direction
u_*	potential velocity component in the x - direction for the case of rotating axis is perpendicular to the free stream direction
U	dimensionless meridional component of velocity, u/U_∞
U	mean velocity in x - direction
$U_{eff,i}$	effective cooling velocities normal to the hot-wire i
U_*	dimensionless potential velocity component in the x - direction for the case of rotating axis is perpendicular to the free stream direction
U_∞	free stream velocity
v	azimuthal (y - direction) component of velocity at any point
v_*	potential velocity component in the y - direction for the case of rotating axis is perpendicular to the free stream direction
v^o	circumferential velocity at a point on the sphere surface, $\omega a Sin\theta$
V	dimensionless azimuthal velocity component at any point, $v/(\omega.a)$
V	mean velocity in y - direction
Vol_i	anemometer output voltages of wire i
V_*	dimensionless potential velocity component in the y - direction for the case of rotating axis is perpendicular to the free stream direction
V^o	dimensionless azimuthal velocity component at a point on the sphere

surface, r/a

w	radial (z - direction) velocity component
w^*	potential velocity component in the z - direction for the case of rotating axis is parallel to the free stream direction
w_*	potential velocity component in the z - direction for the case of rotating axis is perpendicular to the free stream direction
W	dimensionless radial velocity component, w/U_∞
W	mean velocity in z - direction
x	distance along the circular direction of the sphere's surface measured from the north polar
X	dimensionless meridional distance along the surface measured from the north polar, $2x/(Re.a)$
y	distance measured along a circular cross section which is parallel to the equator plane
Y	dimensionless circumferential distance, $2y/(Re.a)$
z	distance from the surface measured along the radial direction
Z	dimensionless distance in the radial direction, z/a

Greek symbols

α	center angle measured from the horizontal axis

α_i^i	direction cosines between unit tangent and normal
θ	center angle measured from the axis of rotation
φ	angle on a horizontal circular cross section
ϕ	any dependent variable
$\phi_N - \phi_T$	dependent variables in question
ρ	density
Γ	exchange (or transport) coefficient
ω	angular velocity of a sphere
υ	kinematic viscosity of fluid
δ	boundary layer thickness
δ_*	dimensionless boundary layer thickness
$\psi_{1,2,3}$	velocity components in three wire coordinate directions

Superscripts

(nr)	normal resolute
(tc)	tangential component
o	on the sphere surface

Subscripts

e	east cell interface

E	node center of east cell
h	high cell interface
H	node center of high cell
i	the coordinate direction
l	low cell interface
L	node center of low cell
m	properties on the maximum cross section
n	north cell interface
(nc)	normal component
N	node center of north cell
P	node center of cell
s	south cell interface
S	node center of south cell
(tr)	tangential resolute
u	x - direction staggered cell
w	west cell interface
W	node center of west cell
x	x - direction
y	y - direction
z	z - direction

CHAPTER 1

INTRODUCTION

1.1   General Approach

The flow field around a rotating body has been the subject of many investigations. These have included ballistics of spinning projectiles, theoretical studies in meteorology where it is regarded as a simple model of large scale atmospheric dynamics, different aspects of jet engines, and flow on the hub of an axial turbomachine. Thus, an understanding of the flow field around a rotating body is pivotal to understand many phenomena.

There are two limiting cases for this kind of problem to a sphere. One case is a stationary sphere in a uniform stream. Numerical solutions for this problem have been given by Dennis and Walker (1971) at Reynolds numbers $Re = 1, 5, 10, 20, 40$, Rimon and Cheng (1969) at $Re = 10, 40, 100, 300, 1000$, Fornberg (1988) at $Re = 100, 200, 500, 1000, 2000, 5000$, Hamielec and Houghton et al. (1967), Mihai and Vasile et al. (1985). In these investigations, series truncation and central differences have used to obtain solutions. Face (1936) also performed experimental work for this case.

1

The second case is steady viscous fluid flow due to a sphere that rotates about an axis with a constant angular velocity in a fluid at rest. This flow is of such a type that in the friction layer the fluid is translated by the centrifugal forces from the poles to the equator, and on the equatorial plane the fluid flows off toward the outside. Theoretical, numerical and experimental solutions have been obtained by many researchers for this case, for example, Dennis, Singh and Ingham (1970, 1981) at $Re = 10, 20, 500$ and $Re = 20, 100, 1000, 5000$, respectively, Singh (1970), Howarth (1951), Banks (1976), Nigam (1974), Kohama and Kobayashi (1983) and Kobashi (1956). Series truncation and central difference are used for the numerical studies, and the momentum integral technique is used to solve the laminar boundary layer equations. In contrast to the first limiting case (nonrotating sphere in a uniform flow), this limiting case does not have boundary-layer character, it means the friction effect is not limited to a thin layer near the wall but takes effect for the entire environment around the rotating body.

On the other hand, limited research results are available for the case of a rotating body in an axial stream. Schlichting (1953) investigated the laminar flow about a rotating body of revolution in an axial free stream by using the momentum integral technique. For the special case of a rotating sphere in a free stream, he obtained the separation point, the drag, and the resisting moment for different values of the spin parameter U_m/U_∞

$$\frac{Circumferential \quad velocity}{Free - stream \quad velocity} = \frac{U_m}{U_\infty} = \frac{R_m\omega}{U_\infty} \tag{1.1}$$

where R_m denotes the radius of the maximum cross section of the body of revolution. U_m is the circumferential velocity, U_∞ free-stream velocity and ω angular velocity. The calculations were aimed at deciding the entire boundary-layer variation as a function of U_m/U_∞. He found that the separation point of the laminar boundary layer advanced to the rear hemisphere because of the rotational motion.

El-Shaarawi, El-Refaie, and El-Bedeawi (1985) numerically studied the steady laminar boundary layer produced by a flow of an incompressible fluid around a rotating sphere whose axis is parallel to the free stream. The effect of spin parameter, Ta/Re^2, Ta represents Taylor number, over the range of $0 \le Ta/Re^2 \le 10,000$ at a fixed value of Reynolds number, $Re = 10,000$ is studied. El-Shaarawi, Kemry and El-Bedeawi (1987) used the same scheme to investigate the effect of Reynolds number of free stream. Results are presented over the range of $5000 \le Re \le 300,000$ for values of $Ta/Re^2 = 0$ and 2.

1.2 Contributions of the Thesis

The work of all the researchers cited has focussed on theoretical, numerical and experimental studies on the limiting cases and one special case - the rotating axis is parallel to the free stream. However, there is no published literature on the case of a rotating sphere whose axis is perpendicular to the free stream. Then, this study is proposed to deal with this case. Here the dominant dimensionless quantities are Reynolds number and the spin parameter. The spin

parameter, Ta/Re^2, is defined as the ratio between the centrifugal and inertia forces

$$\frac{Ta}{Re^2} = \frac{\omega^2 a^2}{U_\infty^2} \qquad (1.2)$$

where Ta is Taylor number, $Ta = (4\omega^2 a^2)/v^2$. Both parameters influence the behavior of a flow field.

The study affords the first step in the calculation of the flow field around an arbitrarily rotating sphere in a free stream. This is a complicated three-dimensional boundary-layer flow problem. The subsequent extension to a multi-body system will be even more complex. To obtain information on the flow field for this situation, three things were concerned with the present study:

i. derivation of the boundary layer equations and corresponding boundary conditions

ii. numerical predictions of the flow fields around rotating sphere for different cases and parameter variation

iii. experimental investigations on the flow field around a rotating sphere whose axis is perpendicular to the free stream.

1.3   Outline of the Thesis

The chapters in this thesis are organized as follows:

Chapter 2 presents a literature survey of the studies relevant from the standpoint of the present work. The contents of that Chapter has been subdivided according to the organization of the thesis.

Chapter 3 introduces the deduction of the boundary layer equations based on the principle of similarity and corresponding boundary conditions by coordinate transformation. The details of the transformation are provided in Appendix I.

The basic transport equations in rectangular and general curvilinear coordinates are described in Chapter 4. These are accordance with the forms obtained from a 'control-volume' based approach. Numerical techniques used in the calculation are discussed in this chapter. The PHOENICS Input Language(PIL) and the FORTRAN codes are put in Appendix II.

Chapter 5 contains the numerical predictions of flow fields around a sphere for different cases and variations of parameters. Results and discussion are given in this Chapter.

Experimental work is the subject of Chapter 6. It includes the design of the measurement system, the choice of the measurement method and comparison of results between calculation and experiment. The experimental techniques presente in Appendix III.

Chapter 7 summarizes the conclusions and gives the recommendations to future work.

CHAPTER 2

LITERATURE SURVEY

There are three types of flow problems for flow field around a sphere. The first one is a very common problem: uniform flow past a stationary sphere. The second one is the steady flow due to a rotating sphere. The third one is boundary layer flow around a rotating sphere in a free stream. The third case is the one on which attention has been focused.

2.1   Uniform Flow past a Stationary Sphere

This is a classical problem and has been the subject of much investigation: for example, Dennis and Walker (1971), Rimon and Cheng (1969), Hamielec et al (1967) and Mihai and Vasile (1985) made computations for this kind of flow at low and moderate Reynolds numbers 10^{1} - 10^{2}. A series truncation method (Dennis and Walker, 1971), and finite difference method (Rimon and Cheng, 1969, Hamielec et al, 1967, and Mihai and Vasile, 1985), are used to solve the stream function - vorticity equations. The reason for solving this set of equations is the axial symmetry of the problem. Wegener (1961) carried out experiments on this problem to find the drag coefficient.

The series method consists in expanding the flow variables as a series in the polar angle θ (Dennis and Walker, 1971) or argument $\mu = Cos\ \theta$ (Dennis et al, 1980), with functional coefficients in the radial variable. The series is substituted into the Navier-Stokes equations and truncated by putting all functional coefficients after a certain stage in the series equal to zero. This gives a finite set of simultaneous ordinary differential equations to be solved for the functional coefficients. These equations are solved numerically and the number of equations to be solved depends on the number of terms retained in the truncated series. The series used are Legendre (Dennis and Walker, 1971) and orthogonal Gegenbauer (Dennis et al, 1980) series. This method gave accurate results at low and moderate Reynolds numbers but is not very suited at higher Reynolds numbers because of the large number of terms in the order of the truncation required. If $Re > 100$, this method is invalid (Dennis et al, 1981).

Finite difference methods are used to approximate the Navier-Stokes equations because of the shortcoming of the series method. They vary considerably in accuracy and efficiency. If central difference is used everywhere then at large values of the Reynolds numbers, difficulties are encountered in obtaining a convergent solution of the finite-difference equations and severe under-relaxation is required. An alternative central finite-difference formulation employing the h^2- extrapolation is described by Dennis et al (1981, 1979) for a large range of Reynolds numbers. It is based on the use of specialized techniques to obtain an approximating set of finite-difference equations to the full partial differential equations that govern the flow. The finite-difference equations obtained involve exponential

coefficients and the matrices associated with them are not necessarily diagonally dominant. It is possible to expand the exponential functions such that both difficulties may be avoided and still maintain second-order accuracy. The numerical solutions included, streamlines, vorticity lines, pressure distribution, drag coefficient, wake bubble growth and separate points.

At high Reynolds numbers 10^2 - 10^3, Fornberg (1988) solved the stream function - vorticity equations by a central second-order finite difference method and obtained results for streamlines, vorticity lines, pressure distributions and drag coefficients. Face (1936) performed an experiment for this case to obtain information about critical Reynolds number. Inchul et al (1990) investigated the stability to this kind of flow by researching the numerical solutions of the equations in stream function form.

2.2 Steady Flow due to a Rotating Sphere

Solutions of the boundary layer equations for incompressible, axial-symmetric flow due to a rotating sphere with a constant angular velocity have been investigated theoretically by Dennis, Ingham and Singh (1980, 1981), Singh (1970), Howarth (1951), Banks (1976), Nigam (1974), Tomotika (1935), Yoden and Yamada (1993), El-Shaarawi et al (1993) and Iliyn (1994). Experimentally by Kohama and Kokayashi (1983), Kobash (1956), Sawatzki (1971) and Oesterle et al (1991). Dennis et al (1980, 1981) studied the problem for a range

of Reynolds numbers $10-10^3$. Dennis et al (1980, 1981) and Yoden and Yamada (1993), solved the stream function-vorticity equations using the method of series truncation for lower Reynolds numbers and a central finite-difference formulation for higher Reynolds numbers. On the other hand, the momentum integral technique is used by Singh (1970), Howarth (1951) and Tomotike (1935) to deal with the equations for the conservation of mass and momentum. Also Banks (1976) and El-Shaarawi et al (1993), Nigam (1974) used finite-difference and power series, respectively, to handle the same set of equations.

At different Reynolds numbers, results obtained included velocity components in radial, azimuthal and transverse directions (Dennis, Singh and Ingham, 1980 and 1981), (Tomotika, 1935), (Banks, 1976) and (El-Shaarawi et al, 1993), the nondimensional torque and skin friction on the surface of the sphere (Dennis, Singh and Ingham, 1980 and 1981), (Singh, 1970) and (Tomotika, 1935), and the streamlines (Dennis, Singh and Ingham, 1980 and 1981), (Singh, 1970) and (Banks, 1976). Vorticity fields and stream function fields are investigated by Yoden and Yamada (1993). Moreover, an important phenomenon is found (Howarth, 1951 and Dennis et al, 1980) regarding streamlines. In steady motion, results show an inflow into the outer edge of the boundary layer confined near the sphere taking place in streamlines parallel to the rotating axis, and outflow from the outer edge of the boundary layer for streamlines perpendicular to the rotating axis or making an obtuse angle with the axis. A region of inflow to the sphere near the pole is balanced by a region of outflow near the equator and as the Reynolds number increases the inflow region increases and the outflow

region becomes narrower. The radial velocity also increases with the Reynolds number at the equator, showing the formation of a radial jet over the narrow region of outflow. In the range considered there is no separation of the flow near the equator.

Experimental results obtained on critical and transition Reynolds numbers (Kohama and Kobayashi, 1983), distributions of velocity component and distribution of boundary layer thickness (Kobashi, 1956) have been compared with theoretical solutions, and the agreement is shown to be satisfactory. Laminar-to-turbulent transition in the boundary layer has been studied by Sawatzki (1971) experimentally. Lift and torque coefficients on a rotating sphere at intermediate Reynolds numbers are measured by Oesterle et al (1991). In a high Reynolds number range ($Re > 10^4$), the lift on a rotating sphere is measured by Maccol (1928), Davies (1949) and Tani (1950). In this case, it is found to be independent of the Reynolds number.

2.3 Boundary Layer Flow around a Rotating Sphere in an Axial Stream

Schlichting (1953), provided the simplified equations of motion according to the calculation method of Prandtl's boundary-layer theory to treat the general case of the rotating body of revolution in a flow that is parallel to the rotating axis

$$\frac{\partial u}{\partial x} + \frac{u}{r}\frac{dr}{dx} + \frac{\partial w}{\partial z} = 0 \tag{2.1}$$

$$u\frac{\partial u}{\partial x} - \frac{v^2}{r}\frac{dr}{dx} + w\frac{\partial u}{\partial z} = u_\bullet\frac{\partial u_\bullet}{\partial x} + \upsilon\frac{\partial^2 u}{\partial z^2} \tag{2.2}$$

$$u\frac{\partial v}{\partial x} + \frac{uv}{r}\frac{dr}{dx} + w\frac{\partial v}{\partial z} = \upsilon\frac{\partial^2 v}{\partial z^2} \qquad (2.3)$$

And the boundary conditions are presented as

$$z = 0: \quad u = 0, \quad v = v^* = r\omega, \quad w = 0$$

$$z = \infty: \quad u = u_*(x), \quad v = 0$$

where u, v and w are the meridional, azimuthal and radial velocity components in the x, y and z-directions, respectively. u_*, potential velocity component in the x-direction. v^o, circumferential velocity on the sphere surface. And ω, angular velocity of the sphere.

El-Shaarawi et al (1985, 1987, 1990, 1992, 1987) investigated the problem numerically by solving the above boundary-layer equations and experimentally by measuring corresponding variables. They concentrated their study on the effect of the spin parameter, Ta/Re^2, over the range $0 \le Ta/Re^2 \le 10,000$ at a fixed value of Reynolds number $Re = 10,000$ and the effect of Reynolds number over the range $5000 \le Re \le 30,000$ for values of Ta/Re^2 $= 0, 1$. The parameter Ta/Re^2 has a physically significant meaning. It represents the ratio between centrifugal and inertia forces. It has effects on the wall shear stress as well.

The basic equations of mass and momentum conservation, are solved with a finite-difference scheme employing a rectangular curvilinear fixed coordinate system. Results of the three velocity components corresponding to different spin parameters are shown as a function of meridional distance. The variations of meridional and azimuthal dimensionless wall shear

stresses are given over a wide range of spin parameters (El-Shaarawi, El-Refaie and El-Bedeawi, 1985). The effect of the Reynolds number is illustrated by El-Shaarawi, Kemry and El-Bedeawi (1987). Detailed experimental work (El-Shaarawi, Kemry and El-Bedeawi, 1987) provided a comparison between calculations and experimental results. Agreements between them are excellent.

The research of Luthander and Rydberg (1935), Tomotika (1938), Schlichting (1953) and Parr (1964), for the flow on a body of revolution spinning about its axis, has a more general treatment of the former case. Numerical and experimental conclusions for critical Reynolds numbers, drag and torque coefficients and velocity distribution agreed well for the case of a sphere.

For the case of a rotating sphere whose axis is parallel to the free stream, mass transfer and convection have also been investigated by El-Shaarawi et al (1990, 1992), Furuta et al (1975, 1977), Chen and Mucoglu (1977), Palec and Daguenᴄt (1984, 1987) and Rajasekaran and Palekar (1985). Other than motion equations, the energy equation is included to solve the problem. The basic computational and experimental methods used here are the same as these used above, but more complicated.

In the above three situations, there is one thing in common: the problem is axially symmetric, and it can be treated as a two-dimensional flow problem. Either stream function -

vorticity equations or momentum equations can be used to solve the problems. Streamlines, the most straightforward physical figures, are presented in their results.

In this study, the problem is symmetric about the equatorial plane. It is a three-dimensional problem. The distribution of velocities and pressures, instead of the streamlines, will be shown with a three-dimensional coordinate system to predict the flow fields.

CHAPTER 3

THEORETICAL ANALYSIS

3.1   Governing Equations

Schlichting (1953) gave the fundamental equations and boundary conditions for boundary-layer flow around a rotating body in an axial stream (Eqs. 2.1 to 2.3). These equations are available only for two-dimensional problems. In the present study, a sphere, rotating with constant angular velocity about a diameter that is perpendicular to the free-stream direction, is considered. This problem is a three-dimensional problem with the flow field being symmetric about the equatorial plane.

Following Schlichting's basic theory (Schlichting, 1979) and assuming the physical properties of the fluid are constant, from the basic spherical boundary-layer equations, the fundamental three-dimensional boundary-layer equations for current problem are deduced. These equations in turn can be simplified to two dimensional equations (Schlichting, 1953), according to the properties of the variables. The details of the procedure are as follows.

Let x, y, z is an orthogonal curvilinear fixed coordinate system as shown in Fig.3.1. The x-axis is measured along the meridional direction, the y-axis is along the circumferential direction of a horizontal cross section, the z-axis is along the radial direction of the sphere, and r is along the radial direction of the horizontal cross section. Meanwhile, let free-stream velocity, U_∞, and sphere radius, a, be denoted as characteristic reference magnitudes. The variables are non-dimensionalized in the following manner:

lengths $\qquad X = x/a, \qquad Y = y/a, \qquad Z = z/a, \qquad R = r/a$

velocities $\qquad U = u/U_\infty, \qquad V = v/U_\infty, \qquad W = w/U_\infty$

pressure $\qquad P = p/(\rho U_\infty^2)$

time $\qquad T = t\, U_\infty/a$

where u, v, and w are the meridional, azimuthal and radial velocity components, respectively; t, the time; and p, the static pressure.

All quantities with a capital letter, except U_∞, are dimensionless. The Reynolds number based on sphere diameter is $Re = 2U_\infty\, a/v$. It will be remembered that in the derivation of the boundary-layer equations dimensionless quantities are used. The reason for this is that for a given body the dimensionless velocity components are functions of the dimensionless coordinates; the functions, moreover, do not depend on the Reynolds number any longer. The practical importance of this principle of similarity with respect to Reynolds number consists in the fact that for a given body shape it suffices to find the solution to the boundary-layer problem only in terms of dimensionless variables.

In the z-direction we know that $\partial p/\partial z$ is very small and may be neglected. Thus, the pressure is depending on x and y alone. From the boundary-layer situation, we have

$$X, U, Y, V, R \sim 0\ (1)$$

$$T \sim 0\ (1)$$

$$Z, W \sim \delta_* = \delta/a \ll 1$$

With these assumptions and without the body forces, the boundary layer equations that govern the problem are as follows:

$$\frac{\partial u}{\partial x} + \frac{\partial v}{\partial y} + \frac{u}{r}\frac{dr}{dx} + \frac{\partial w}{\partial z} = 0 \tag{3.1}$$

$$u\frac{\partial u}{\partial x} + v\frac{\partial u}{\partial y} - \frac{v^2}{r}\frac{dr}{dx} + w\frac{\partial u}{\partial z}$$
$$= u_*^o\frac{\partial u_*^o}{\partial x} + v_*^o\frac{\partial u_*^o}{\partial y} - \frac{(v_*^o)^2}{r}\frac{dr}{dx} + \upsilon\frac{\partial^2 u}{\partial z^2} \tag{3.2}$$

$$u\frac{\partial v}{\partial x} + v\frac{\partial v}{\partial y} + \frac{uv}{r}\frac{dr}{dx} + w\frac{\partial v}{\partial z}$$
$$= v_*^o\frac{\partial v_*^o}{\partial y} + \frac{u_*^o v_*^o}{r}\frac{dr}{dx} + \upsilon\frac{\partial^2 v}{\partial z^2} \tag{3.3}$$

Here, in x and y momentum equations, pressure terms are substituted by known potential flow expressions according to Schlichting's (1979) analysis; u_*^o and v_*^o are potential velocity components in x and y-directions on the surface of the sphere, respectively. The pressure increase across the boundary layer is of the order δ^2, i.e., very small. At the outer edge basic equations are applied to obtain expressions for the pressure gradients by outer edge parameters; then they are connected to momentum equations.

3.2 Boundary Conditions

There are two kinds of boundary conditions as follows

i.   At the surface of the sphere, $0^\circ < \theta < 90^\circ$, $0^\circ \le \varphi \le 360^\circ$, $z = 0$

$$u = w = 0 \qquad (3.4)$$

$$v = \omega\, a\, \sin\theta \qquad (3.5)$$

where θ is the center angle measured from the axis of rotation; φ, the angle on a horizontal circular cross section; and ω, the angular velocity of the sphere.

ii.   Far away from the surface of the rotating sphere, the flow is a two-dimensional potential flow. It has the following two velocity components (Milne-Thomson, 1968) in the coordinate system shown in Fig.3.2.

$$u^* = -U_\infty \left[\, 1 + a^3 / 2\, (a + z)^3\, \right]\, \sin\alpha \qquad (3.6)$$

$$w^* = U_\infty \left[\, 1 - a^3 / (a + z)^3\, \right]\, \cos\alpha \qquad (3.7)$$

where u^* and w^* are potential velocity components in the x and z-directions, respectively for the rotating sphere whose axis is parallel to the free stream direction; and α, the center angle measured from the horizontal axis. The expressions must be translated (sees Appendix I) to conform with coordinate system used in this thesis (Fig.3.1), then these become:

$$u_* = U_\infty \left[\, 1 + a^3 / (a + z)^3\, \right]\, \cos\varphi\, \cos\theta \qquad (3.8)$$

$$v_* = -U_\infty \left[\, 1 + a^3 / 2\, (a + z)^3\, \right]\, \sin\varphi \qquad (3.9)$$

$$w_* = U_\infty \left[\, 1 - a^3 / (a + z)^3\, \right]\, \cos\varphi\, \sin\theta \qquad (3.10)$$

3.3 Nondimensional Governing Equations and Boundary Conditions

Introducing the dimensionless parameters given in the section 3.1, the nondimensional governing equations and boundary conditions may be written as follows

$$\frac{\partial U}{\partial X} + \frac{\partial V}{\partial Y}\frac{\sqrt{Ta}}{Re} + \frac{U}{R}\frac{dR}{dX} + \frac{Re}{2}\frac{\partial W}{\partial Z} = 0 \tag{3.11}$$

$$U\frac{\partial U}{\partial X} + \frac{\sqrt{Ta}}{Re}V\frac{\partial U}{\partial Y} - \frac{Ta}{Re^2}\frac{V^2}{R}\frac{dR}{dX} + \frac{Re}{2}W\frac{\partial U}{\partial Z}$$
$$= U^o\frac{\partial U^o_.}{\partial X} + \frac{\sqrt{Ta}}{Re}V^o\frac{\partial U^o_.}{\partial Y} - \frac{Ta}{Re^2}\frac{(V^o_.)^2}{R}\frac{dR}{dX} + \frac{\partial^2 U}{\partial Z^2} \tag{3.12}$$

$$U\frac{\partial V}{\partial X} + \frac{V\sqrt{Ta}}{Re}V\frac{\partial V}{\partial Y} + \frac{UV}{R}\frac{dR}{dX} + \frac{Re}{2}W\frac{\partial V}{\partial Z}$$
$$= \frac{\sqrt{Ta}}{Re}V^o\frac{\partial V^o_.}{\partial Y} + \frac{U^o_. V^o_.}{R}\frac{dR}{dX} + \frac{\partial^2 V}{\partial Z^2} \tag{3.13}$$

The corresponding nondimensional boundary conditions may be expressed as

i.   At $Z = 0$ (surface of the sphere)

$$U = W = 0 \tag{3.14}$$
$$V = \frac{v^o}{\omega a} = \sin\theta \tag{3.15}$$

where v^o is a circumferential velocity at a point on the sphere surface.

ii.   At $Z \geq \delta.$ (outer edge of the boundary layer)

$$U = U_. = [\ 1 + 1\ /\ (1 + Z)^3\ ]\cos\varphi\ \cos\theta \tag{3.16}$$

$$V = V_* = - [\ 1 + 1\ /\ 2\ (1 + Z)^3\ ]\ \sin \varphi \qquad (3.17)$$

$$W = W_* = [\ 1 - 1\ /\ (1 + Z)^3\ ]\ \cos \varphi\ \sin \theta \qquad (3.18)$$

where δ_* is the dimensionless boundary layer thickness.
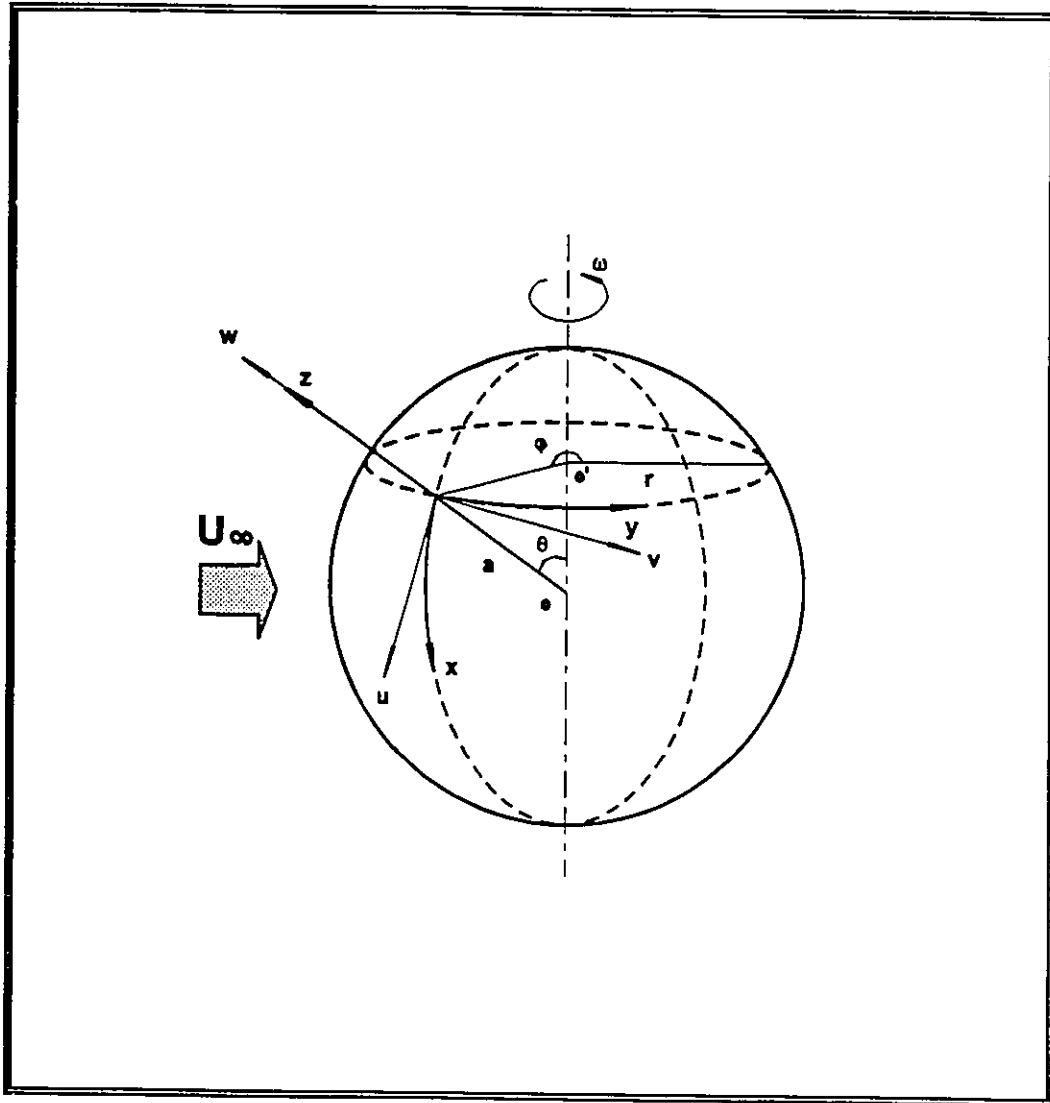
Figure 3.1   Spherical coordinate system
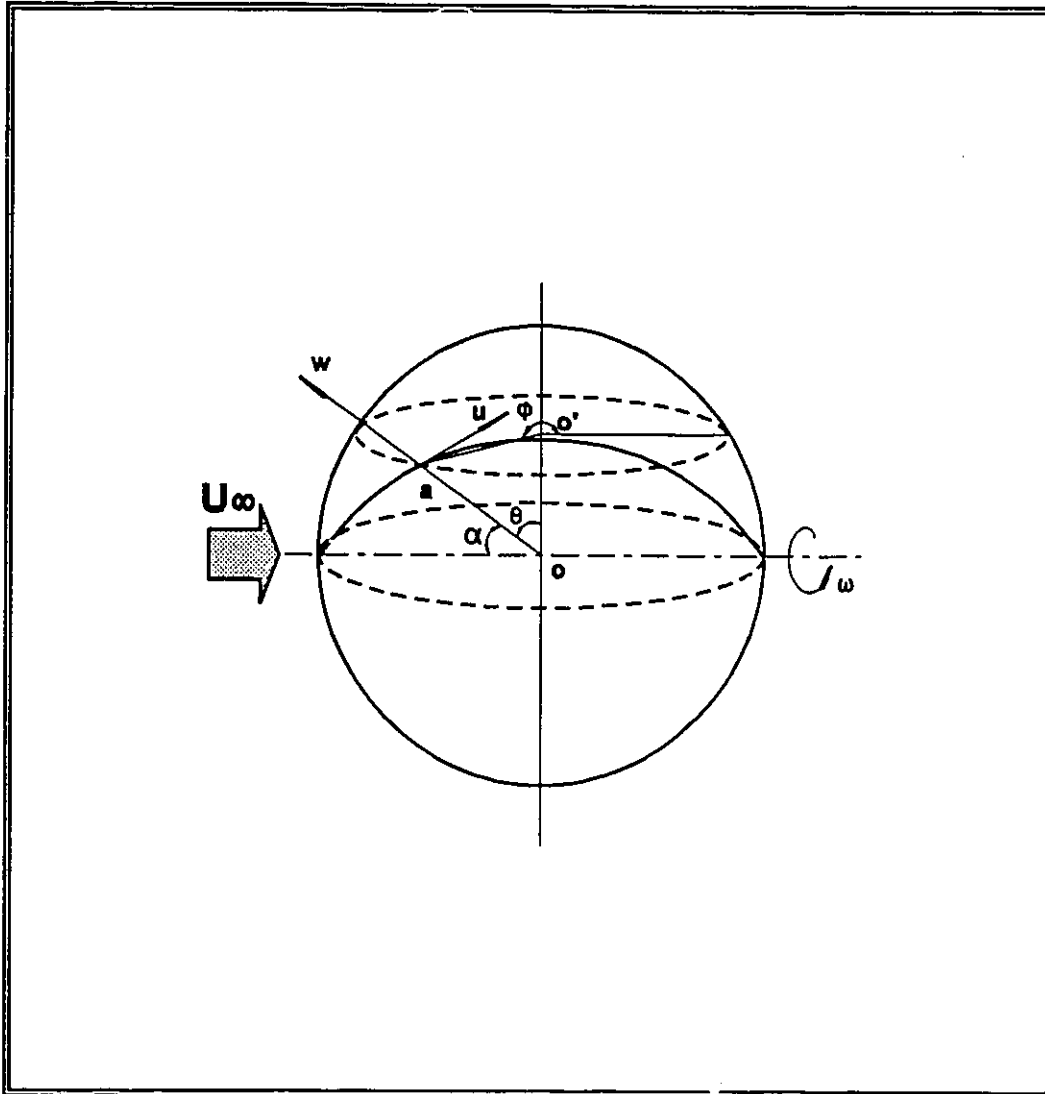
Figure 3.2   Coordinate system for original flow

CHAPTER 4

NUMERICAL METHOD

4.1 Basic Equations

The basic equations of fluid mechanics, assuming the fluid is incompressible with constant properties can be written in general form (Patankar, 1980) as:

$$\frac{\partial}{\partial t}(\rho\phi) + \bar{\nabla} \cdot (\rho\bar{u}\phi) = \nabla \cdot \Gamma\nabla\phi + S$$

$$\textit{transient} + \textit{convection} = \textit{diffusion} + \textit{source}$$

(4.1)

The transport of some property ϕ is a result of the combined influence of transience, convection, diffusion and source-related effects. The Navier-Stokes' equations may be regarded as the equation for the derivatives of three velocity components incorporating viscous and pressure gradient effects, while the continuity equation is obtained by taking ϕ to be unity, with only convective activity.

In this thesis, steady, laminar and turbulent, incompressible, constant-property flows are considered. Thus transient terms have been omitted from these equations, and the

diffusion terms have been simplified. Other than this, the general form has been retained so that the more universal forms can easily be recovered.

4.2 Numerical Scheme

4.2.1 Finite - volume Equations

The basic solution procedure used in the remainder of the study is the finite-volume method that uses a modified version of the SIMPLE (Semi-Implicit Method for Pressure-Linked Equations) algorithm (Patankar and Spalding, 1972 and Patankar, 1980).

The methodology involves constructing a grid made up of many cells connected in a structured manner. Figure 4.1 shows a typical cell. The location of the node P is a weighted average of the eight cell corners. Assuming the nodal value of ϕ at P, ϕ_P is related to its six neighbors by a set of linear algebraic equations having the form

$$a_W(\phi_W-\phi_P) + a_E(\phi_E-\phi_P) + a_S(\phi_S-\phi_P) + a_N(\phi_N-\phi_P) +$$
$$a_L(\phi_L-\phi_P) + a_H(\phi_H-\phi_P) + a_T(\phi_T-\phi_P) + S = 0 \qquad (4.2)$$

where the subscripts W, E, S, N, L, H refer respectively to the west, east, south, north, low, and high neighbors of P and ϕ_T refers to the value of ϕ at the previous time step. S is the source term. The above equation is termed a finite-volume equation, as it approximates the

differential equations of motion, integrated over the cell volume. The linking coefficients are evaluated by considering the combined influence of transience, convection, diffusion and source-related effects.

The above equations may be solved by various iterative schemes; point-by-point, line-by-line, slab-by-slab, or whole-field solution procedures (Spalding, 1980). The general equation integrated over a control volume is presented in discretized form as

$$a_P \phi_P = a_N \phi_N + a_S \phi_S + a_E \phi_E + a_W \phi_W \\ + a_H \phi_H + a_L \phi_L + a_T \phi_T + b$$

(4.3)

where b and a_p are employed to express not only sources but boundary conditions, corrections to left-hand-side terms, under-relaxation practices, etc.

4.2.2 Body-fitted Coordinates

During the simulation process, due to the particular curved shape, a special coordinate system, body-fitted coordinates (BFC), is used to generate the grids in the spherical domain. The theoretical fundamental of BFC is actually a coordinate transformation from curvilinear to Cartesian coordinates. The use of body-fitted coordinates is a natural extension of the finite-volume method (Malin et. al., 1985).

In BFCs, as with regular grids, the scalar variables are stored at the cell center, i.e. the arithmetic mean of the cell corners. Meanwhile, velocities are stored at the centers of cell faces. The direction of the stored velocity is along the line joining adjacent cell centers (local grid direction). The magnitude of the stored velocity is obtained by resolving the total velocity vector (by projection) in the direction of the line joining the cell centers. The stored velocity is therefore known as a resolute.

As Figure 4.2 shows, these resolutes are OA, OB and OC, respectively. The velocity components in local grid directions, 1 and 2, are OQ and OP, respectively. Components and resolutes are equivalent only when the grid is orthogonal. If p, q, r are the velocity components in the local grid directions, and $\vec{e}_1$, $\vec{e}_2$, $\vec{e}_3$ are the unit vectors defined in these directions, i.e., 1,2 and 3, then the velocity vector can be expressed as

$$\vec{V} = p\vec{e}_1 + q\vec{e}_2 + r\vec{e}_3 \tag{4.4}$$

And the velocity resolutes are formed by $u = \vec{e}_1 \cdot \vec{V}$, $v = \vec{e}_2 \cdot \vec{V}$, $w = \vec{e}_3 \cdot \vec{V}$, respectively. The velocity components are written in terms of the resolutes as

$$p = A_p u + B_p v + C_p w \tag{4.5}$$
$$q = A_q u + B_q v + C_q w \tag{4.6}$$
$$r = A_r u + B_r v + C_r w \tag{4.7}$$

where the A's, B's and C's are functions of angles between the coordinate directions.

In fact, in the calculation program the stored velocity values are the tangential resolutes. For convenience, in the following discussion the compact notation u_e, v_n, w_h will be used instead of $u_{e(tr)}$, $v_{n(tr)}$, $w_{h(tr)}$. Similarly P-E, P-N, P-H refer to the tangential-displacement components, $dx^{(tc)}$, $dy^{(tc)}$, $dz^{(tc)}$, will be expressed as dx, dy, dz. Finally the areas A_e, A_n, A_h refer to normal components $A_{e(nc)}$, $A_{n(nc)}$, $A_{h(nc)}$. These are the cell-face vector areas.

Without transient and source-terms, the resolute form of the transport equation may be written as (Beale, 1993)

$$\frac{\partial}{\partial x}(\frac{1}{\alpha_x{}^x}J_x{}^{(nr)}) + \frac{\partial}{\partial y}(\frac{1}{\alpha_y{}^y}J_y{}^{(nr)}) + \frac{\partial}{\partial z}(\frac{1}{\alpha_z{}^z}J_z{}^{(nr)}) = 0 \qquad (4.8)$$

where $\bar{J}$ is the total flux that combined the convection and diffusion terms, and defined as

$$\bar{J} = \rho\,\bar{u}\phi - \Gamma\bar{\nabla}\phi \qquad (4.9)$$

And $\alpha_x{}^x$ denotes the cosine of the angle between the x-tangent and x-normal directions, $\alpha_y{}^y$ and $\alpha_z{}^z$ the y- and z- direction cosines. Because the volume of the parallelepiped bounded by the tangential components dx, dy, dz is

$$\lim_{dV \to 0} dV = \alpha_x{}^x dA_x dx = \alpha_y{}^y dA_y dy = \alpha_z{}^z dA_z dz \qquad (4.10)$$

Eq. (4.8) can be integrated to obtain

$$A_e J_e{}^{(nr)} - A_w J_w{}^{(nr)} + A_n J_n{}^{(nr)} - A_s J_s{}^{(nr)} + A_h J_h{}^{(nr)} - A_l J_l{}^{(nr)} = 0 \qquad (4.11)$$

Thus, the transport equations may be discretized as described above, subjected to only two modifications.

The first modification to the finite-volume method is that the normal resolutes of $\vec{J}$ must be computed from the stored tangential values. For the convection flux, the procedure is as follows. The stored values are the tangential velocity resolutes, u_e, v_n, w_h. Considering the east face convection flux, m_e. Values of u_e, v_n, w_h are used to construct the components of a vector, $\vec{u}$, based on the inverse of the direction cosines between the grid lines P-E, P-N, P-H. The magnitude of the convection flux normal to A_e is then obtained as the projection of these components normal to the east face

$$m_e = \rho \vec{A}_e \cdot \vec{u}_e = \rho A_e^{(nr)} u_{e(nc)} = \rho A_{e(nc)} u_e^{(nr)} \tag{4.12}$$

All three tangential resolutes contribute to the construction of the normal resolute $u_e^{(nr)}$, so that

$$m_e = \rho A_e (F_u u_e + G_u v_n + H_u w_h) \tag{4.13}$$

F, G, and H, are geometric factors related to angles between the coordinate and the cell-face directions. Convection coefficients at the other interfaces are computed in a similar fashion.

A similar treatment is used for the diffusion flux. Since grad ϕ is a vector resolute, it is also necessary to construct the tangential components of the diffusion flux vector and

project these in the normal direction (using the same geometrical factors, F, G, and H, above). Considering the normal diffusion flux resolute across the east face

$$\nabla \phi_e = F_u \frac{(\phi_E - \phi_P)}{|\vec{PE}|} + G_u \frac{(\phi_N - \phi_P)}{|\vec{PN}|} + H_u \frac{(\phi_H - \phi_P)}{|\vec{PH}|} \tag{4.14}$$

With similar terms for the other resolutes.

A second set of modifications is applied to the momentum-equation terms. When integrating over a finite-volume, it is necessary to refer values to locally-fixed directions. Consider the east neighbor of u_e, u_{eE} say, in the u-momentum equation. To construct the finite-volume equation associated with a locally oblique curvilinear coordinate system, the components of a vector are constructed in a fashion similar to Eq. (4.13), from velocity resolutes u_{eE}, v_{nE}, w_{hE}. These are then projected in direction P-E, i.e. parallel to u_e. This treatment of u_e and u_w accounts for grid curvature. Divergence effects may be similar treated in regard of u_{eS}, u_{eN} in the u-momentum equations. Curvature and divergence terms are referred to as Coriolis and centrifugal effects, respectively.

An element of bias has been introduced by using the triplet u_e, v_n, w_h in constructing the components of a vector at e, the use of higher order schemes e.g. involving u_e, u_w, v_n, v_s, w_h, w_h while reducing the error.

The BFC equations are solved by the regular-grid solution methods in the software used which is based on the SIMPLEST algorithm. Equations are solved by sweeps in the z direction, which are repeated until convergence is achieved. The pressure-correction equation can be solved whole field. The only modification in the solution procedure for BFC's is in the pressure-correction sequence, when the grid is non-orthogonal.

4.2.3 Relaxation

Fluid flow and heat transfer problems are governed by partial differential equations that are nonlinear and very often are strongly coupled. These facts make it difficult to obtain a convergent solution and sometimes solution controlling parameters must be enforced to get and enhance convergence. There are two relaxation methods provided for control divergence behavior.

i. False - time -step relaxation

$$a_P \phi_P = \sum_{F - W,E,S,N,H,L} a_F \phi_F + a_T \phi_T + b + \frac{\rho V_P}{\Delta t_f} (\phi_P - \phi_{P,old}) \qquad (4.15)$$

where ρV_P is the in-cell mass, the denominator Δt_f is the so-called false time-step and $\phi_{P, old}$ is the previous variable value. Based on the general finite volume equation, Eq. (4.3), an additional source term was added to the equation. It showed that the value of the false time-

step controls the rate at which the dependent variable is going to change from sweep to sweep. The two extremes are:

(a) Δt_f = very large value ($1.0E10$ say) → $\rho V_p / \Delta t_f \to 0$

(b) Δt_f = very small value ($1.0E\text{-}10$ say) → $\phi_P = \phi_{P,\,old}$

In the first case, the added term vanished entirely meaning that there is no relaxation at all. In the second case, there is so much relaxation that the dependent variable gets 'frozen', i.e., it is not allowed to change from one sweep to the next one.

ii.   Linear relaxation

$$\phi_{P,new} = \phi_{P,old} + c \left(\phi_{P,calculated} - \phi_{P,old} \right) \qquad (4.16)$$

The dependent variables are updated from one sweep to the next one are constrained by adding a linear fraction of the previous value of ϕ to the current value. c is a relaxation factor. Thus, setting $0 < c < 1.0$ slows the changes in ϕ_p from sweep to sweep.

In the calculation procedure of this study, the false-transient relaxation method was chosen for all velocity components, while the linear relaxation method was chosen for pressure p. In the latter, there is no false transient.

4.2.4   Rotating Coordinate System

Because of the rotation of the sphere, a rotating coordinate system was also considered with BFC. For a coordinate system rotating with constant angular velocity, ω, the resolutions of the apparent body-force per unit volume are

$$F_i = \vec{e}_i \, [\, -2\rho\vec{\omega} \times \vec{Q} - \rho\vec{\omega} \times (\, \vec{\omega} \times \vec{R} \,) \,] \qquad (4.17)$$

where vectors of $\vec{e}_i$, $\vec{\omega}$, $\vec{Q}$ and $\vec{R}$ are the total unit vector, the rotation vector, total velocity vector and the radius vector, respectively. The first term, $-2\rho\vec{\omega} \times \vec{Q}$, is the Coriolis force that is perpendicular to vectors of $\vec{Q}$ and $\vec{\omega}$. The second term, $-\rho\vec{\omega} \times (\, \vec{\omega} \times \vec{R})$, is the centrifugal force. These forces are incorporated into the mathematical model as additional volumetric momentum sources. Obviously, this is the case for rotating sphere situations, so the author has considered it in the corresponding programs.

4.2.5 Cyclic Boundary Conditions

Cyclic boundary conditions are required whenever the two ends of the calculation domain in the x-direction join up with one another. The general rule is that whenever identical conditions are to be expected at $x = 0$ and $x = $ last x, and finite flow is to be expected through that surface, then the boundaries are cyclic.

For both rotating sphere cases, rotating axes are parallel and perpendicular to the free stream, the cyclic boundary condition occur in the circumferential direction of BFC.

Therefore, at the positions $\varphi = 0^\circ$ and $\varphi = 360^\circ$, a cyclic boundary condition is employed to handle the repeat conditions of the two planes.

4.3 Computer Code and Application

The computer codes used for the numerical study were the PHOENICS (Parabolic, Hyperbolic or Elliptic Numerical Integration Code Series) versions 1.5 to 2.0. All computations are made on a Sunspark station operating in a UNIX environment.
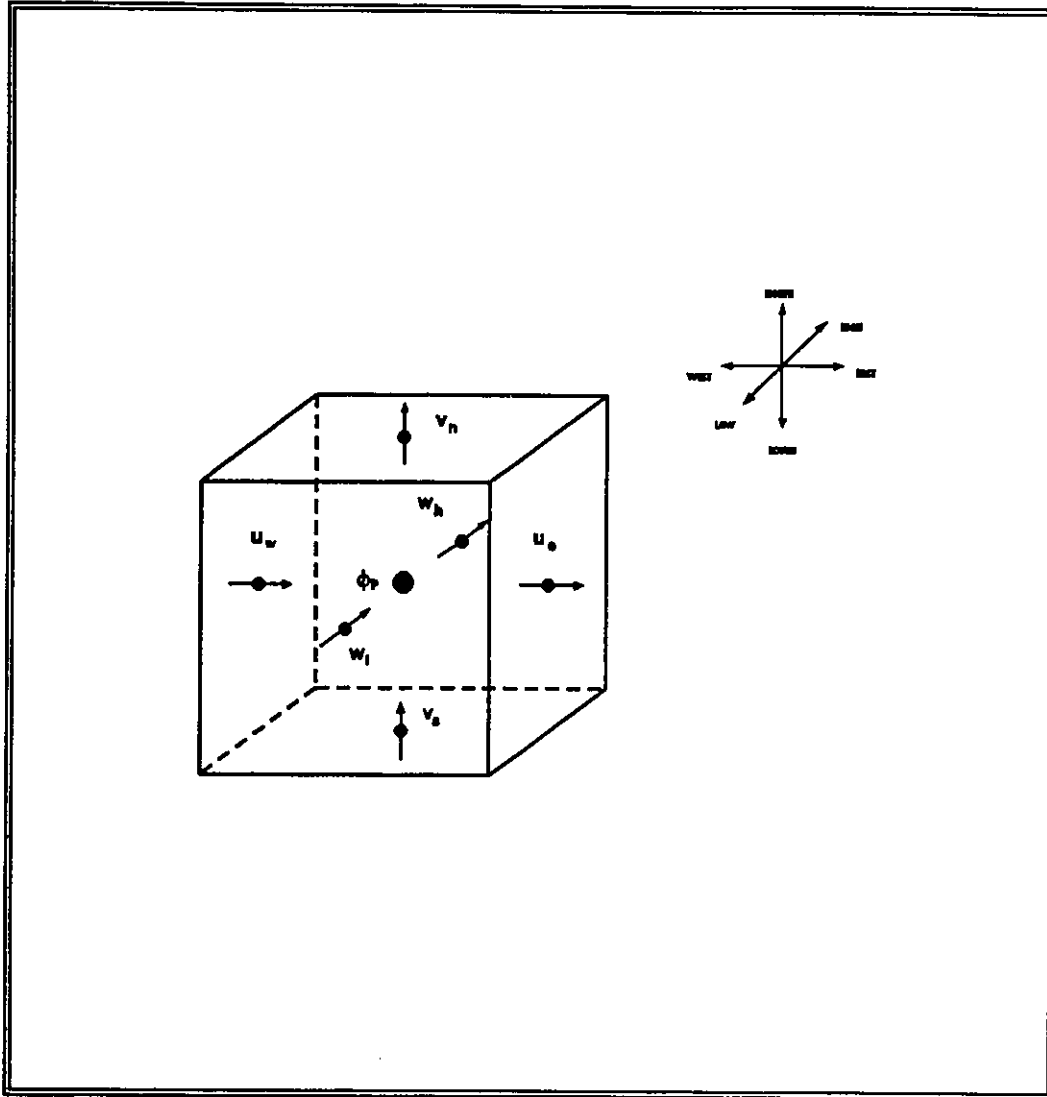
Figure 4.1   Control volume for calculation
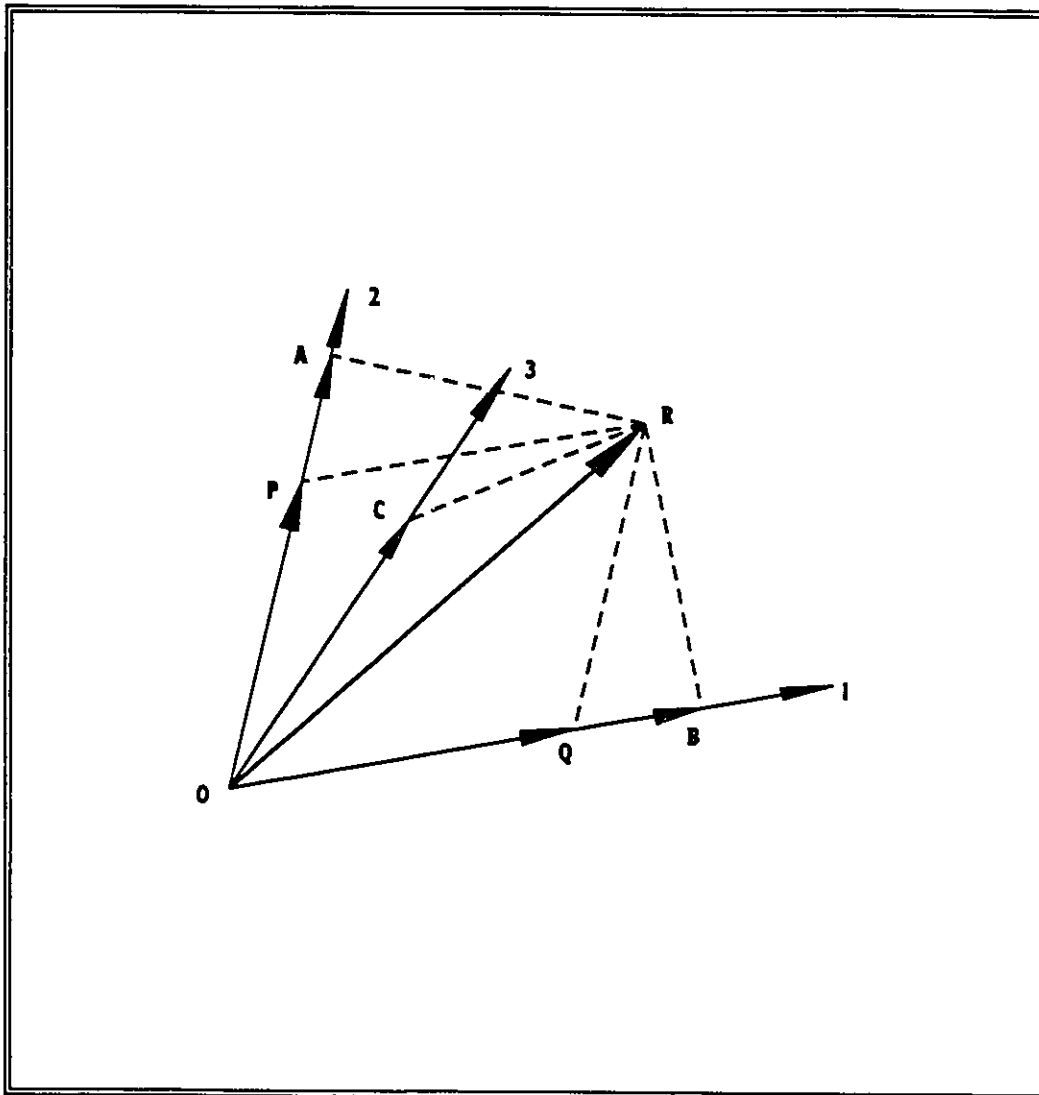
Figure 4.2 Resolutes and components of vector

CHAPTER 5

NUMERICAL PREDICTION OF

FLOW FIELDS AROUND SPHERES

5.1   Grid Generation

Two kinds of grids, cylindrical and spherical, are considered for the geometric symmetry of

the flow field domain. The general strategy involves the use of body-fitted-coordinate (BFC)

grids, connected in a structured fashion that has desirable features as listed below:

i.   equivalent to a distorted Cartesian grid

ii.   grid lines must continue right across the grid

iii.   parallel grid lines must remain parallel

iv.   one set of grid lines should be aligned with the main flow direction to reduce

        numerical false-diffusion errors

v.   concentrating grid lines in regions of interest (boundary layers, wakes etc.)

5.1.1   Cylindrical Grid

For problems of flow around a stationary sphere or a rotating sphere whose axis is parallel to the free stream direction, it is convenient to use a cylindrical grid system illustrated in Figure 5.1 because of axial symmetry. Using a curvilinear coordinate system, let x be the radial direction, y the circumferential direction and z the axial direction. The free stream direction is the same as the z-direction. To match the spherical surface, the Laplace solver with *10* iterations is used. There are *10* radial cells, *20* circumferential cells and *30* axial cells. The size of the cells is not distributed uniformly in the axial direction, with high concentration near the polar area. Due to the procedure of the grids generation, the first and the last planes on the circumferential direction are overlapped. A cyclic boundary condition is introduced to handle this situation.

5.1.2   Spherical Grid

For problems of the flow field due to a rotating sphere and the flow field around a rotating sphere whose axis is perpendicular to the free stream direction, it is more convenient to use a spherical grid system as shown in Figure 5.2. In the latter case, the flow field is hemispherically symmetric about the equatorial plane. Here x is along the circumferential direction of horizontal plane, y the radial direction and z the circumferential direction of vertical plane, respectively. Only one half of the sphere above the equatorial plane is considered because of hemispherical symmetry. The free stream direction is along with the x-direction. There are *31* cells in the circumferential direction of horizontal plane, *15* cells in

the radial direction and *11* cells in the circumferential direction of vertical plane. The size of the cells is exponentially (exponential coefficient equal to *1.2*) distributed in the radial direction, with high concentration near the surface of the sphere.

It worth mentioning that the first radial plane and the last radial plane in the *x*-direction are the same plane, again the cyclic boundary condition is used to treat it. Furthermore, the last circumferential plane in the *z*-direction, in fact, became a line on the rotational axis. Therefore, one-dimensional boundary condition is all that is necessary.

5.2   Flow Fields past a Stationary Sphere

Two cases are included in this section. One is potential flow field past a sphere at low Reynolds number. The other is the vortex flow field past a sphere at moderate Reynolds number. An important difference between them is that whether or not a separated wake appears behind the sphere. Calculated results for velocity and pressure distributions, are given with detailed discussions. Results are compared with other researchers' results.

5.2.1   Potential Flow Field

Results

Some work has been carried out on the flow field around a stationary sphere. Figures 5.3 and 5.4 show the results of velocity and pressure distributions on two symmetrical planes, respectively with Reynolds number equal to *2.2*, the free stream velocity is *1 m/s* and inlet reference pressure *1 N/m²* (the unit of all pressure graphics). Where the flow is potential flow, the Darcy law i.e. a Laplace-equation form, is applied. This usage eliminates the convection and diffusion terms and is the recommended way of solving potential flows in BFC.

Discussion

As shown in Figures 5.3, the problem is axially symmetric. The result shows that the smallest velocity occurs at the front polar point area. Around the equatorial plane, velocity has the largest value. This result is in excellent agreement with classical calculation results, such as Rimon and Cheng (1969), and Dennis and Walker (1971), shown in Figures 5.7 and 5.8. As the Reynolds number is very small, no separation present.

Figure 5.4 indicates that the pressure has the largest value at the entrance of the whole calculation domain and the smallest value at the exit. The pressure changes along the free stream direction smoothly, but there is no change on each of the cross sections. This result is somewhat different from the results of Rimen and Cheng (1969) and Dennis and Walker (1971). Their results have the smallest pressure value at the point on where the largest velocity gradient occurs. The reason for this is the use of the Darcy law in the calculation.

5.2.2   Vortex Flow Field around a Sphere

Results

Another case of this kind of problem is vortex flow around a stationary sphere. When the free stream velocity is increased to a certain value, the flow is disturbed and a vortex occurs behind the sphere. Using a standard k-ε turbulence model, the evolution of near wake structure, at Reynolds number equal to *22*, free stream velocity *60 m/s* and outlet reference pressure *10 N/m²*, is shown in Figure 5.5. Figure 5.6 is the pressure distribution.

Discussion

Figures 5.5 and 5.6 show that at the stagnant point, the velocity has the smallest value, while the pressure has the largest value. Around the equatorial plane, velocity has largest value due to the curved surface, the pressure has smallest value correspondingly. Near the rear polar point, velocity is reversed and the dead water phenomena occurs. Here the pressure is smaller than the rest positions of this area because the dead water phenomenon.

One of the important points is to decide the Reynolds number at which a separated wake first appears behind the sphere and to examine the subsequent development of the wake with Reynolds number. $Re = 20.5$, has given by Dennis and Walker (1971) and *24* by Rimon

and Cheng (1969) for the onset of separation.

Comparing the pressure distributions on the whole flow field with the case of potential flow, Figure 5.4, we conclude that pressure has no change corresponding to the velocity variation on a cross section if a velocity potential exists. The inlet side has the largest pressure and outlet the smallest. Here, the pressure distribution is in good agreement with the results of Rimon and Cheng (1969) when Reynolds numbers are in the same range.

Results given by Rimon and Cheng (1969) and Dennis and Walker (1971) are shown in Figures 5.7 and 5.8. In the rear polar point area, there is a dead water area due to the separation. This is because when the free stream velocity is increased, Reynolds number also increases. In this situation, a separation point occurs in the rear half sphere. The size of the dead water area depends on the position of the separation point which is a function of the free stream velocity.

5.3   Flow Fields around a Rotating Sphere

Three different flow fields in this kind of problem will be discussed. They are:

i.   flow field around a rotating sphere whose axis is parallel to the free stream

ii.   flow field due to a rotating sphere

iii.   flow fields around a rotating sphere whose axis is perpendicular to the free stream

The first two cases are axisymmetrical problems, so they can be treated as two-dimensional problems. The last case is a three-dimensional problem. Due to the desired features of structured grids in section 5.1, cylindrical grids are used for the first case, and spherical grids for the last two cases.

5.3.1   Flow Field around a Rotating Sphere - Axis is Parallel to the Free Stream

Results

The results given are based on a constant angular velocity of *1 rad/s*, free stream velocity of *10 m/s* with inlet reference pressure of *10 N/m²*, Reynolds number of *6.25×10⁶*, and spin parameter $Ta/Re^2 < 1$. Due to the rotation of the sphere, a rotating coordinate system is used for the reason mentioned in section 4.2.4. Also, the procedure for the generation of the grids required a treatment of cyclic boundary conditions as explained in section 4.2.5 for the first and last radial planes. Figures 5.9 and 5.10 are velocity distributions on two special cross section planes and two symmetrical planes, respectively. One cross plane is at upstream and another one downstream. Figure 5.11 is pressure distribution on two symmetrical planes.

Discussion

Figure 5.9 illustrates the velocity distributions on two cross section planes at the positions of

two polar points. On the upstream cross section, only the velocity of the free stream affects the velocity distribution because there is no other flow interference. Meanwhile, on the downstream cross section, besides the effect of the velocity of the free stream, the behavior of the rotation also has an effect. This also shows in Figure 5.10, at the back of the half sphere, the tangential velocities along circumferential direction of cross sections are large enough to interfere with the flow field. Beyond this area, the effect keeps until the outlet plane. Here, the problem is still symmetry about the rotating axis, so the stagnant point on the front polar having the smallest velocity value.

Comparing the result of pressure distribution, Figure 5.11, with the result of vortex flow, Figure 5.6, at the position around the stagnant point the pressure distributions are the same because there is no difference in flow condition here. On the contrary, due to the effect of rotation the dead water area disappears and the pressure is smaller than the vortex case at the rear area of the sphere and downstream.

Here an important spin parameter, Ta/Re^2, the ratio between the centrifugal and inertia force, is introduced. It plays a significant role with Reynolds number in the boundary layer equations. It has an effect on a separation angle, dimensionless torque, resisting momentum and frictional drag (El-Shaarawi et al, 1985).

Far away from the surface of the sphere, the flow is of a two-dimensional potential

type. The two velocity components for such a potential flow are adopted from Milne-Thomson (1968). On the surface, only circumferential velocity, $v_0 = r\omega$, is relevant.

5.3.2   Steady Flow due to a Rotating Sphere

Results

The steady flow due to a rotating sphere is a limiting case and has attracted much attention so far. As the problem is symmetric about the rotating axis, we consider only one radial plane of half spherical grids with a sphere radius of *0.065 m* and an extent radius distance of *0.300 m*, a constant angular velocity of *100 rad/s* and Reynolds number of 5.3×10^4. A rotating coordinate system and cyclic boundary condition are used for the same reason as mentioned in section 5.3.1. The results are shown in Figures 5.12 for velocity distribution and Figure 5.13 for pressure distribution, respectively.

Discussion

Figure 5.12 illustrates that there is a region of inflow to the sphere near the pole, which is balanced by a region of outflow near the equatorial plane. This is as indicated by Singh (1970), Banks (1976) and Dennis et al (1980). As Reynolds number increases, the inflow region increases and the outflow region is narrower. The angle at where the transition

between of them takes place is dependent on the variation of Reynolds number, shown in Figure 5.14.

As shown in Figure 5.12, in the whole flow field, the velocity decreases rapidly from the surface of the sphere to the outer edge of the spherical area. On the other hand, the pressure increased rapidly along this direction, illustrated in Figure 5.13. At the equatorial plane, the radial velocity increases with Reynolds number indicating the formation of a radial jet over the narrowing region of outflow. There is no evidence of any separation.

5.3.3 Flow Fields around a Rotating Sphere - Axis is Normal to the Free Stream

The contributions of the present work are the numerical predictions of the flow fields around a rotating sphere whose axis is perpendicular to the free stream. This has never been investigated before. This problem is three-dimensional and it is symmetric only about the equatorial plane. The effects of two parameters as following are studied:

i.   Reynolds number, Re

ii.   spin parameter, Re/Ta^2

The discussions are detailed for three cases those are:

i.   low Reynolds number and high spin parameter

ii.   moderate Reynolds number and low spin parameter

iii.   high Reynolds number and low spin parameter

For each case, the turbulence k-ε model is used, the reference pressure always taken as 1 N/m^2 at the surface of the sphere. Figure 5.15 show the positions of equatorial plane and three radial planes on where the velocity and pressure distributions are illustrated.

Low Reynolds Number and High Spin Parameter

Considering a sphere has a radius of 0.065 m and an extent radius distance of 0.3 m, with Reynolds number equal to 5×10^4, rotating at a constant angular velocity of 88 rad/s, spin parameter of $Ta/Re^2 = 2$, and free stream velocity of 5.7 m/s, Figures 5.16, 5.17 and 5.18 illustrate the results of velocity and pressure distributions on equatorial and radial planes.

The results illustrate the velocity of the free stream is too small to have an effect on rotational action. The pressure distributions on the two sides of the symmetrical plane of the free stream almost the same. Near the surface of the sphere, the pressures have negative values and velocity vectors are very large. The pressures decrease rapidly along the free stream direction. Velocity gradient along radial direction is very large near the sphere surface, and is very small at the rest area.

Moderate Reynolds Number and Low Spin Parameter

Using the same radius of the sphere and the extent radius distance as the first case, with

Reynolds number equal to 1×10^5, rotating at a constant angular velocity of *88 rad/s*, spin parameter of $Ta/Re^2 < 1$, and the free stream velocity of $U_\infty = 11.4$ *m/s*, Figures 5.19, 5.20 and 5.21 show the results.

The results illustrate that when the value of the free stream increased, i.e. increased Reynolds number, the rotation behavior is correspondingly reduced. Comparing this set of the results with the lower Reynolds number case, the situation is almost the same. This is because the Reynolds numbers are at the same range - lower than the critical Reynolds number of a sphere, about $3 \times 10^5 - 3 \times 10^6$. The evidence indicates that the increase of the free stream has a larger influence on the flow field than increasing the angular velocity, for a Reynolds number lower than the critical value. Near the surface of the sphere, on the left side of the symmetrical plane of the free stream, two velocities acted together along same direction, meanwhile on the right side they resisted each other duo to the different velocity directions.

High Reynolds Number and Low Spin Parameter

For high Reynolds numbers, larger than or equal to the critical Reynolds number of a sphere, using the same radius of the sphere and the extent radius distance as above. At first, considering the case of Reynolds number equal to 2×10^5, rotating at a constant angular velocity of *177 rad/s*, spin parameter of $Ta/Re^2 < 1$, and the free stream velocity of $U_\infty = 23$ *m/s*, Figures 5.22, 5.23 and 5.24 illustrate the results. Then, considering a Reynolds number

equal to 5×10^5, rotating at a constant angular velocity of *250 rad/s*, spin parameter of *Ta/Re²* < *1*, and the free stream velocity of *60 m/s*, Figures 5.25, 5.26 and 5.27 show the results of velocity and pressure distributions on equatorial and radial planes, respectively.

Because the velocity of the free stream and the angular velocity are at the same scale, the influence of the velocity of the free stream is very strong, it can almost eliminate the action of rotation. These phenomena are illustrated in Figures 5.22, 5.23, 5.25 and 5.26. The figures also show that at the left side of the symmetric plane of the free stream, the effect of the rotation is much stronger because of the overlap of the two velocities. At the right side of the symmetrical plane, near the surface of the sphere, the rotational effect is larger. Along the radial direction from the surface to the outer edge, the effect decreases gradually due to the resistance of the velocity of the free stream. At a certain point, the total velocity equals zero, from this point to the outer edge of the flow field, the value of free stream velocity increases gradually, finally reaching the largest value of the free stream. The position where velocity equals zero depends on the relation between the free stream and angular velocities.

Figures 5.24 and 5.27 present the corresponding changes of pressure distribution on the flow field. On the two sides of the symmetrical plane of the free stream, the pressure varies according to the changes of the velocity, but there is no large difference between the two sides.

PHOTON
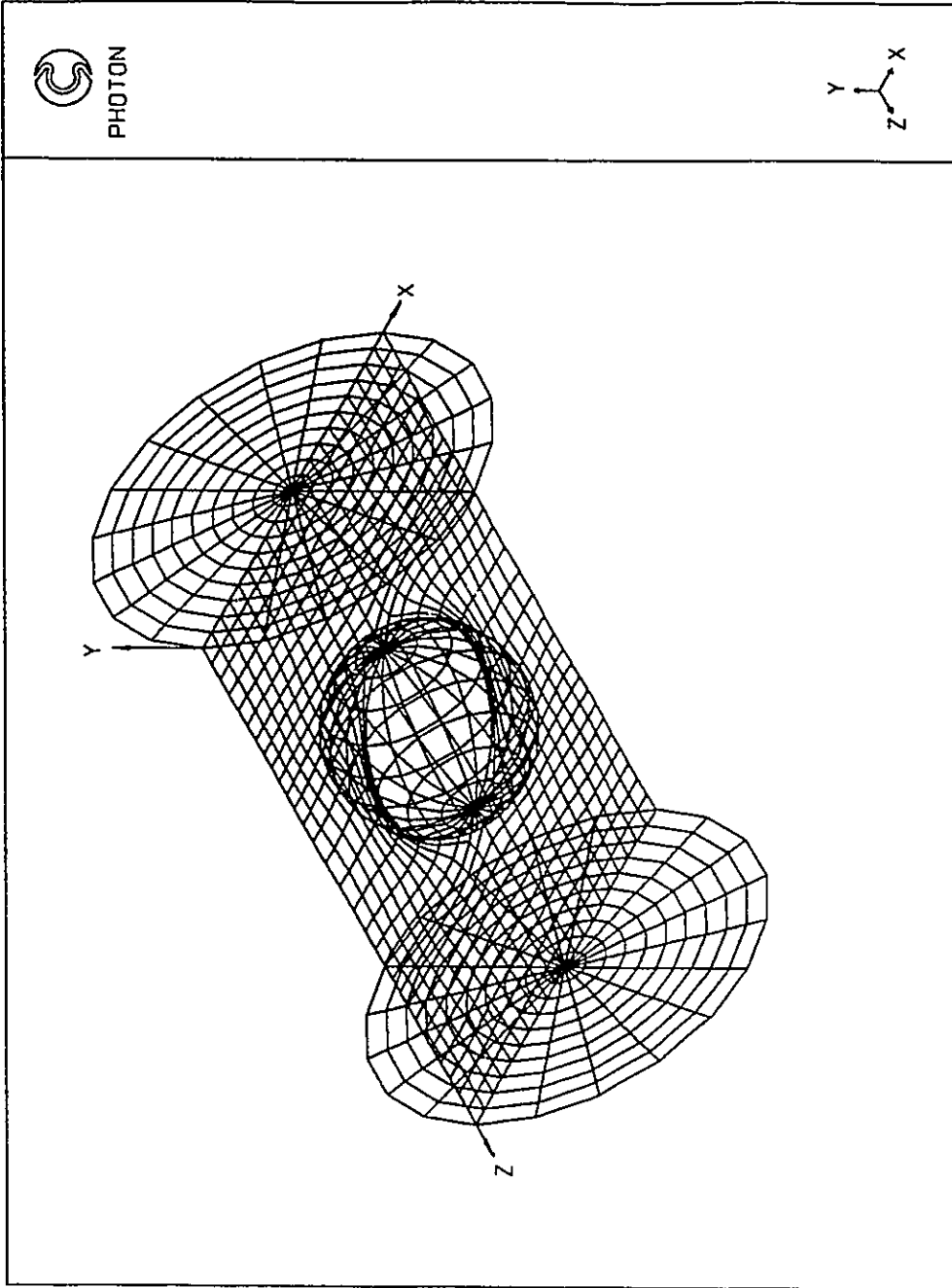
Figure 5.1   Sketch of cylindrical grids

PHOTON
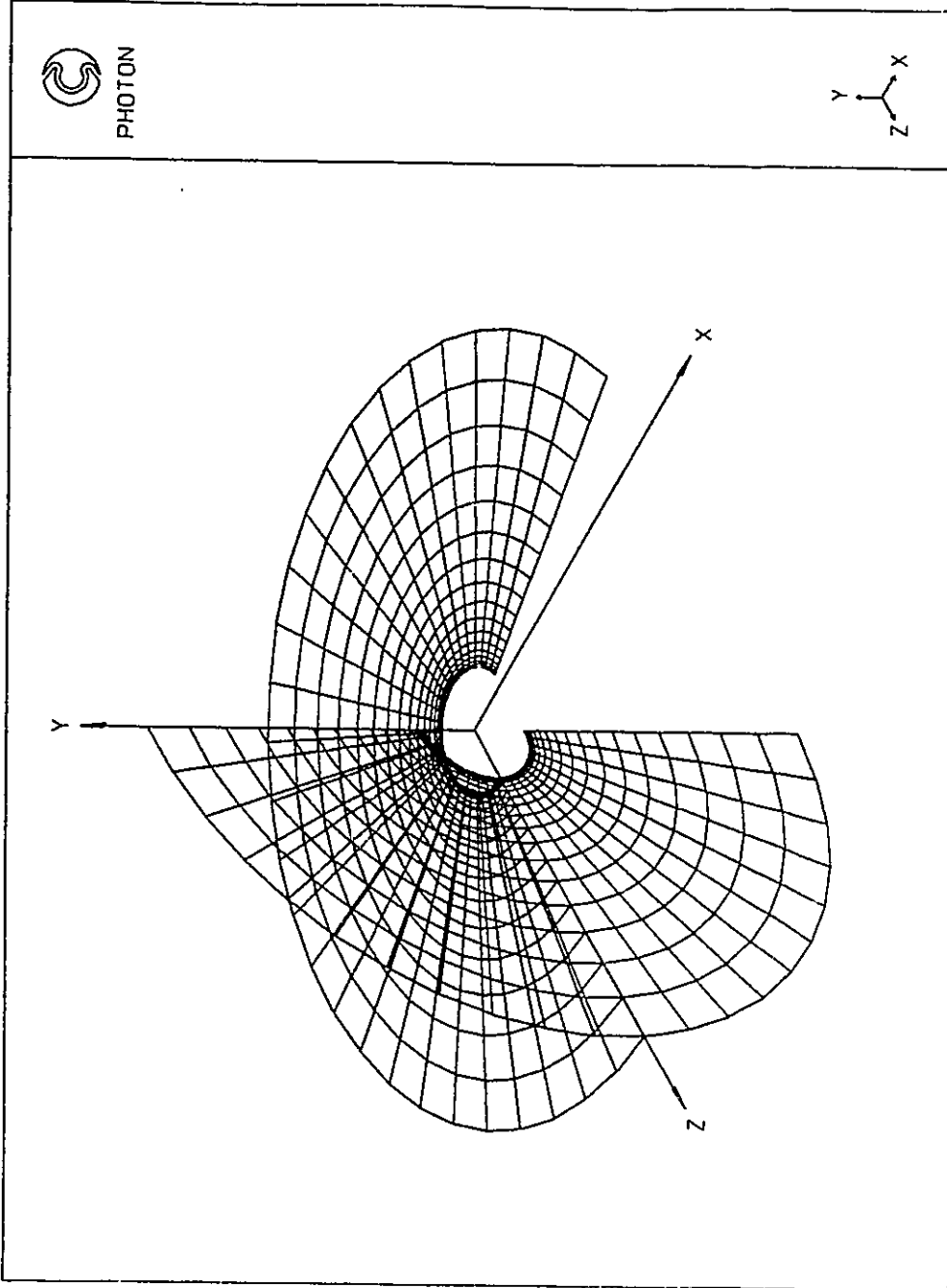
Figure 5.2   Sketch of spherical grids
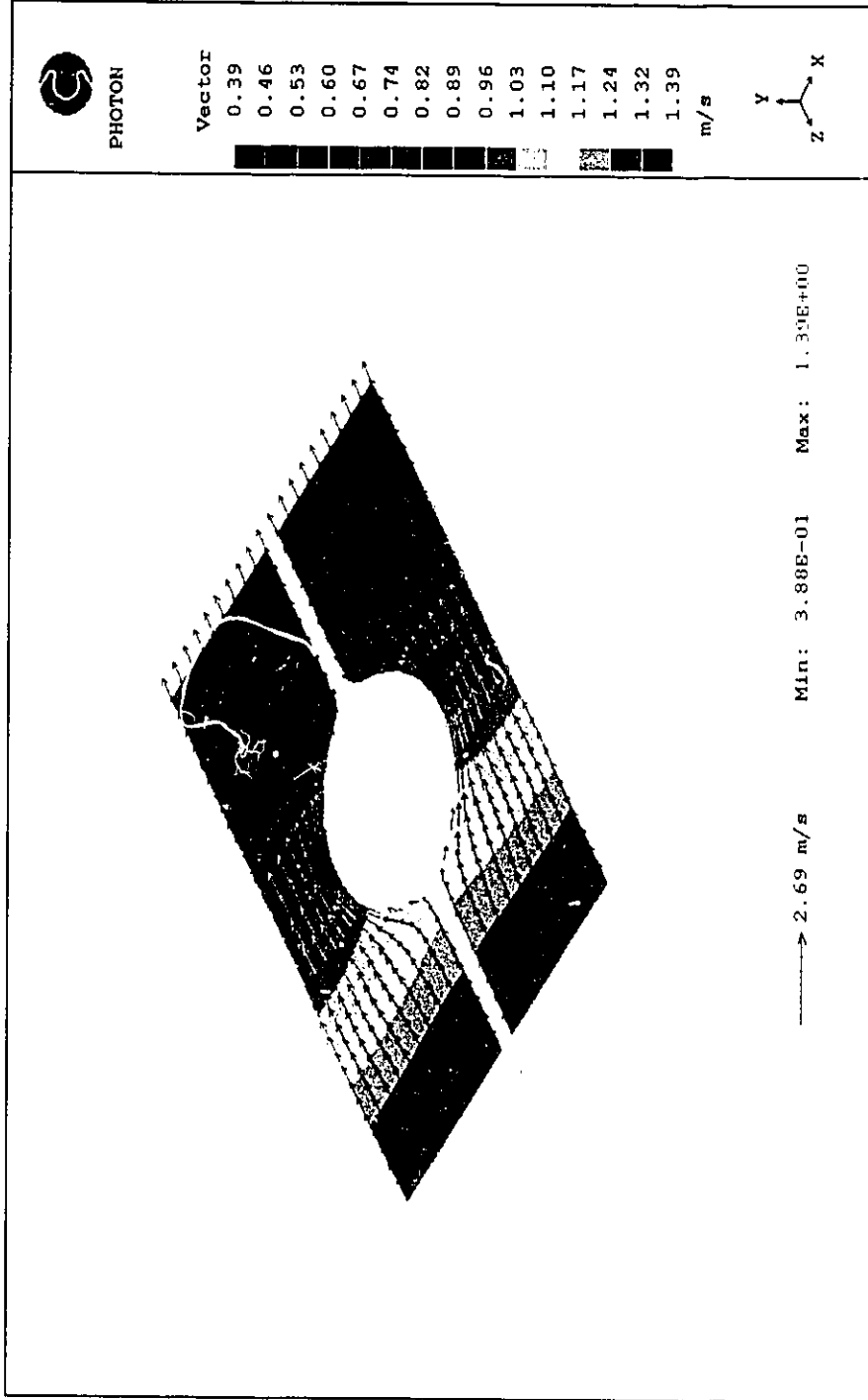
Figure 5.3 Velocity distributions on symmetrical planes for potential flow

51

Figure 5.4   Pressure distributions on symmetrical planes for potential flow
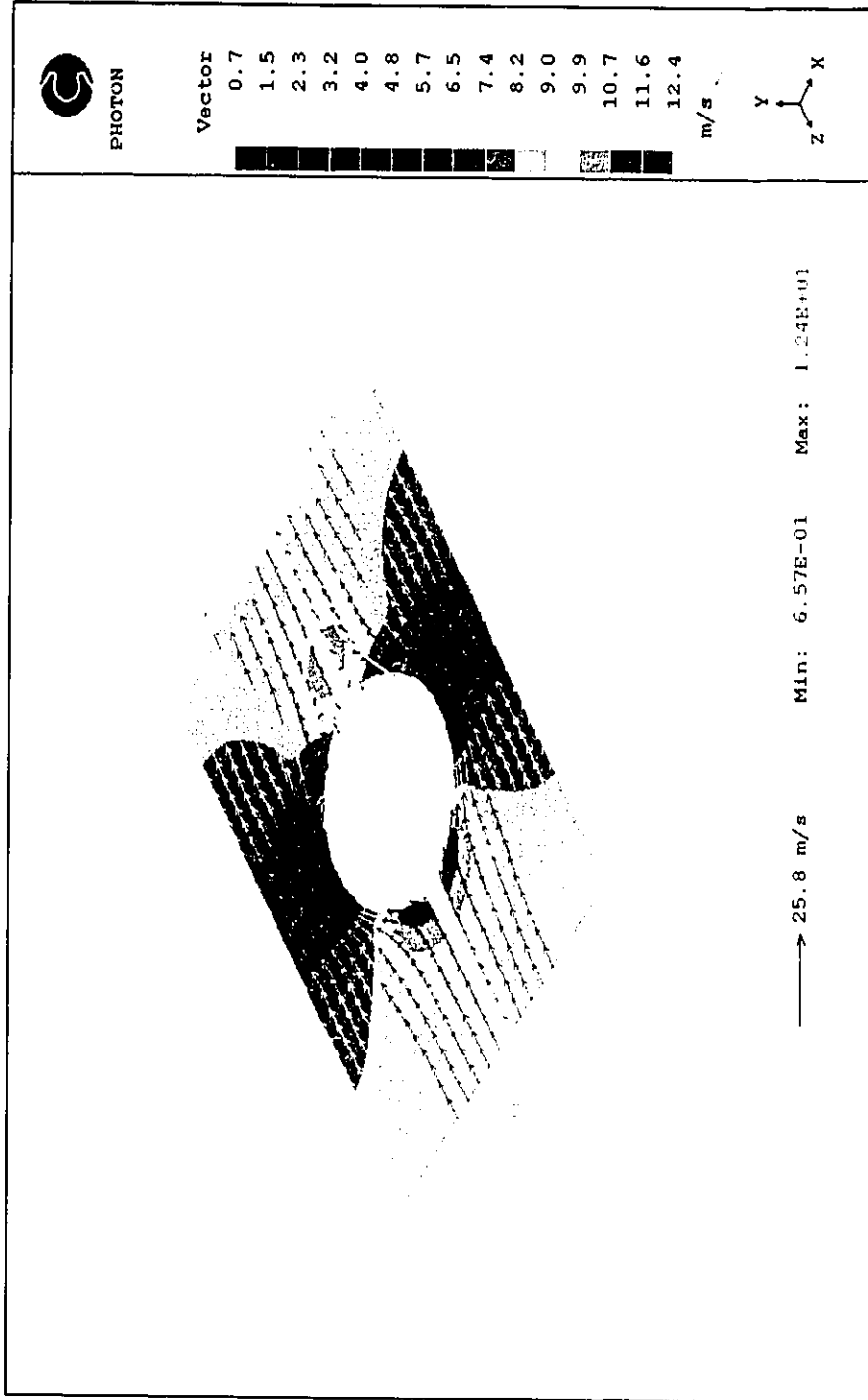
Figure 5.5 Velocity distributions on symmetrical planes for vortex flow
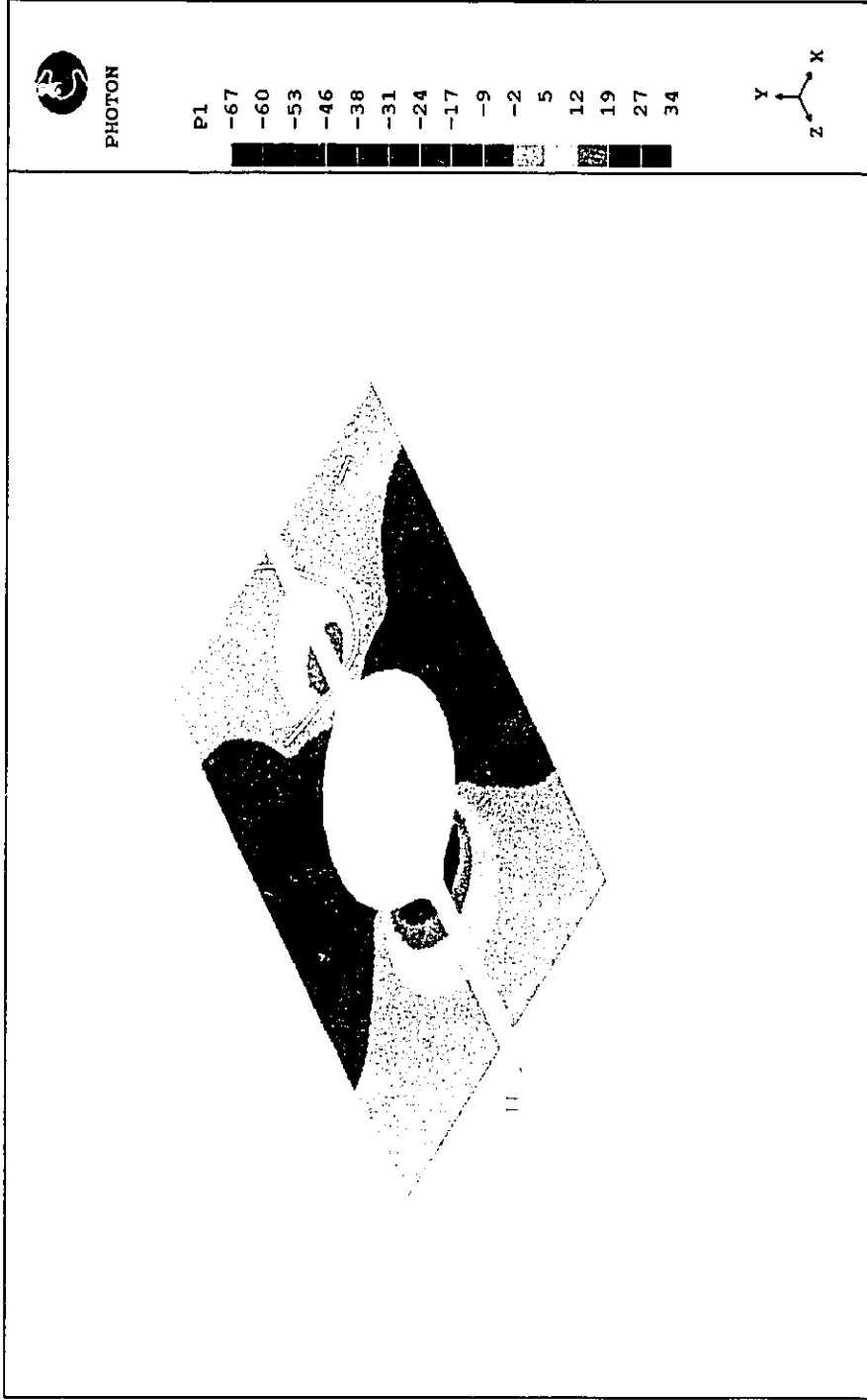
Figure 5.6   Pressure distributions on symmetrical planes for vortex flow
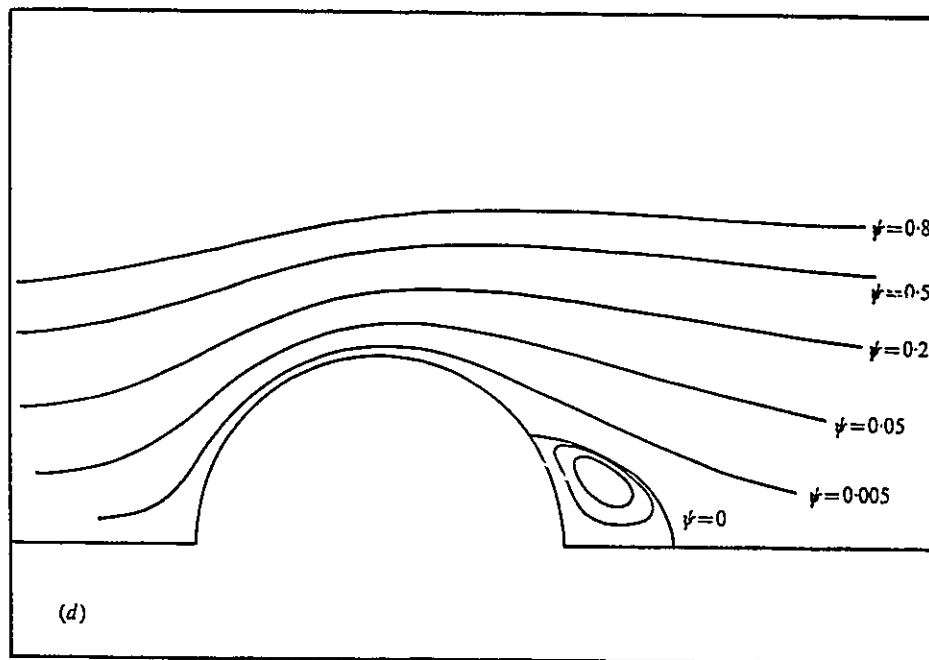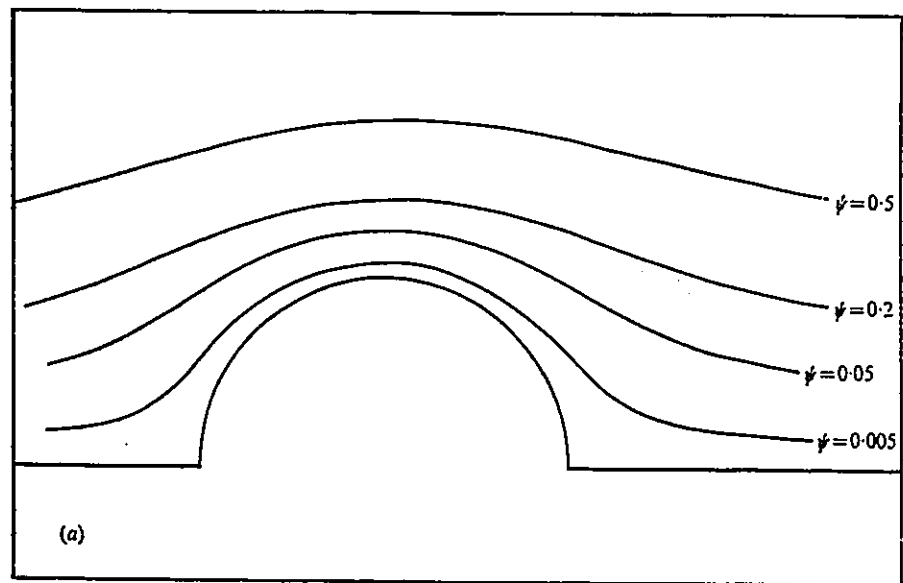
Figure 5.7   Dennis' stream lines, *Re = 1, 40*
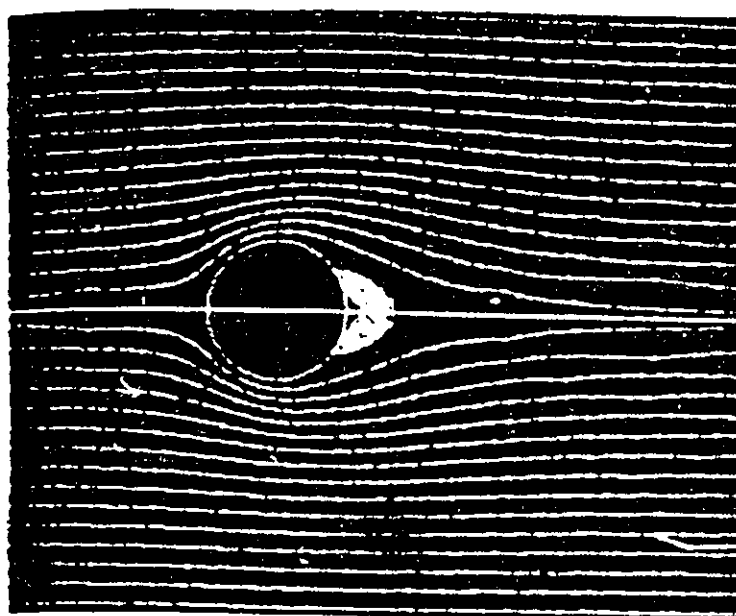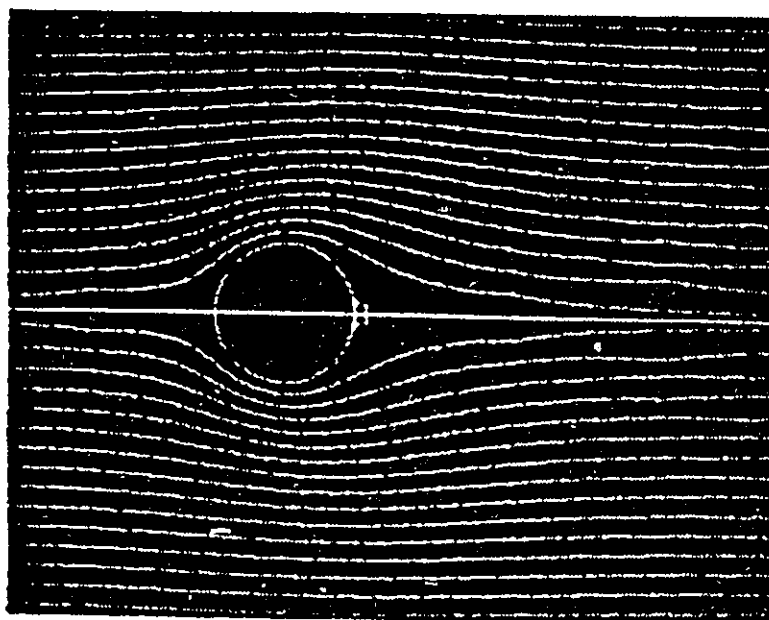
Figure 5.8   Rimon's stream lines, *Re = 1, 40*
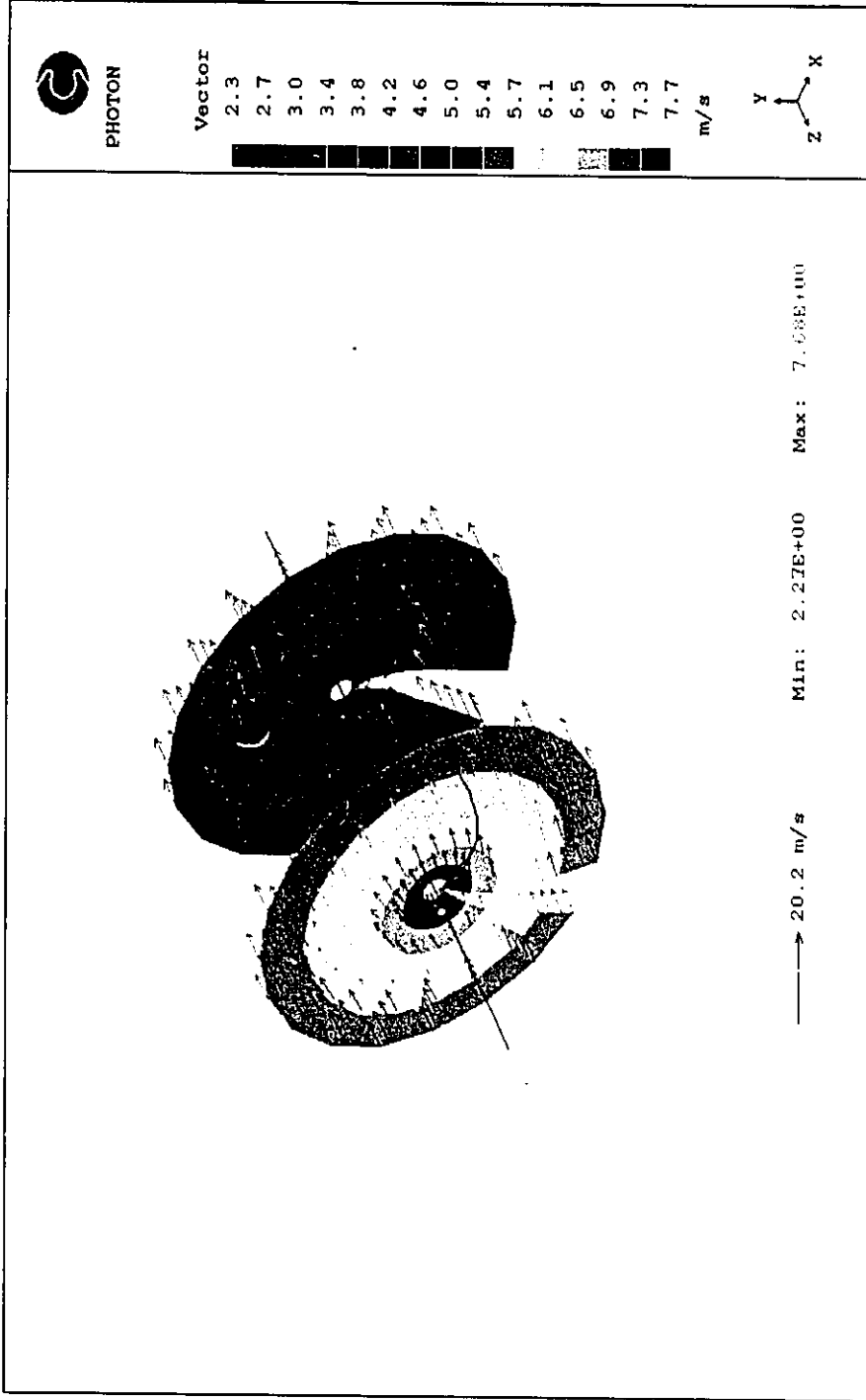
Figure 5.9 Velocity distributions on cross sections for parallel rotating sphere
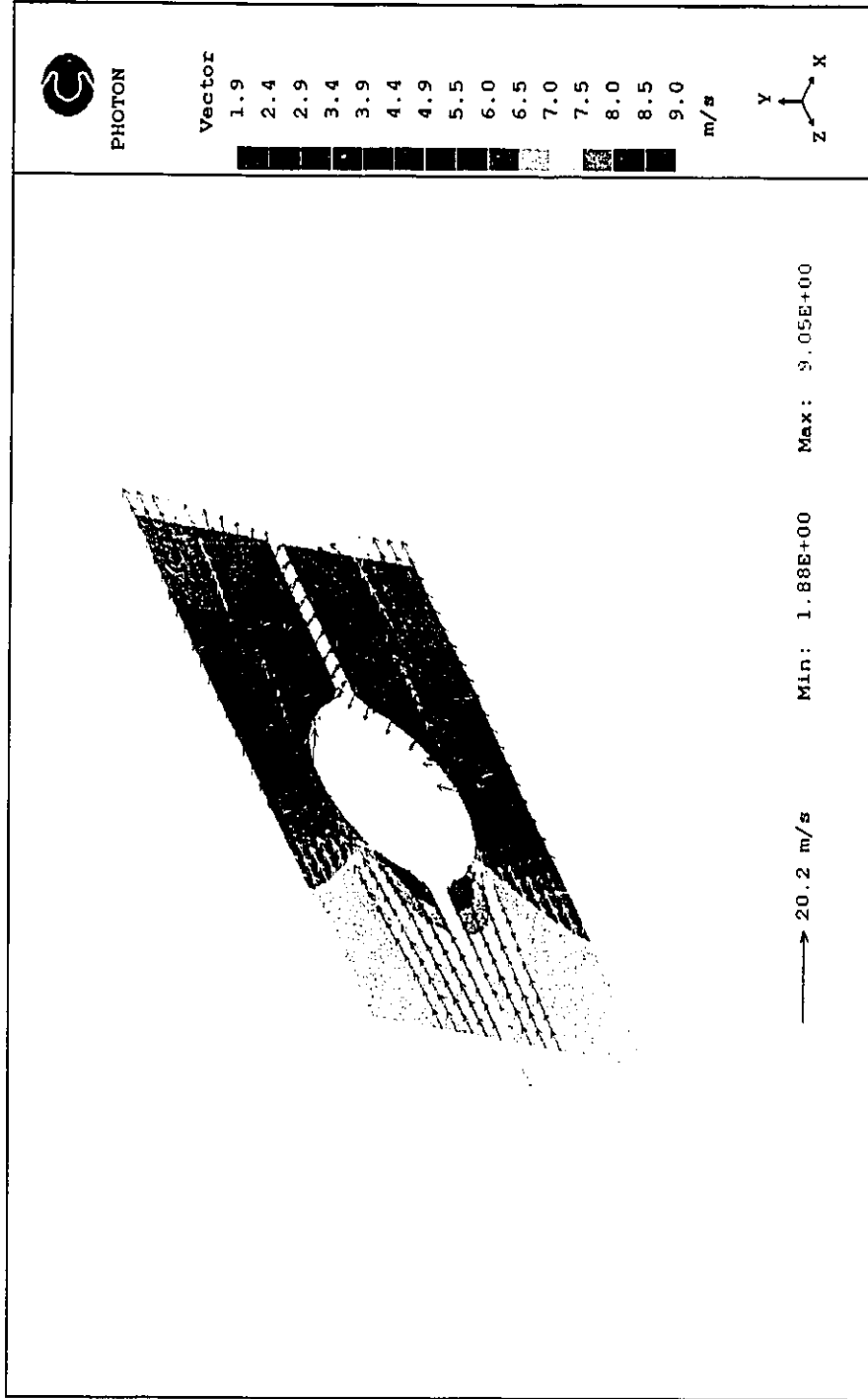
Figure 5.10 Velocity distributions on symmetrical planes for parallel rotating sphere
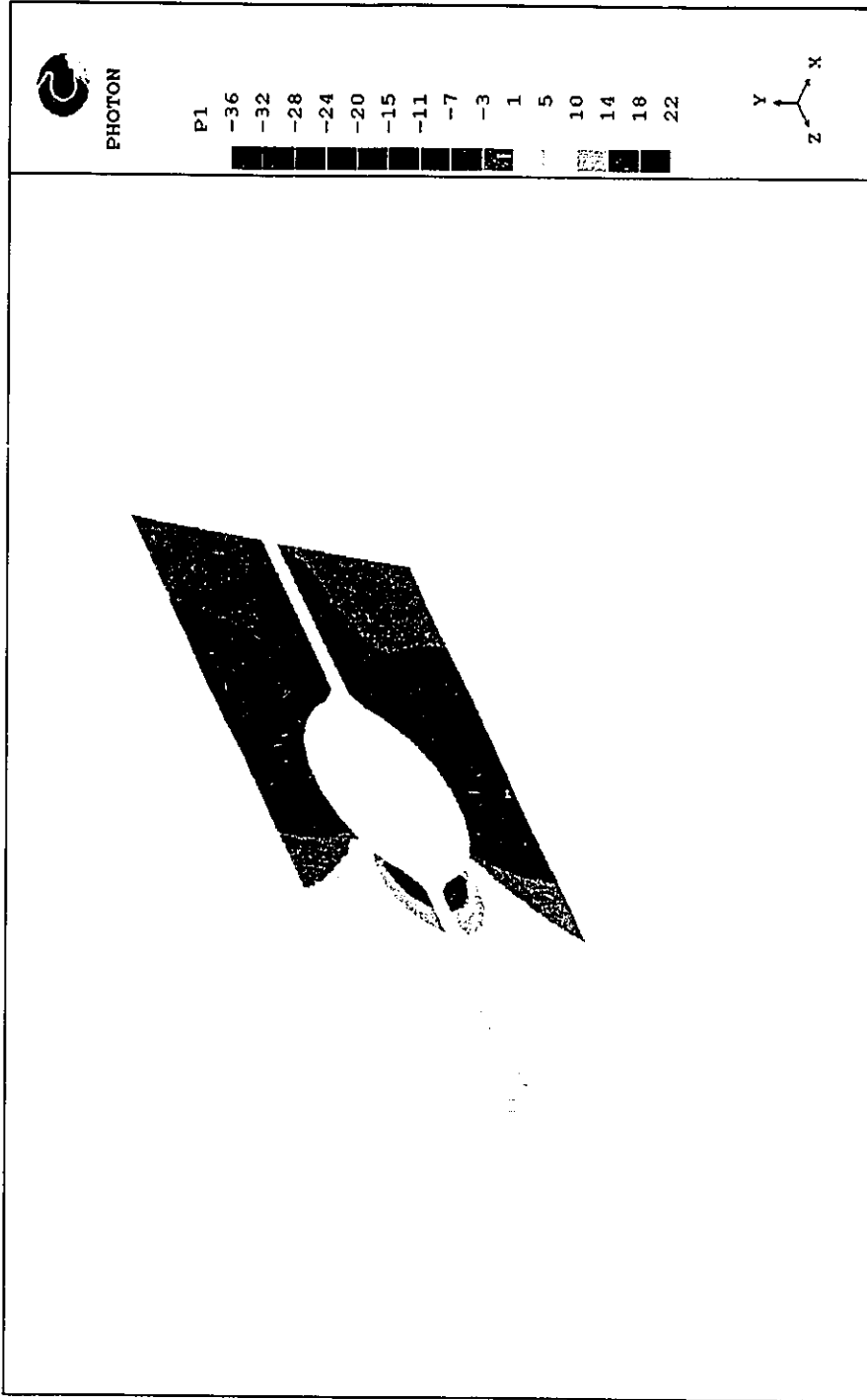
Figure 5.11 Pressure distributions on symmetrical planes for parallel rotating sphere
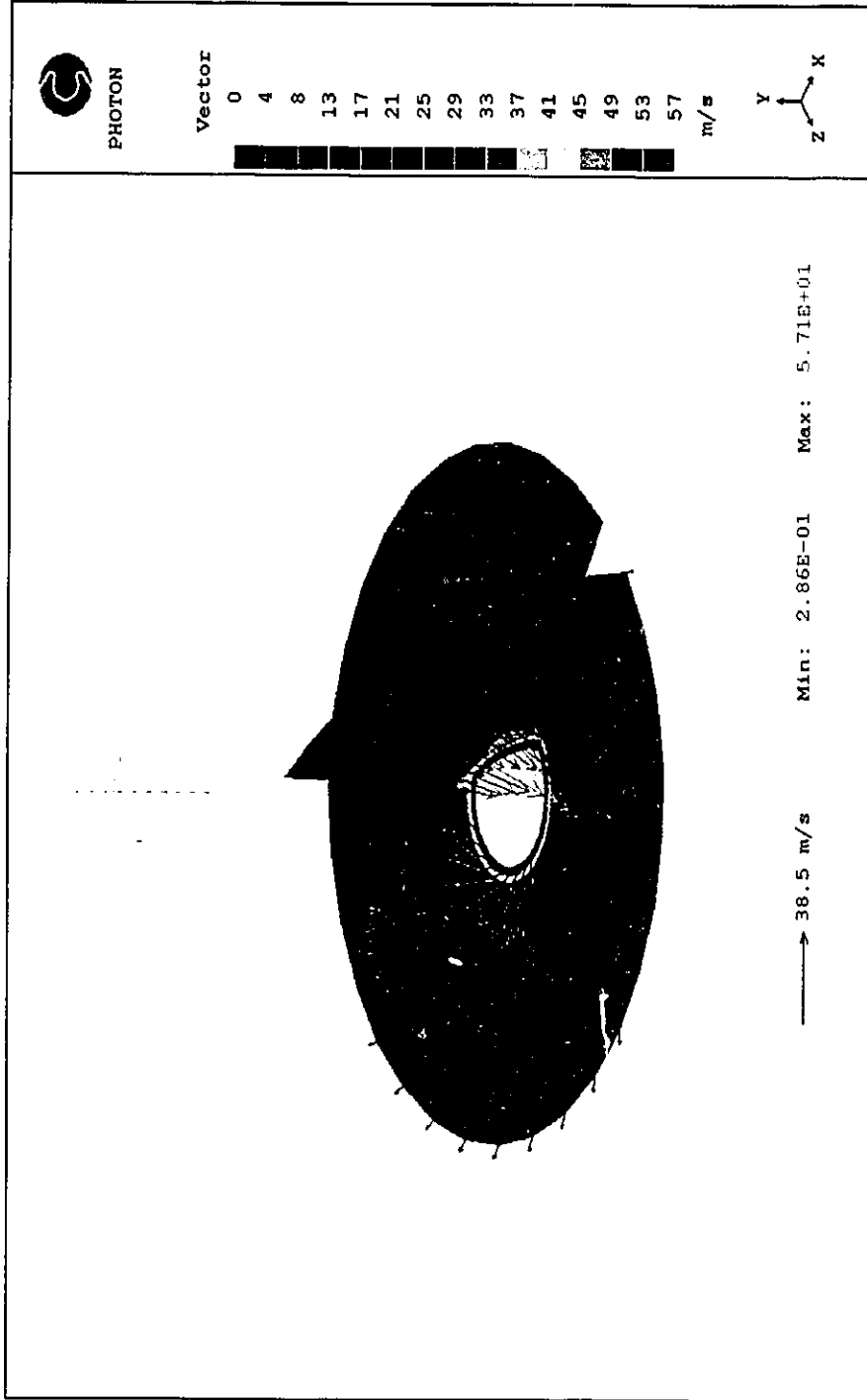
Figure 5.12 Velocity distributions on radial and equatorial planes for rotating sphere
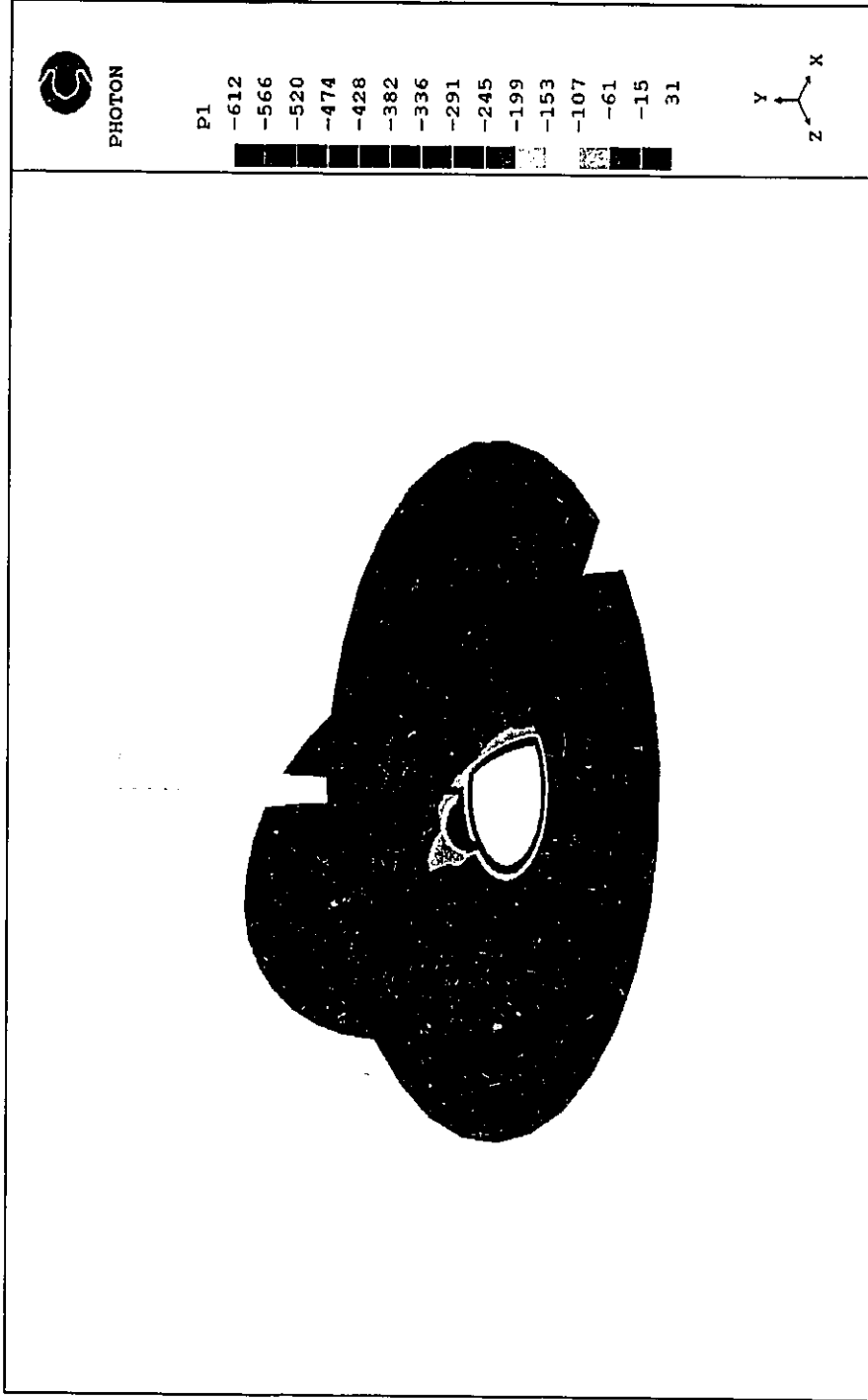
Figure 5.13 Pressure distributions on radial and equatorial planes for rotating sphere
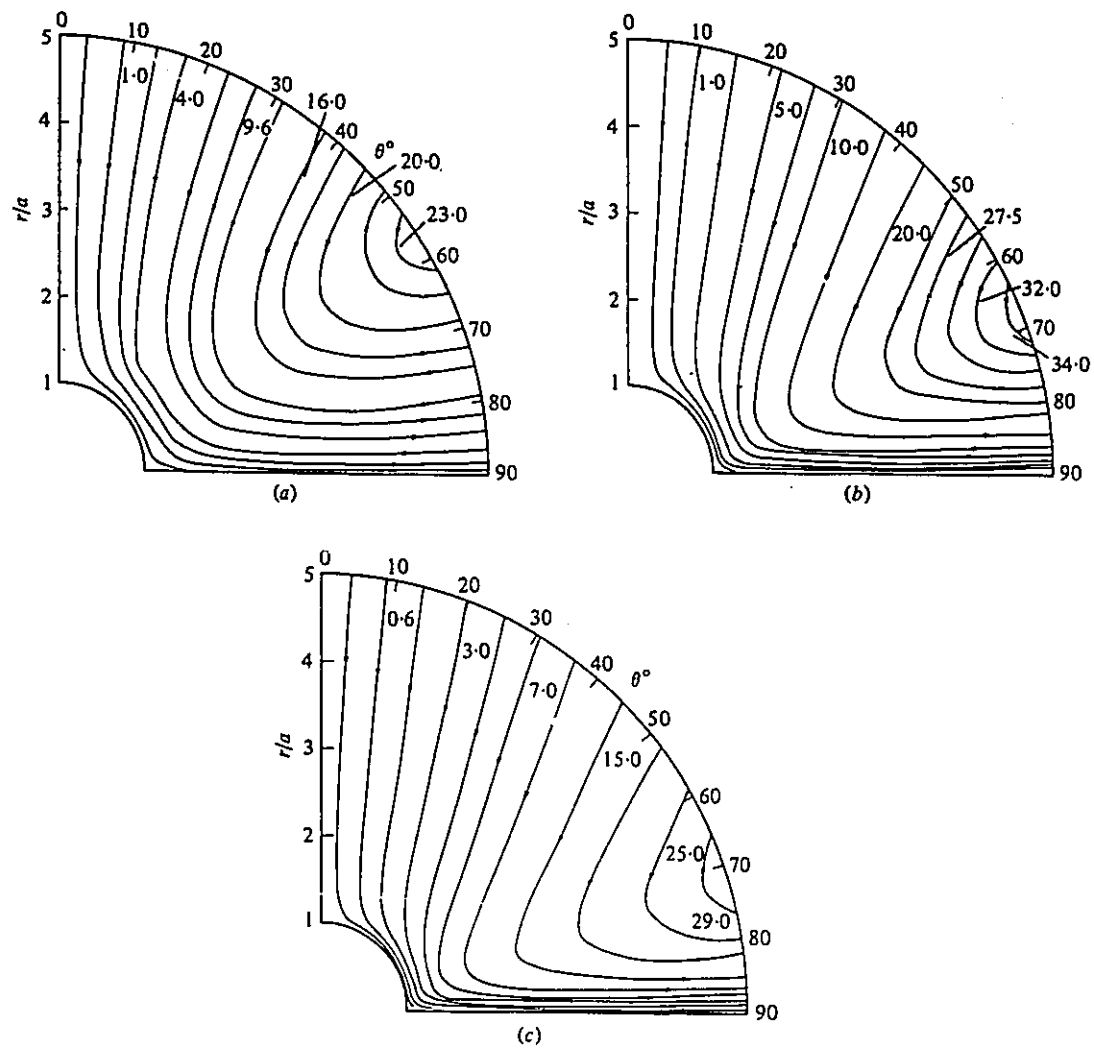
Figure 5.14   Dennis' stream lines
Re = 10, 50, 100

62

PHOTON

I=24

I=4

I=14

U
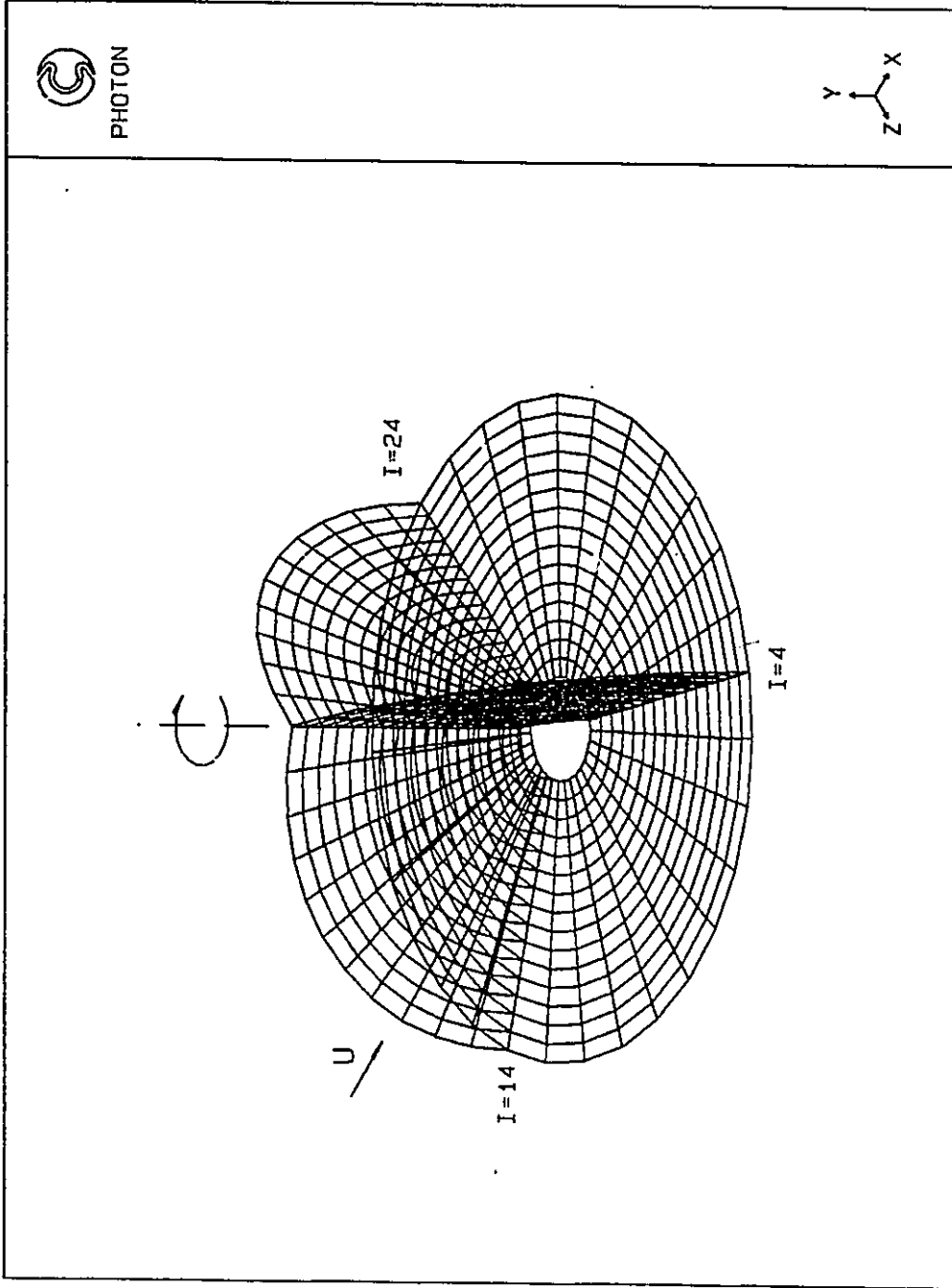
Figure 5.15   Positions for results
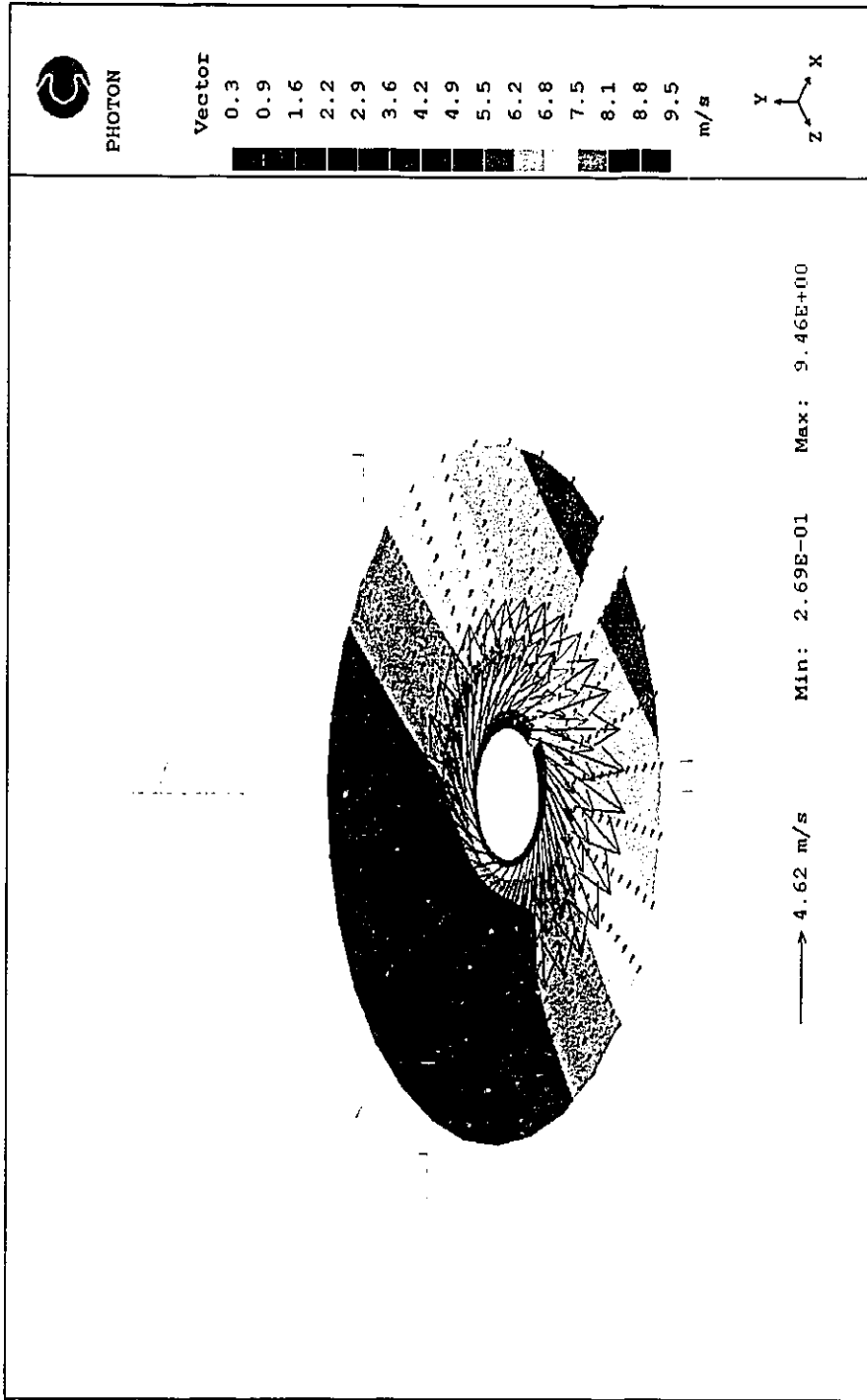
Figure 5.16 Velocity distribution on equatorial plane
$Re = 5 \times 10^4$, $U_\infty = 5.7 m/s$, $Ta/Re^2 = 2$
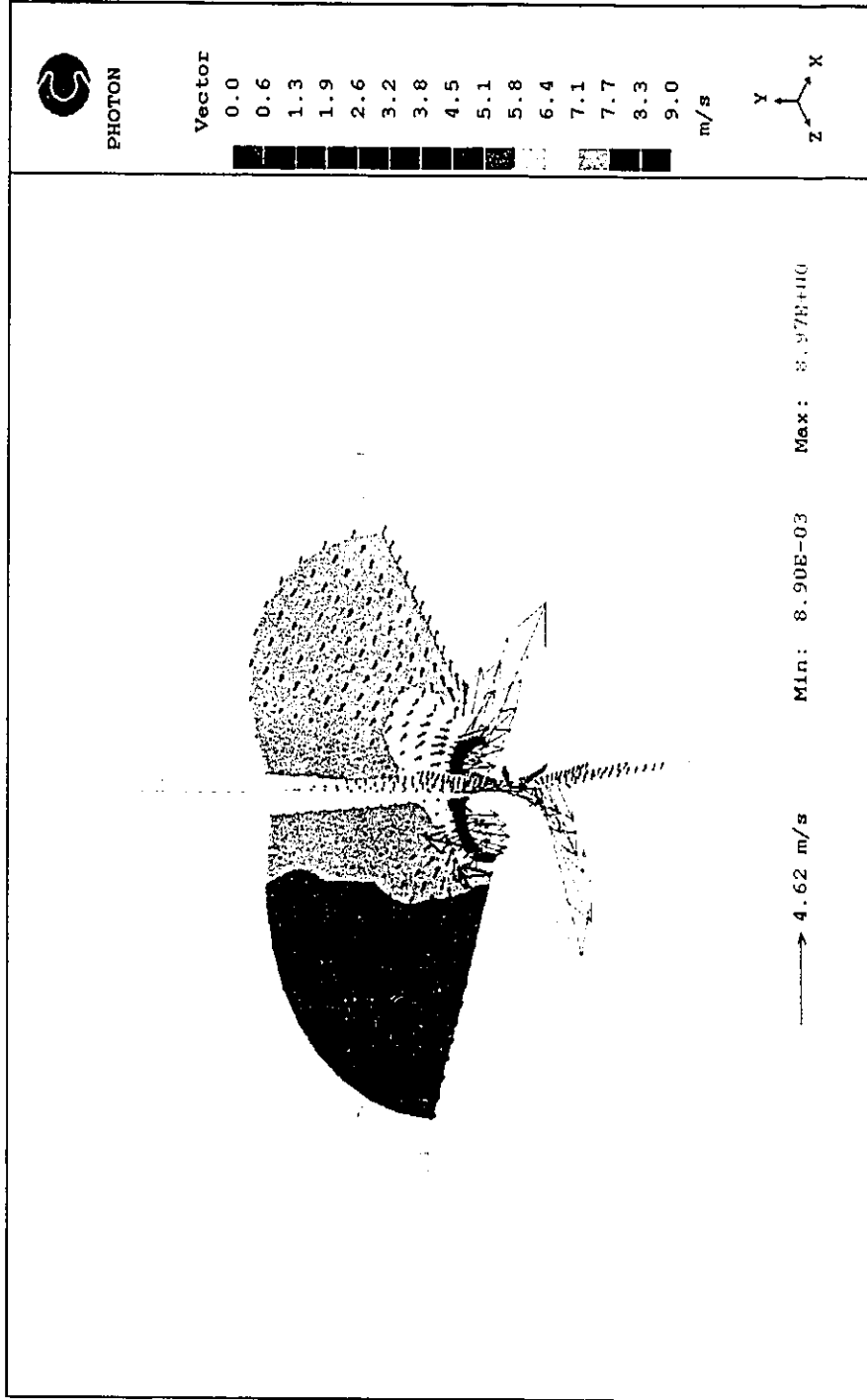
Figure 5.17 Velocity distributions on radial planes
$Re = 5 \times 10^4$, $U_\infty = 5.7 m/s$, $Ta/Re^2 = 2$
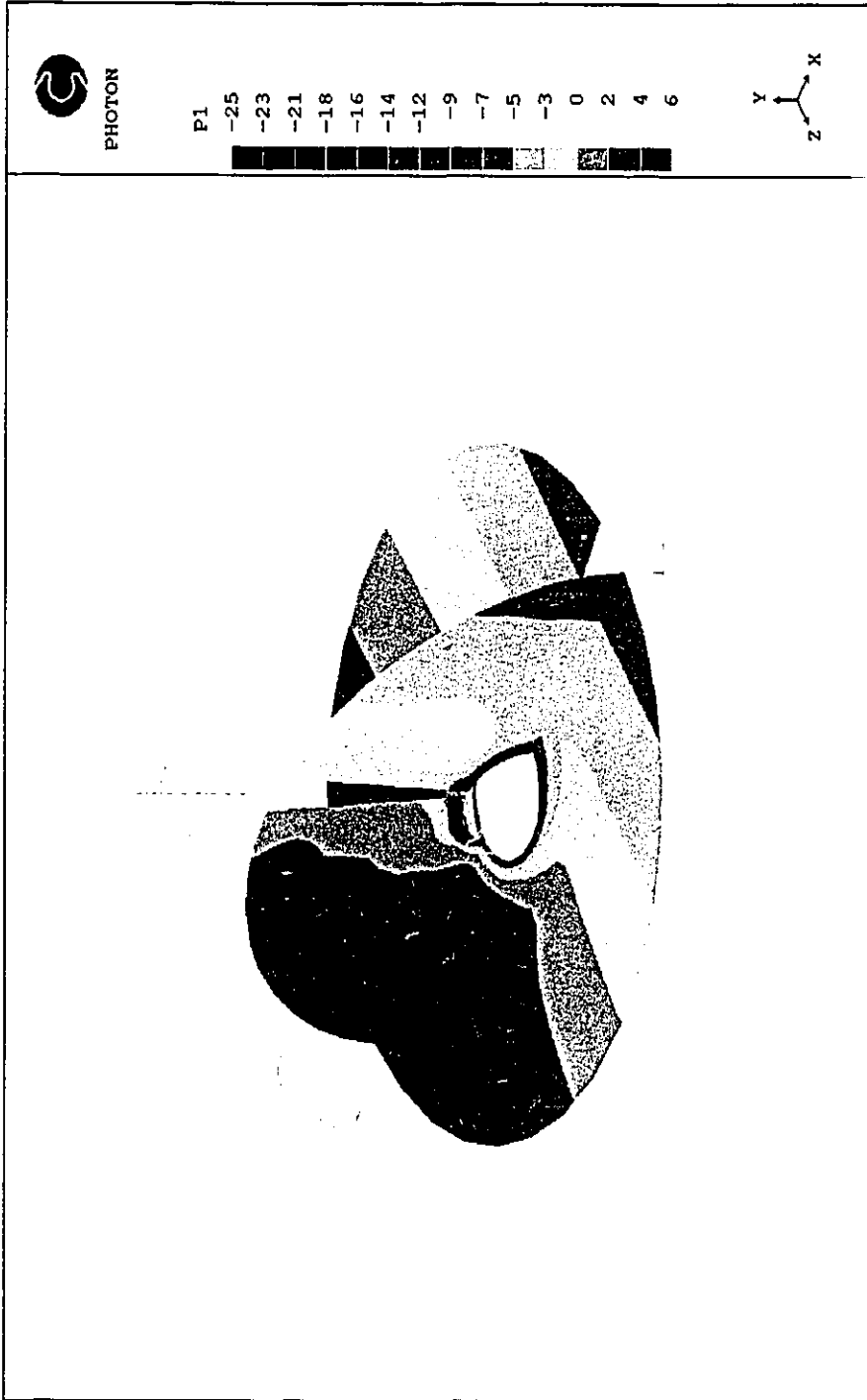
Figure 5.18 Pressure distributions on equatorial and radial planes
$Re = 5 \times 10^4$, $U_\infty = 5.7 m/s$, $Ta/Re^2 = 2$
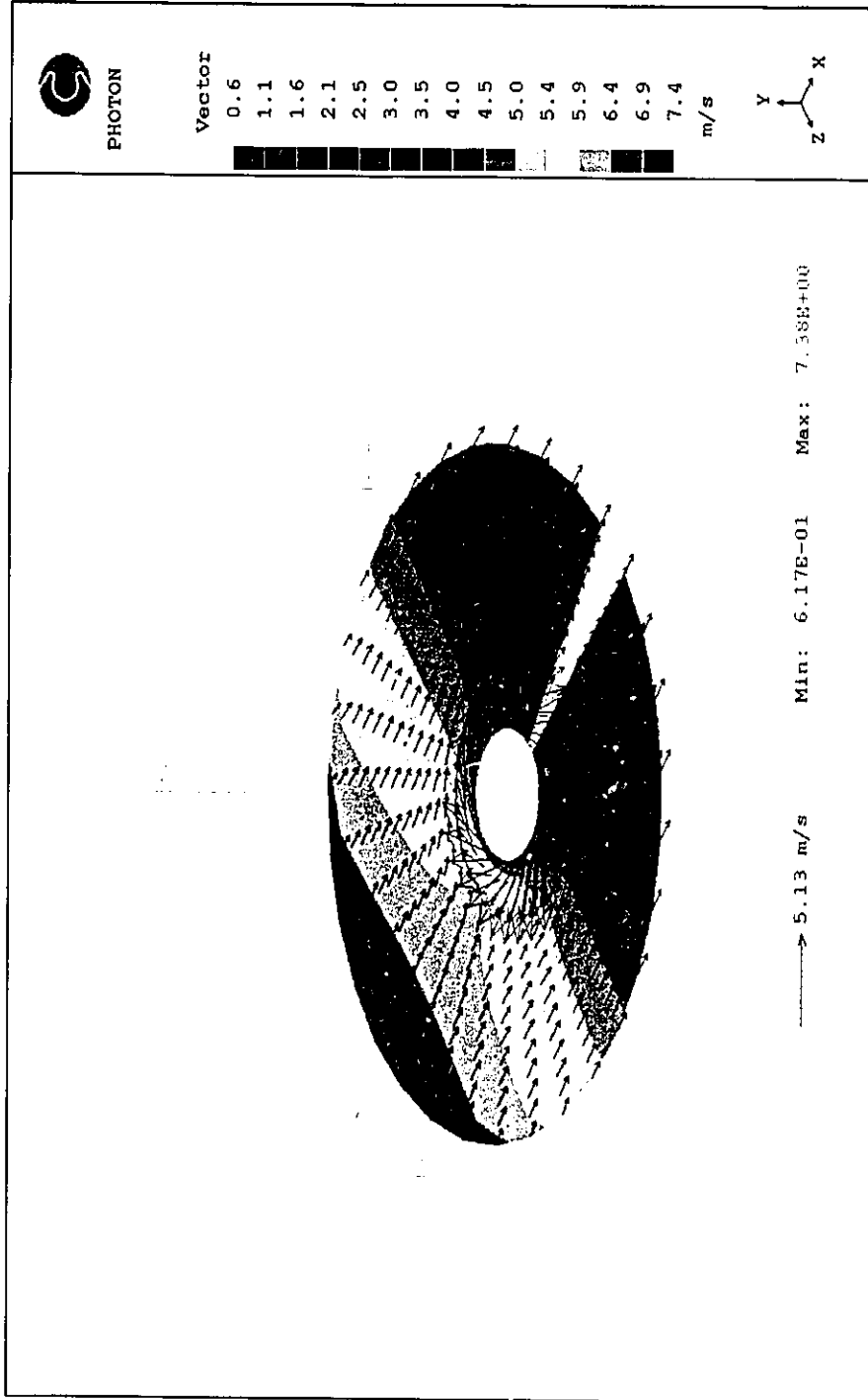
Figure 5.19 Velocity distribution on equatorial plane
$Re = 1 \times 10^5$, $U_\infty = 11.4m/s$, $Ta/Re^2 < 1$
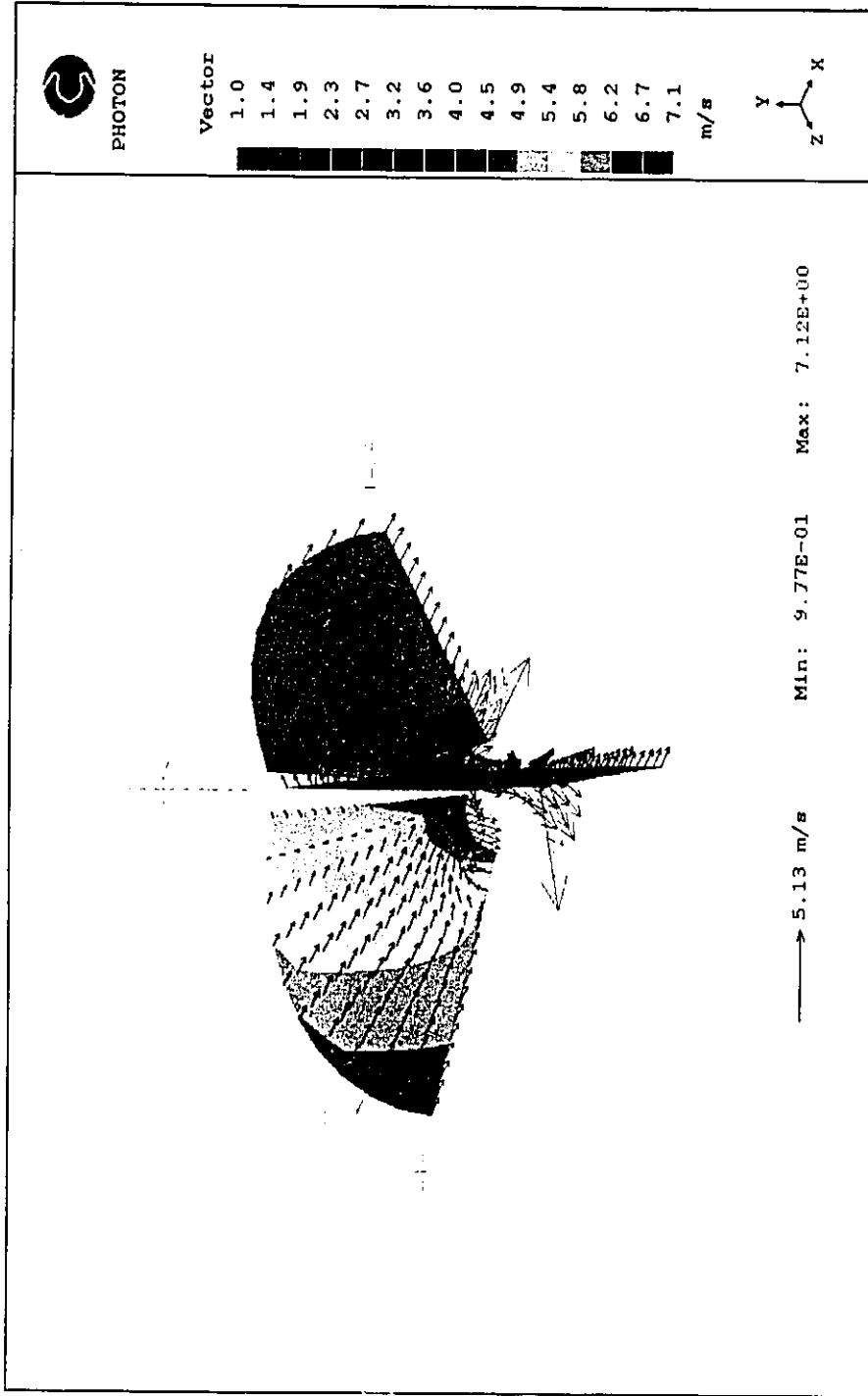
Figure 5.20   Velocity distributions on radial planes
$Re = 1 \times 10^5$, $U_\infty = 11.4m/s$, $Ta/Re^2 < 1$

Figure 5.21 Pressure distributions on equatorial and radial planes
$Re = 1 \times 10^5$, $U_\infty = 11.4 m/s$, $Ta/Re^2 < 1$
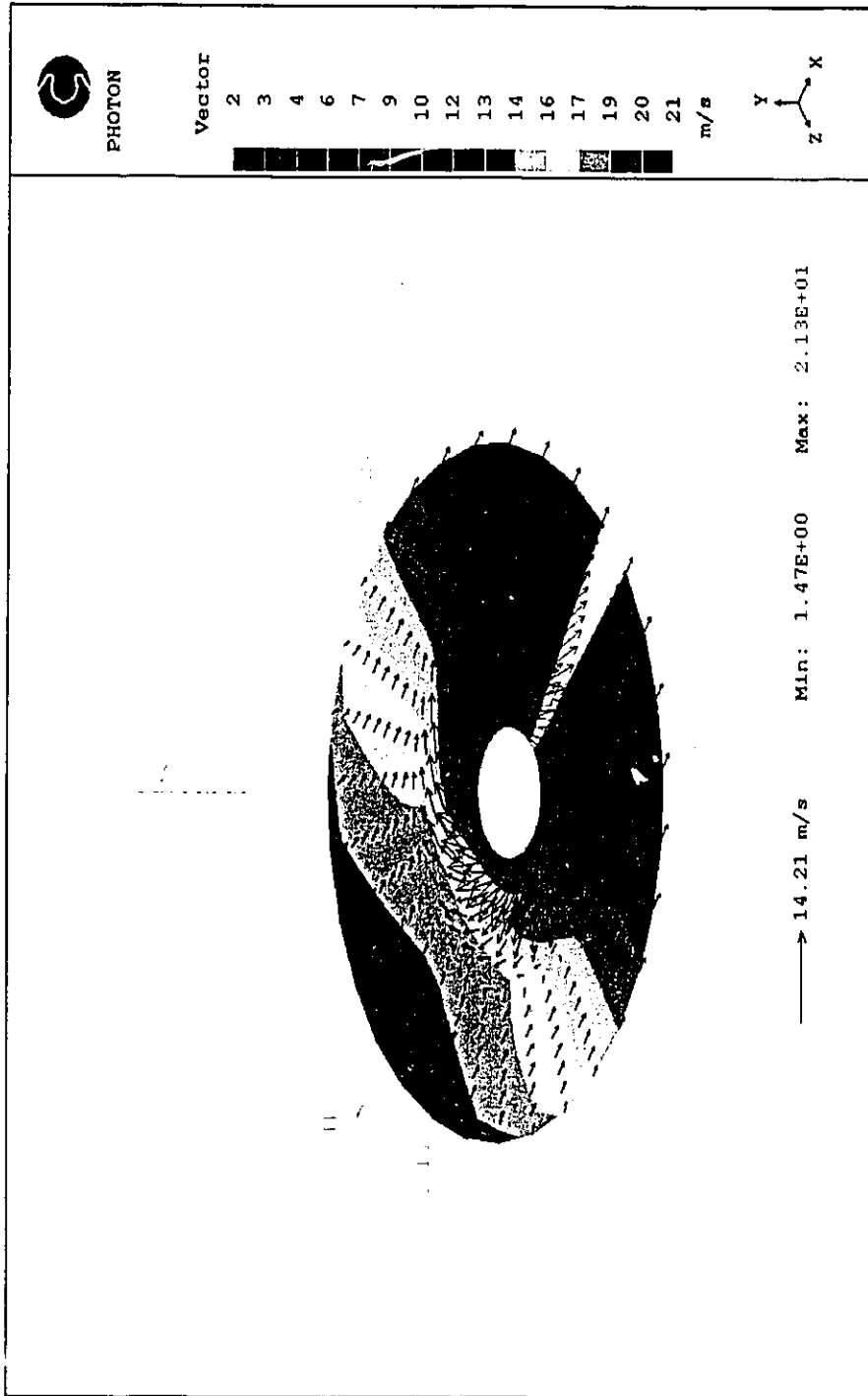
Figure 5.22 Velocity distribution on equatorial plane
$Re = 2 \times 10^5$, $U_\infty = 23m/s$, $Ta/Re^2 < 1$
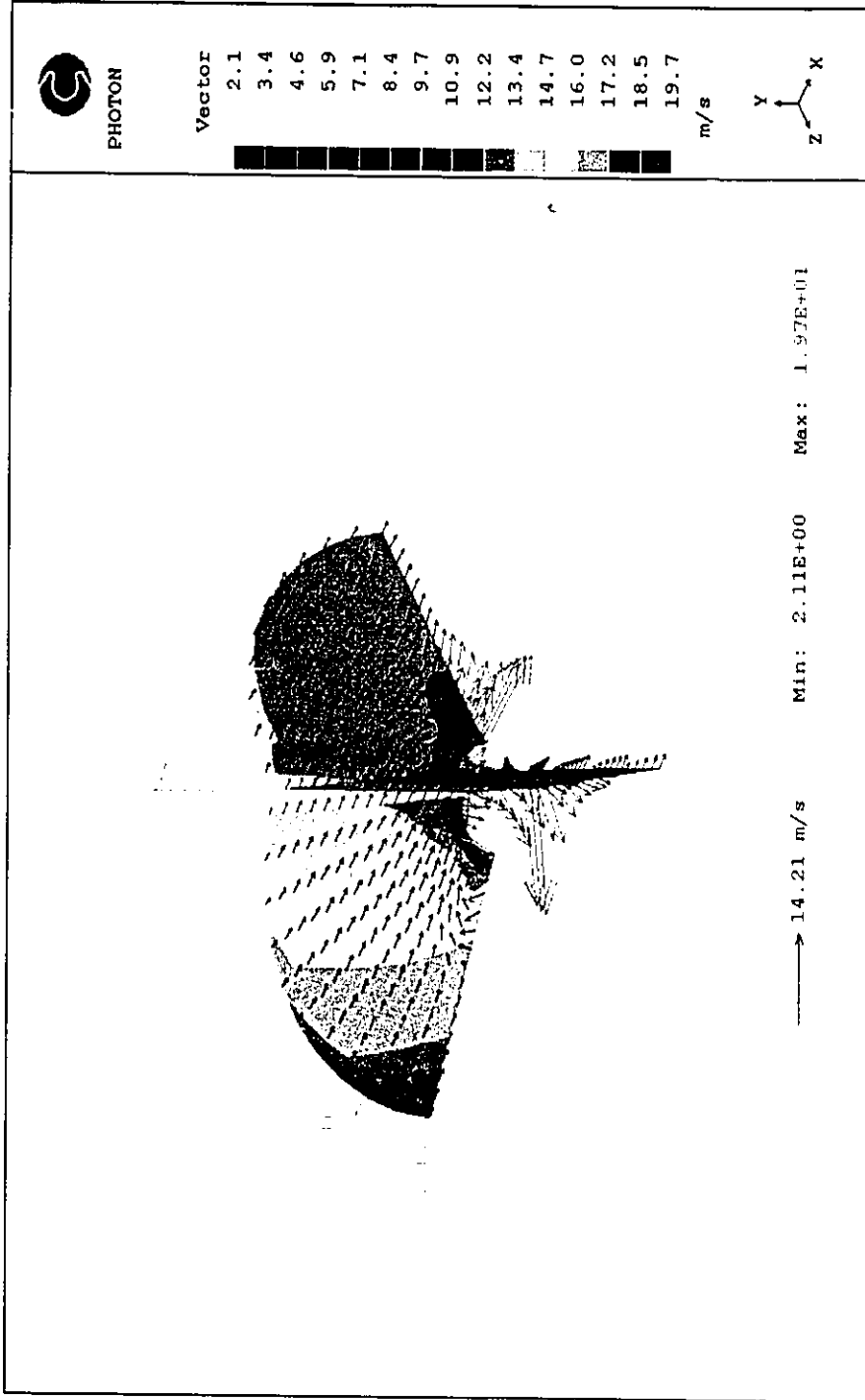
Figure 5.23 Velocity distributions on radial planes
$Re = 2 \times 10^5$, $U_\infty = 23m/s$, $Ta/Re^2 < 1$
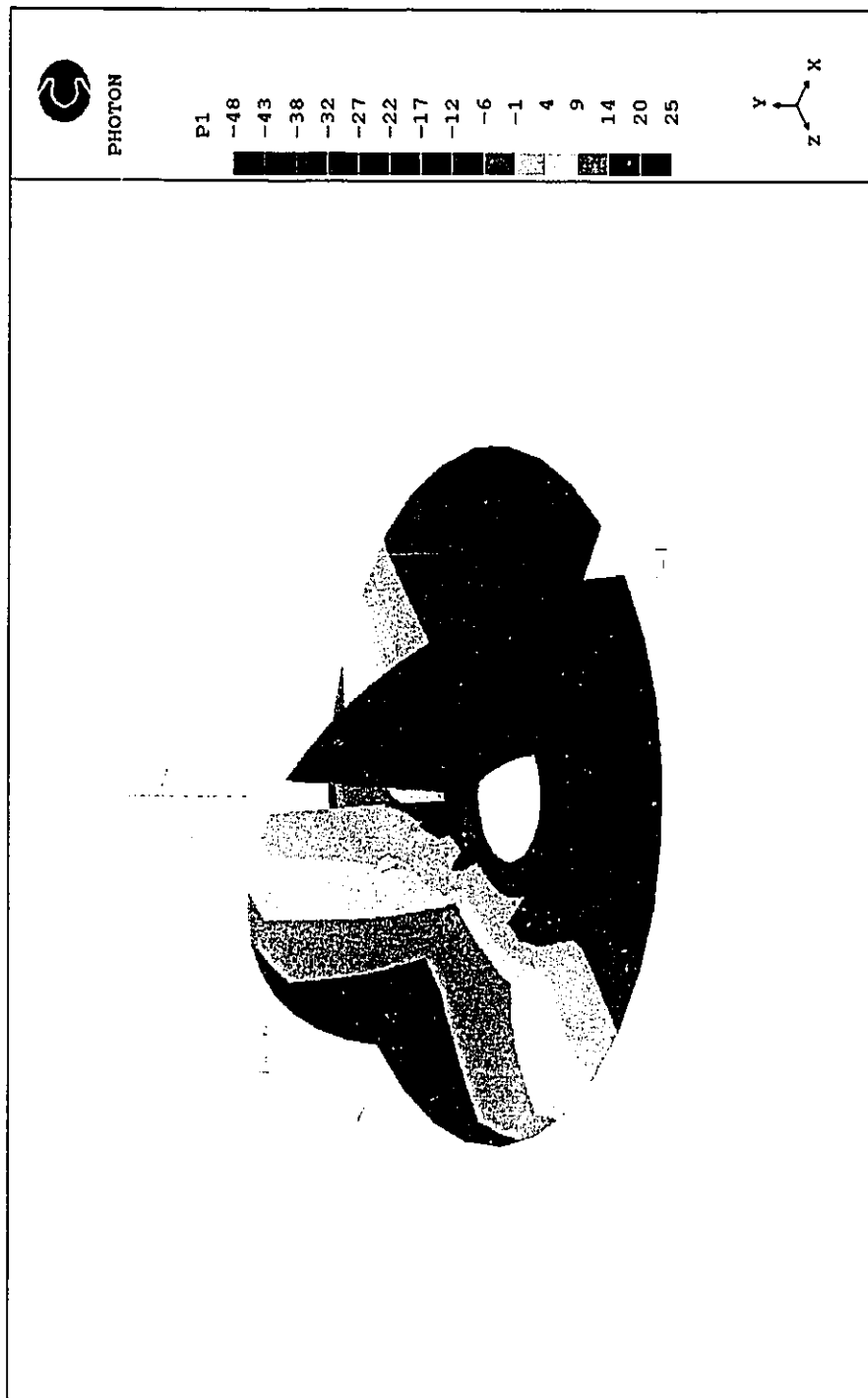
Figure 5.24 Pressure distributions on equatorial and radial planes
$Re = 2 \times 10^5$, $U_\infty = 23 m/s$, $Ta/Re^2 < 1$
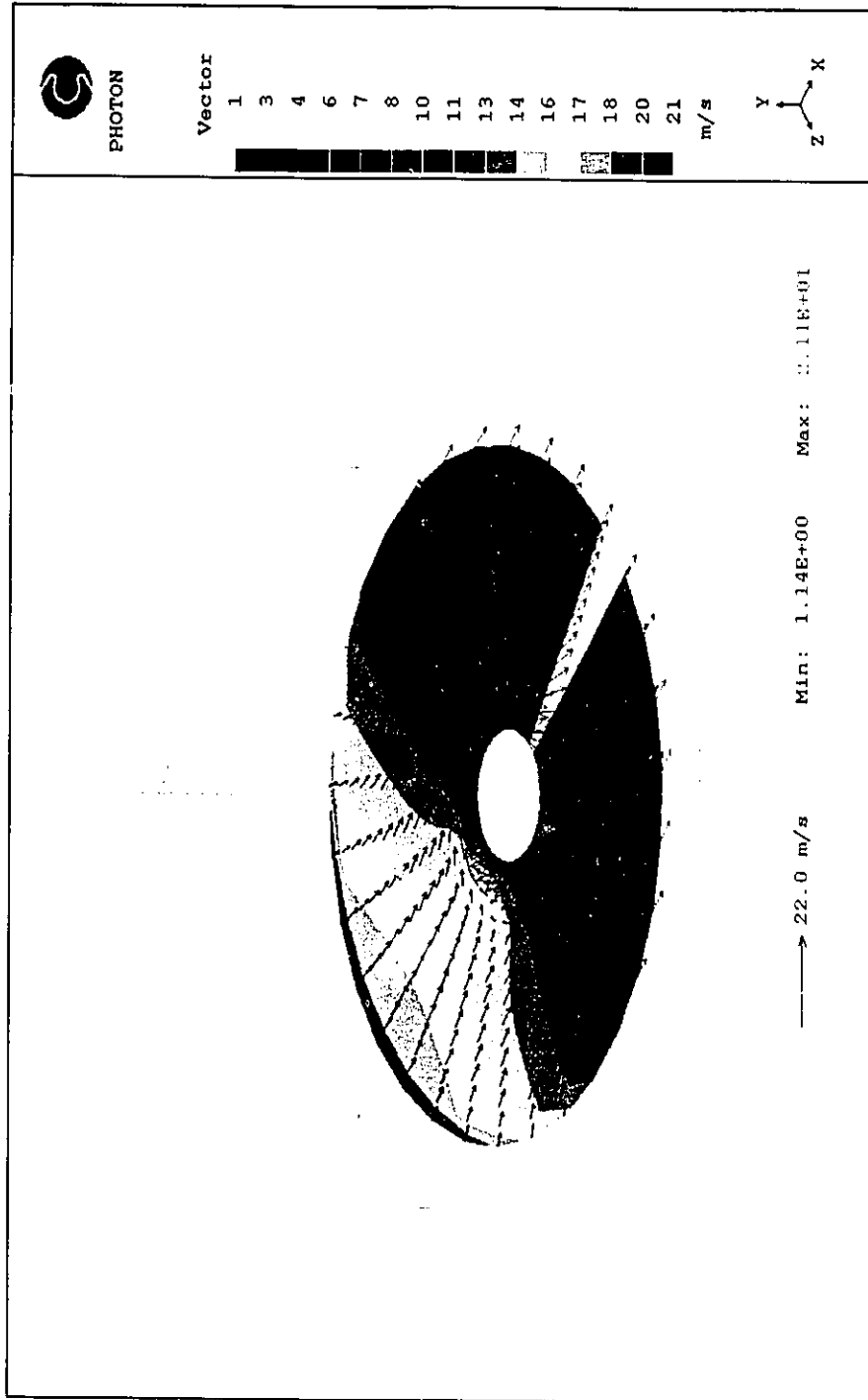
Figure 5.25 Velocity distribution on equatorial plane
$Re = 5 \times 10^5$, $U_\infty = 60m/s$, $Ta/Re^2 < 1$
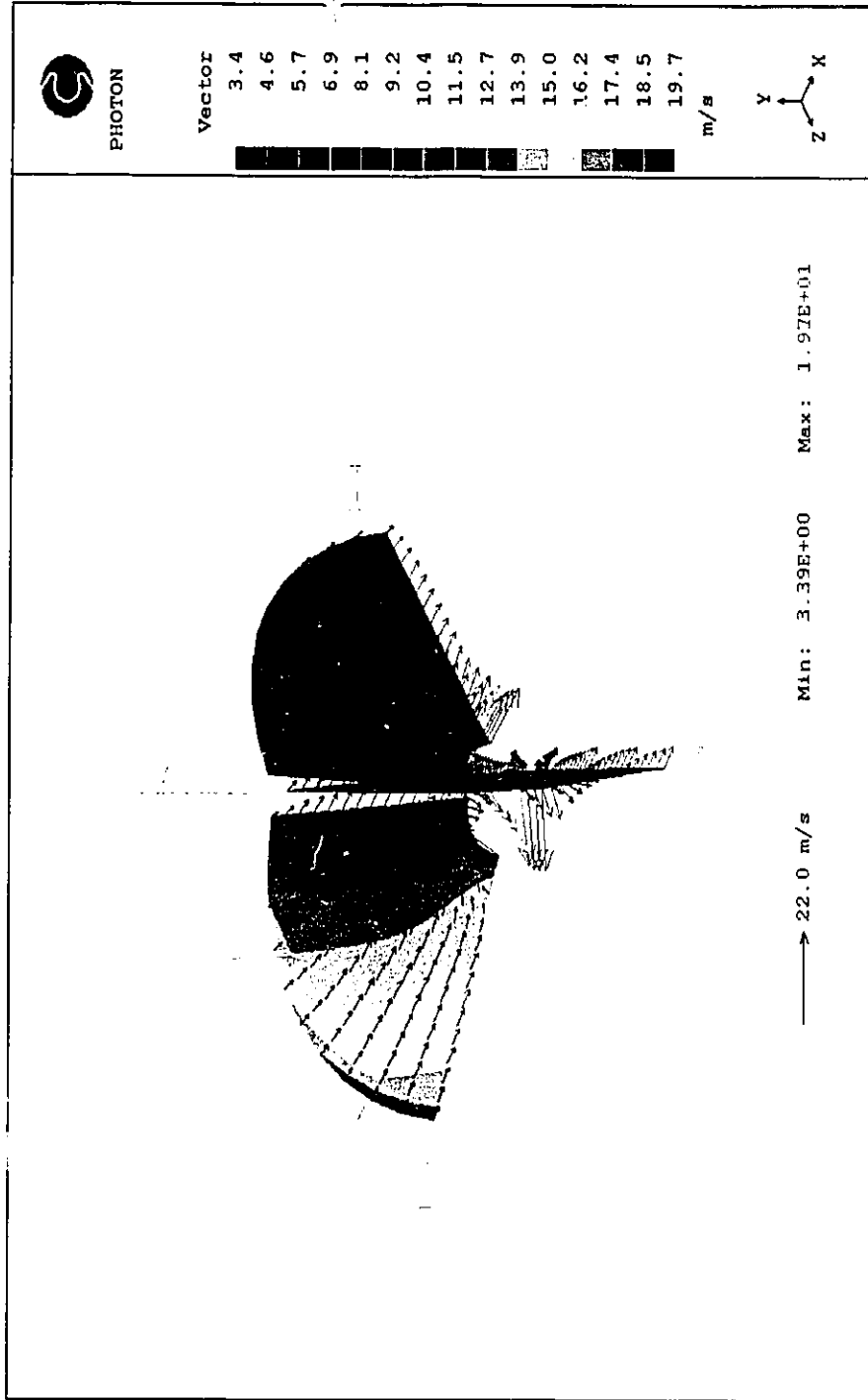
Figure 5.26 Velocity distributions on radial planes
$Re = 5 \times 10^5$, $U_\infty = 60m/s$, $Ta/Re^2 < 1$
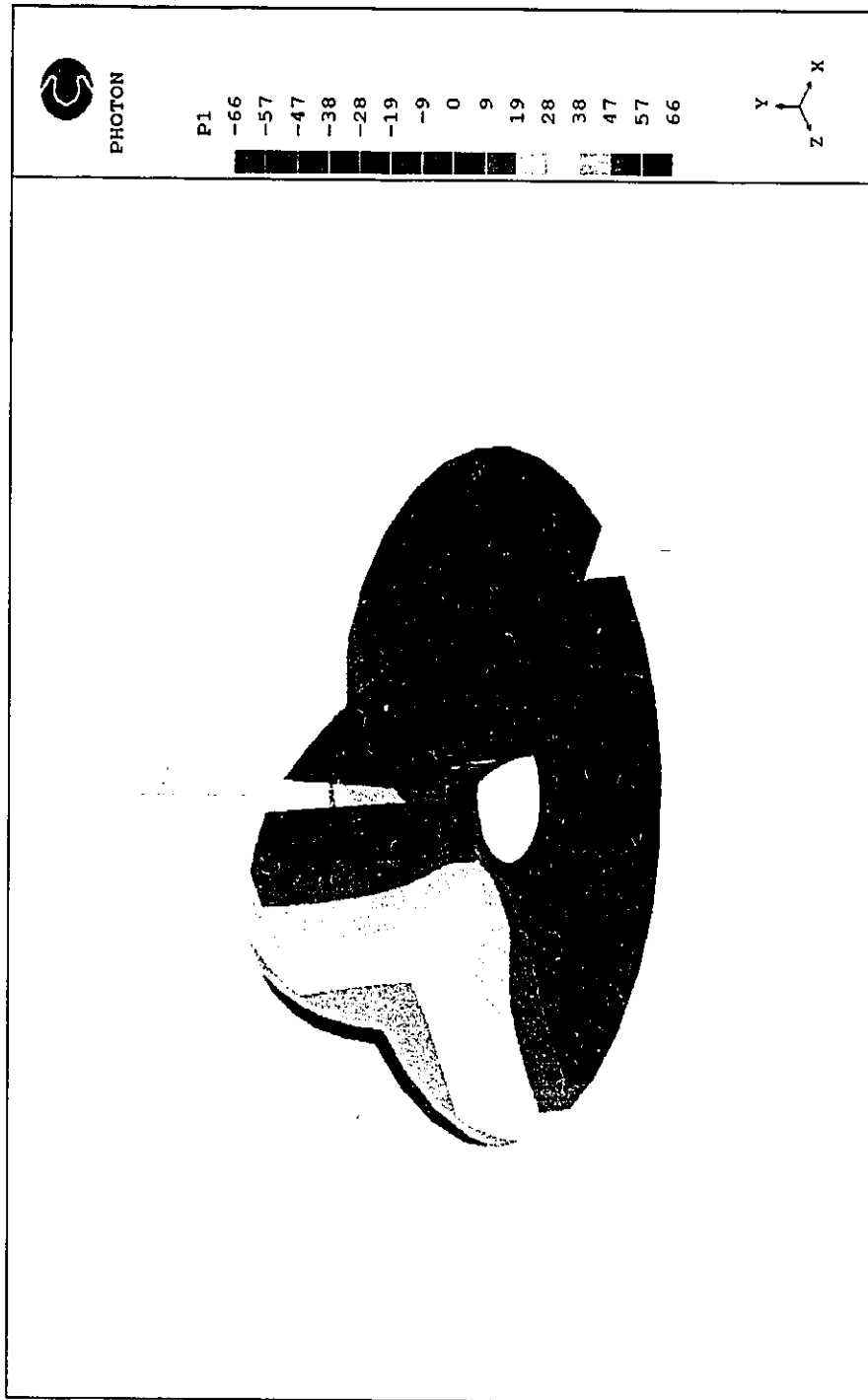
Figure 5.27 Pressure distributions on equatorial and radial planes
$Re = 5 \times 10^5$, $U_\infty = 60 m/s$, $Ta/Re^2 < 1$

CHAPTER 6

EXPERIMENTAL INVESTIGATION

OF VERTICALLY ROTATING SPHERE

6.1   Introduction

The problem of a rotating sphere in a free stream has received very little experimental
attention in the literature. To the author's knowledge, the velocity distribution around a
rotating sphere whose axis is perpendicular to the free stream direction has never been
investigated experimentally. Thus, based on imposed potential velocities at the edge of the
boundary, the numerical results of the flow about a rotating sphere in a perpendicular free
stream have been obtained. The actual velocities at the boundary layer edge may be different
from the potential ones. Therefore, the actual velocity at the boundary layer edge and the
velocity components within the boundary layer were measured experimentally. Furthermore,
a comparison between numerical and experimental results should lead to a good
understanding of the actual flow behavior and any limitations of the theoretical work.

The objectives of the experimental work were:

i.   design and construction of the experimental apparatus, including the sphere support

mechanism and a three-dimensional hot-wire probe positioning device.

ii.   the experimental measurements of the flow field using a triple-sensor probe.

The apparatus was designed such that a sphere could be rotated at different speeds about

an axis perpendicular to the flow in a large wind tunnel. A traversing mechanism for the

triple-sensor probe was also incorporated into the equipment so that measurements could

be made at different positions from the surface of the sphere.

6.2   Wind Tunnel

The experiments were performed in an open circuit boundary layer type wind tunnel with a

615 mm × 615 mm octagonal test section; *1800 mm* length. The wind tunnel had a free

stream velocity range of *0.2 m/s ≤ U_∞ ≤ 30 m/s* and a turbulence intensity about *0.3 %* for *1*

m/s ≤ U_∞ ≤ 12 m/s, rising to *0.9 %* at *U_∞ = 20 m/s*. The thickness of the boundary layer was

about *25mm*. The maximum velocity variation outside boundary was about *3.7%*. A pitot

static tube was placed on the bottom of the upstream part to measure the flow velocity.

6.3   Test Model

In designing the test model, several design aspects were considered for finding the best

parameters to be used in the experiments. Selection of the size of the sphere was dependent

on the size of the test section of the wind tunnel and the range of the desired Reynolds numbers to be used in the experiments. Generally, the sphere should be *3* to *5* diameters away from the walls of the wind tunnel, and the projected area of the sphere should account for no more than *5%* of the tunnel cross-sectional area. The critical Reynolds number ranges from 3×10^5 to 3×10^6 (Janna, 1987) for a sphere in the laminar flow case. An initial steady-state air speed of the wind tunnel was approximately *4-5 m/s*. Referring to the results of the numerical prediction, meanwhile considering the limitation of the wind tunnel, it was decided that a *Re* about 1×10^5 and sphere diameter of *9 cm* was most suitable for the experiments. The Reynolds number is lower than the critical *Re* number range of the sphere. It was confirmed by examining the plot of drag coefficient versus *Re* for a sphere (Janna, 1987) that shows that the drag coefficient is fairly constant over the range of *Re* 10^3 to 10^5. The accuracy and precision of the measurements were important in the design of the support apparatus and probe positioning device. An accuracy of *0.1 mm* was needed in the experiments. With the above considerations in mind, the following parameters were used:

diameter of sphere	$d = 9\ cm$
Reynolds number	$Re = 1 \times 10^5$
spin parameter	$Ta/Re^2 = 0 - 2$
wind tunnel speed	$U_\infty = 5 - 25\ m/s$
angular velocity	$\omega = 800 - 2000\ rpm$
blockage	$< 4.4\%$

6.4   Apparatus and Procedure

6.4.1   Design of Support Apparatus

The support mechanism was designed such that it allowed the sphere to rotate in a smooth and stable manner with the rotating axis of the sphere perpendicular to the free stream direction. Meanwhile, the vibrations of the drive must be reduced to insure constant sphere position and precision in the test measurements. It also had to be designed to minimize its contribution to flow field interference.

The sphere support apparatus is shown in Figure 6.1. The sphere was connected to a shaft supported by pillow block bearings and connected to a d.c. motor though a flexible coupling. The assembly was supported by a steel frame at the external of the wind tunnel to position the sphere in the center of the cross-section of the tunnel. The sphere was chosen to be *9 cm* in diameter from the above considerations. Its material chosen was an ultra high molecular weight plastic with a density of *9.411 × 10⁻⁴ kg/cm³*. The sphere was attached to the shaft by drilling a slightly smaller hole in the sphere and inserting the shaft with interference fits into an appropriate adhesive. The shaft was *20 mm* diameter to make the shaft stiff enough to avoid vibration of the sphere and keep cantilever bending of the shaft to under *0.1mm*. A long cantilevered shaft was specified to facilitate placement of the apparatus external to the tunnel.

Two FAFNIR SAS *1.25"* ball bearing pillow blocks were chosen to support the shaft. The pillow blocks were fixed to a steel plate that was fixed to the frame of the wind tunnel. The experiment required that measurements be taken over a range of rotational speeds; thus a variable speed drive train was necessary. The motor was attached to the shaft via a standard flexible coupling, *AL-090* (LOVEJOY).

6.4.2 Design of Probe Positioning Device

The simplest approach would be manually sliding the probe to the desired location. This was achieved accurately with the help of vernier scales. The design incorporated two components: the x - y - z positioning table and a rotatable sealing disk.

An x - y - z positioning table was selected from a UniSlide Catalog of VELMEX (1991) which had a triple x - y - z stage with *12.5"* travel in x-direction (*A2515Q1-S2.5*), *7.5"* in y and z-directions (*A1509Q1-S1.5*). Overall dimensions of *375mm* × *225mm* × *225 mm*, and an accuracy of *0.001"*. The x-y-z table could move independently in three perpendicular directions. In the measurement x is free stream direction, y is cross flow direction and z is vertical direction.

The sensing wire of the hot-wire anemometer was located in the measurement region of the working section of the wind tunnel and was connected to the electric circuiting

externally. The probe axis was horizontal and was supported by a probe holder. The holder

was mounted in the y-direction of the x-y-z table whose frame was fixed to the main frame

of the wind tunnel. The probe holder was inserted into the wind tunnel through a rotatable

sealing disk in a perspex side window. The advantage of this design is that it was simple, with

minimal sealing problems, and was well suited for spherical objects. The front view of the

measurement system and the rotational sealing disk are shown in Figure 6.2.

6.4.3   Probe and Data-logging System

A DANTEC triple-hot-wire probe *55P91* was used, Figure 6.3, with a simultaneous data-

logging system, Figure 6.4. The system consisted of a multi-channel anemometer set, which

included a DANTEC *56C01/56C16* CTA(constant temperature anemometer) bridges

mounted inside a DANTEC main frame *56B12* and a DANTEC *55M01/55M10* CTA bridge

along with a DANTEC power unit *55M05*, a multi-channel data acquisition and analysis

system which included a DAS *20 A/D* board and a software package *ACQWIRE*, and a DELL

316SX computer. The triple-sensor probe had three identical wire sensors mounted mutually

perpendicularly to each other. Appendix III shows how the triple-wire probe works.

The relationship between anemometer voltage and sensed velocity for each wire is

adequately expressed by Lomas (1986) as:

$$Vol_i^2 = A_i + B_i U_{eff_i}^{n_i} \qquad (i = 1, 2, 3) \qquad (4.1)$$

where Vol_i are anemometer output voltages, A_i, B_i and n_i are constant for a given probe which are decided using Collis and Williams law in calibration, and U_{eff} are the effective cooling velocities normal to the hot-wire, the relations between these velocities and the wire coordinate velocities are expressed in Appendix III. The triple-sensor probe was calibrated by a DISA calibration rig *55D41/42*. The cone pressure measured with a pitot-tube which was read by a Betz micromanometer-used as a reference for calibration. Figures A3.2a, b and c are the calibration curves and the corresponding percentage errors in the fit for three hot wires, respectively. The maximum error was less than *5%*.

The output voltages from the anemometers were fed to the three input channels of a data acquisition system, a *12-bit A/D* converter that could sample at up to *100 kHz*. In the experiments, according to a Strouhal number of a stationary sphere at the range of Reynolds number investigated, the sample frequency was set at *1 kHz* and the sample number *8 k* for each wire. The sample data for three channels were read simultaneously and then transferred to the computer where data-processing was performed by *ACQWIRE*.

6.5 Experimental Results and Discussions

The triple-sensor probe was intended to be used for measuring the mean and some turbulent flow quantities in the three-dimensional complex flows. One major problem of using an orthogonal triple-sensor probe is its slight non-orthogonality due to imperfections in

manufacture. Andreopoulos (1983) investigated this influence by measurements. He found that if the effects of corresponding yaw and pitch sensitivity variations with the flow angle or non-orthogonality are ignored, errors in the Reynolds stress measurements are generated, but the effect on the mean flow is very small. In the present tests, the mean velocity components were considered, so the effects of the above were very small.

All measurements were performed on the equatorial plane. In order to compare with the calculated results, three cases were measured:

i.   velocity distribution around a rotating sphere whose axis was perpendicular to the free stream direction, $\omega = 835$ rpm and $U_\infty = 11.3$ m/s.

ii.   velocity distribution around a rotating sphere whose axis was perpendicular to the free stream direction, $\omega = 1689$ rpm and $U_\infty = 23$ m/s.

iii.   turbulent properties at one point for different rotational speeds, $\omega = 500, 1000, 1500, 2000$ rpm.

For the first case, Figure 6.5 illustrates the vector distribution at different radial directions of equatorial plane, and Figure 6.6 the mean velocities at four radial directions. Figure 6.6a and 6.6b are two horizontal and two vertical radial directions respectively. In Figure 6.5, there are eight radial directions which had equal angles, 45°, between two of the radial directions and each with 7 points. The nearest point to the surface was 7.5 mm away-limited by the diameter of the triple-sensor probe. The 3 mm increase point by point along the

radial direction which was limited by the size of the test section of the wind tunnel.

Figure 6.5 provides a qualitative velocity distribution plot. Directions of free stream and rotational speed are shown in the Figure. It can be seen, that in the horizontal and vertical radial directions, velocities are parallel to the free stream. At the top of the vertical direction, tangential velocities of the rotation and free stream are same direction. Meanwhile, at the bottom vertical direction, both velocities are at adverse directions and the total velocities are smaller than the top's. Between each horizontal and vertical direction, directions of velocity were changed according to the two velocity directions.

As Figure 6.6a shows, in two horizontal directions the mean velocity components W are very small and almost no change. Mean velocity components U vary along radial direction, the upstream side values are decreased within negative values and the downstream side values are increased within positive values. Meanwhile, Figure 6.6b illustrates that in the vertical directions mean velocity components U have small variations and all the values are negative. Mean velocity components W also have small variations with the values almost equal to zero.

For the second case, Figure 6.7 has vector distributions at the same positions as the first case. The directions of free stream and rotation speed are shown in the Figure. In the horizontal direction, at the upstream side, the velocities somewhat decline with the rotational

direction and at the downstream side the velocity directions are exactly the tangential directions of the sphere and near the surface of the sphere the magnitudes of the velocity are smaller because of the influence of the vortex. For the rest of the radial directions, the general cases of the velocity distribution are the same as the first case.

Figure 6.8 presents the mean velocity components, U and W, in horizontal directions, Figure 6.8a, and vertical directions, Figure 6.8b. Figure 6.8a indicates that on the upstream side the mean velocity components U decrease and reach negative values, and on the downstream side the variation shows a peak. The lower plot indicates that in the upstream horizontal direction the mean velocity components W maintain a constant value. Meanwhile, at the downstream horizontal direction it decreases quickly along the radial direction. Variations of mean velocity components in vertical directions are shown in the Figure 6.8b. At the top vertical direction both mean velocity components have small variation. At the bottom, the mean velocity components U show smooth variations; however, the profile for W is not smooth; fluctuations are present. The later is due to the action of the adverse velocity directions. All components U have negative values according to the free stream direction.

Considering the influence of turbulence, the third case gives the turbulent properties at one point (-5, 0, 0), the point nearest to the surface of the downstream horizontal radial direction. Figure 6.9 presents the spectra for different rotational speed and figures 6.10 a, b and c show the auto-correlations of wire 1, 2 and 3 to same set rotational speeds respectively.

In figures 6.9 and 6.10, plots a, b, c and d correspond to rotational speeds $\omega = 500$, *1000*, *1500* and *2000* respectively. When the rotational speed increases the variations of spectrum and auto-correlation are smaller. With frequency increase the spectra go to zero and with time delay the auto-correlations go to zero. This means that the larger the rotational speed the smaller of the influence of turbulence. The influences occurred at the lower frequency and initial time period.

6.6   Comparisons with Calculated Results

Figure 6.11a, b, and c are the comparison of calculated and measurement results. The comparisons are based on the conditions of the second case and using the Cartesian coordinate system shown at the bottom right of Figure 5.2. Because of the limitation of the experiment, the experimental data could not be obtained at positions that were very close to the surface of the sphere. In general, the numerical and experimental results are reasonable and agree well, though the experimental values seem smaller than the calculated values. The discrepancy between them may have resulted from the imposed turbulence model used in the calculations are not the exact turbulence situations in the experiment.

The variations of the velocity components in free stream direction (Figure 6.11a) are changed due to the different radial positions, while in vertical direction (Figure 6.11b), the variations are the same. The two components maintain a constant value after a certain

distance from the sphere surface. For the components in the cross flow direction (Figure 6.11c), the variations are also different due to the different radial positions. Position $\varphi = 0^\circ$ is the downstream center line, near the sphere surface the area is a vortex area, the directions of the radial velocity components are totally different from the outer edge area.
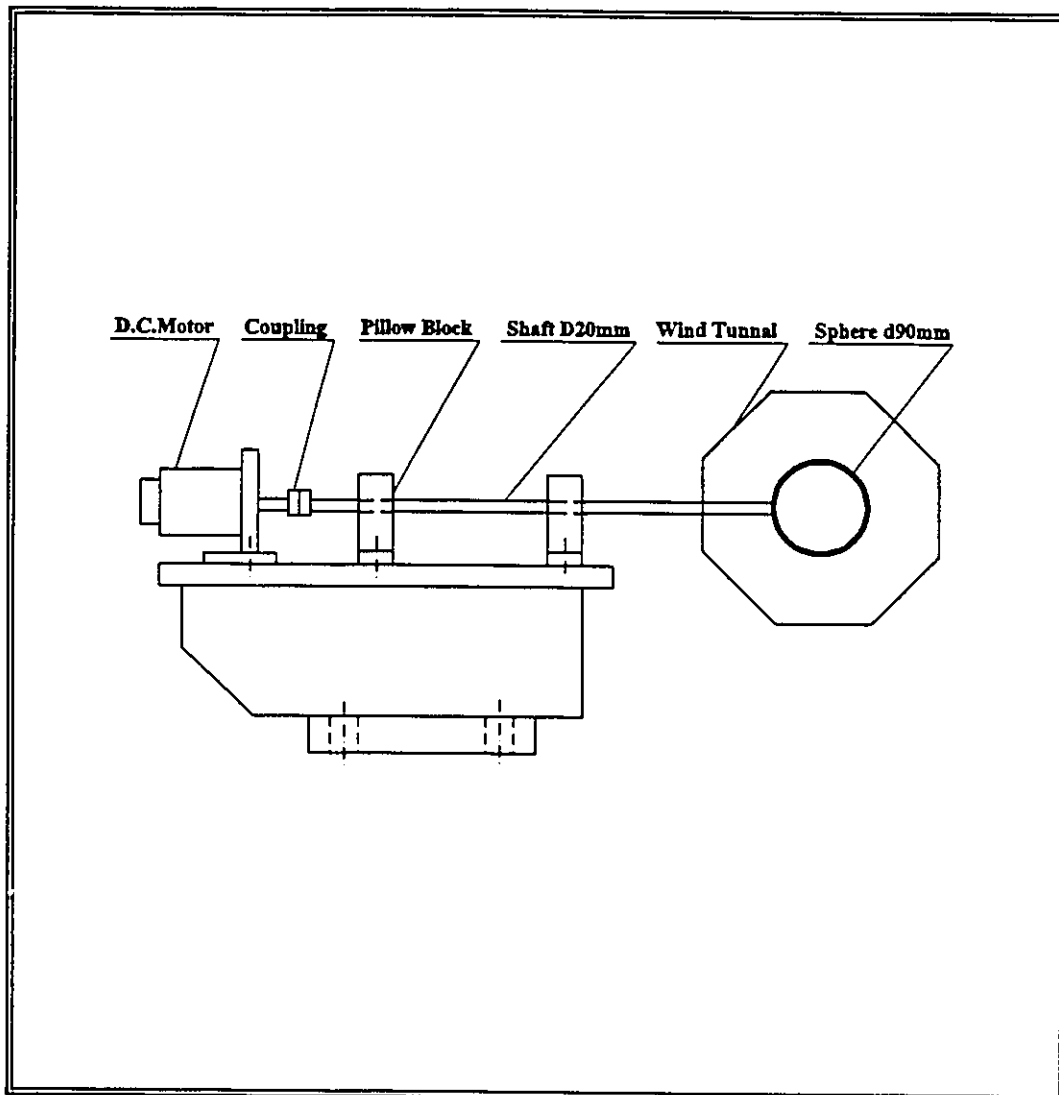
Figure 6.1   Sphere support mechanism
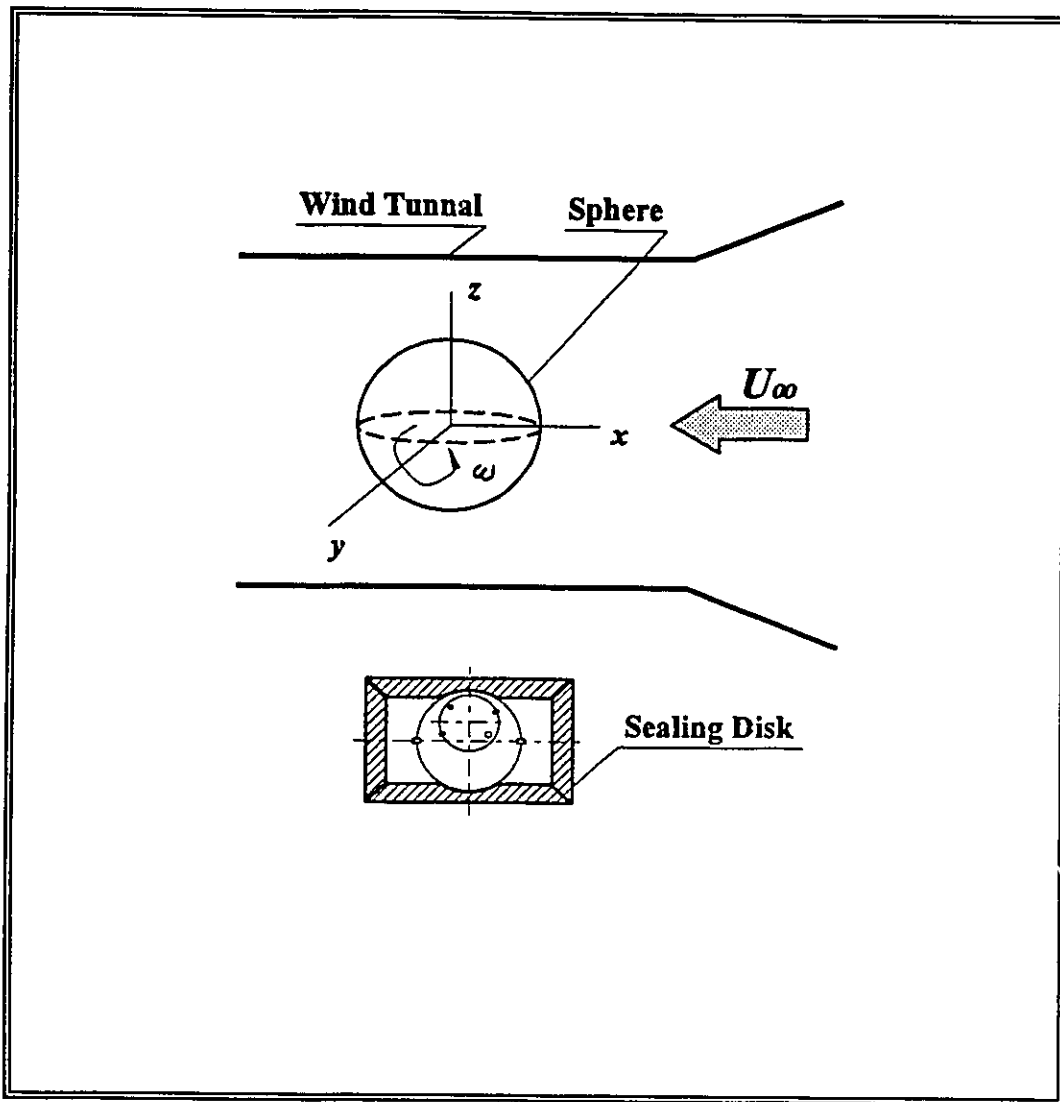
Figure 6.2   Front view and sealing disk
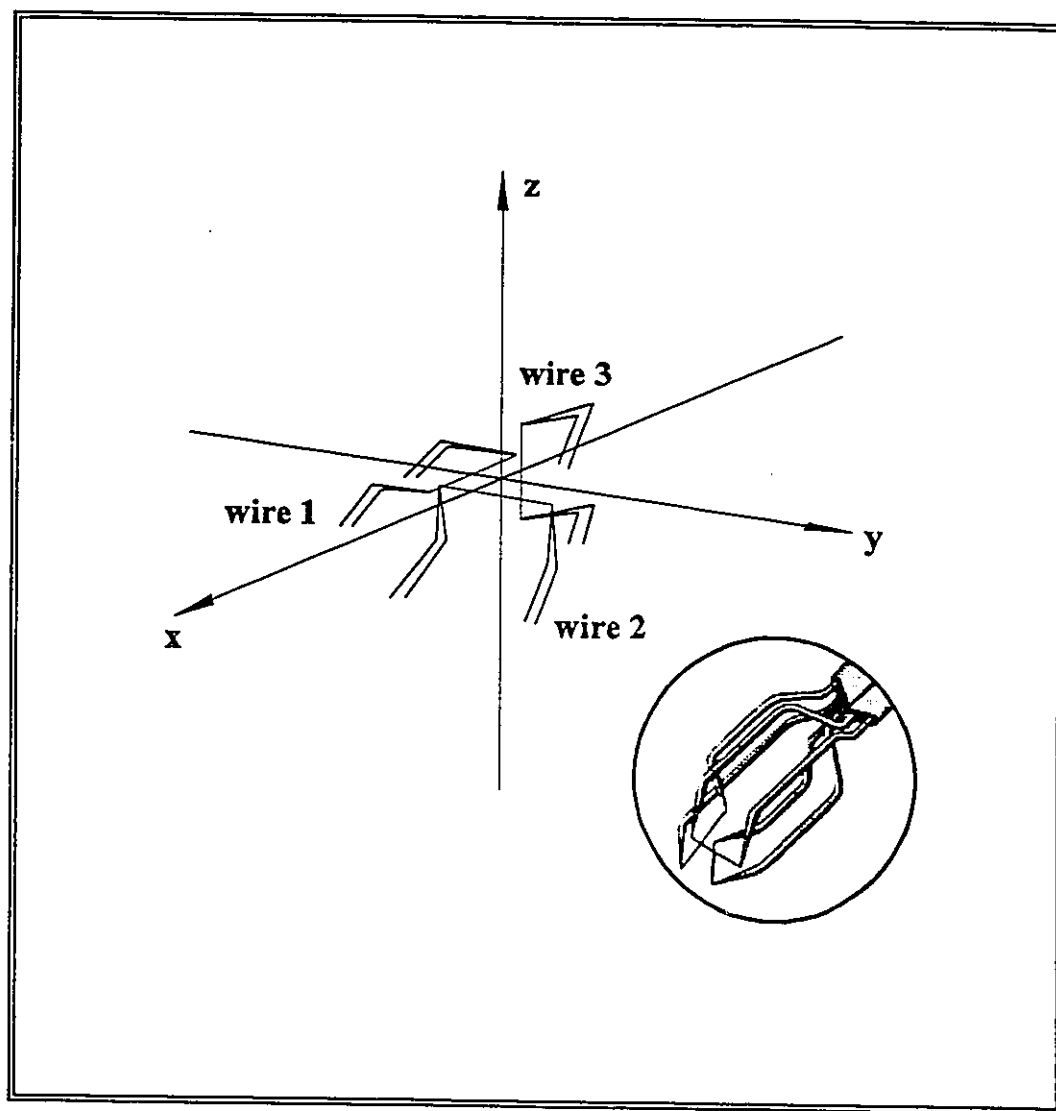
Figure 6.3   Triple - sensor probe
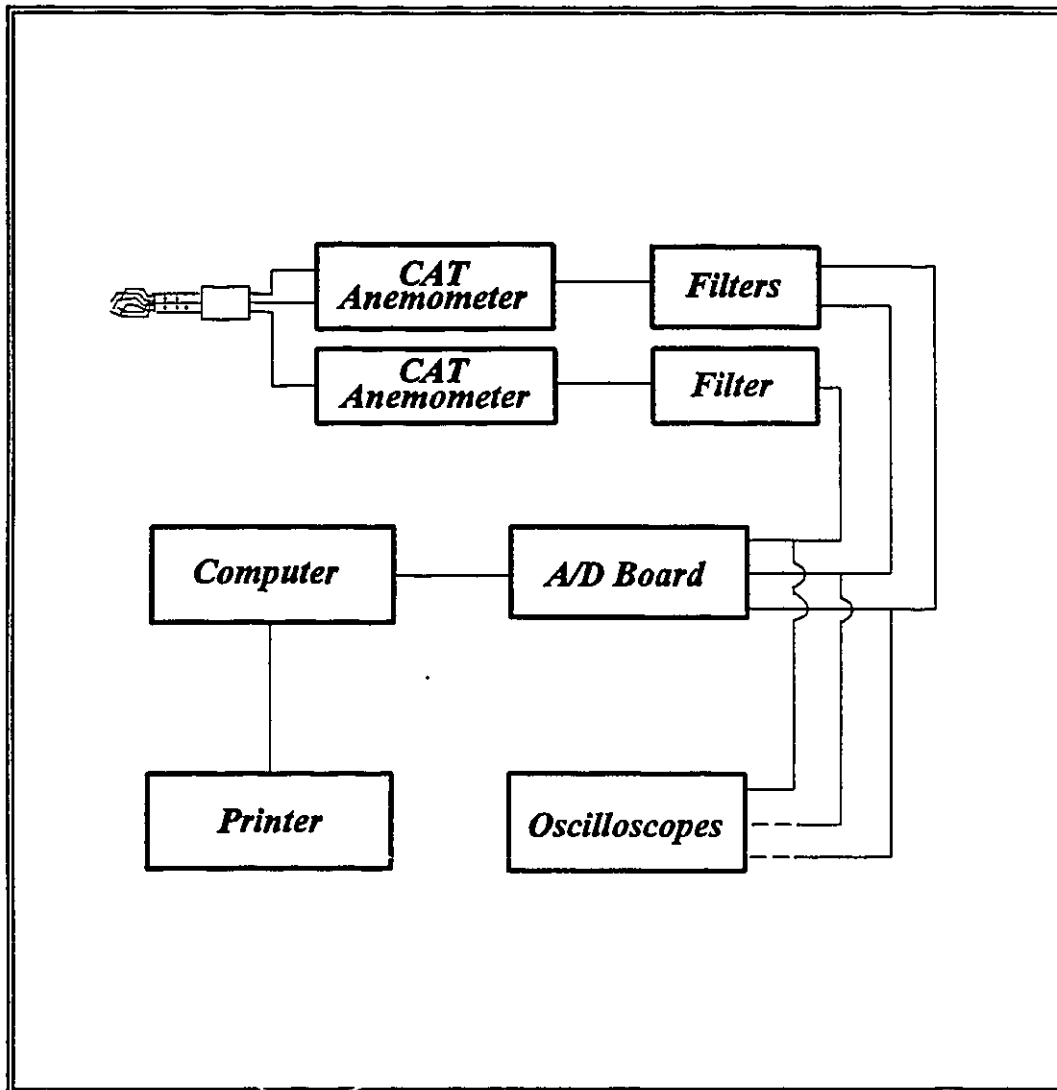
Figure 6.4   Probe and data-logging system
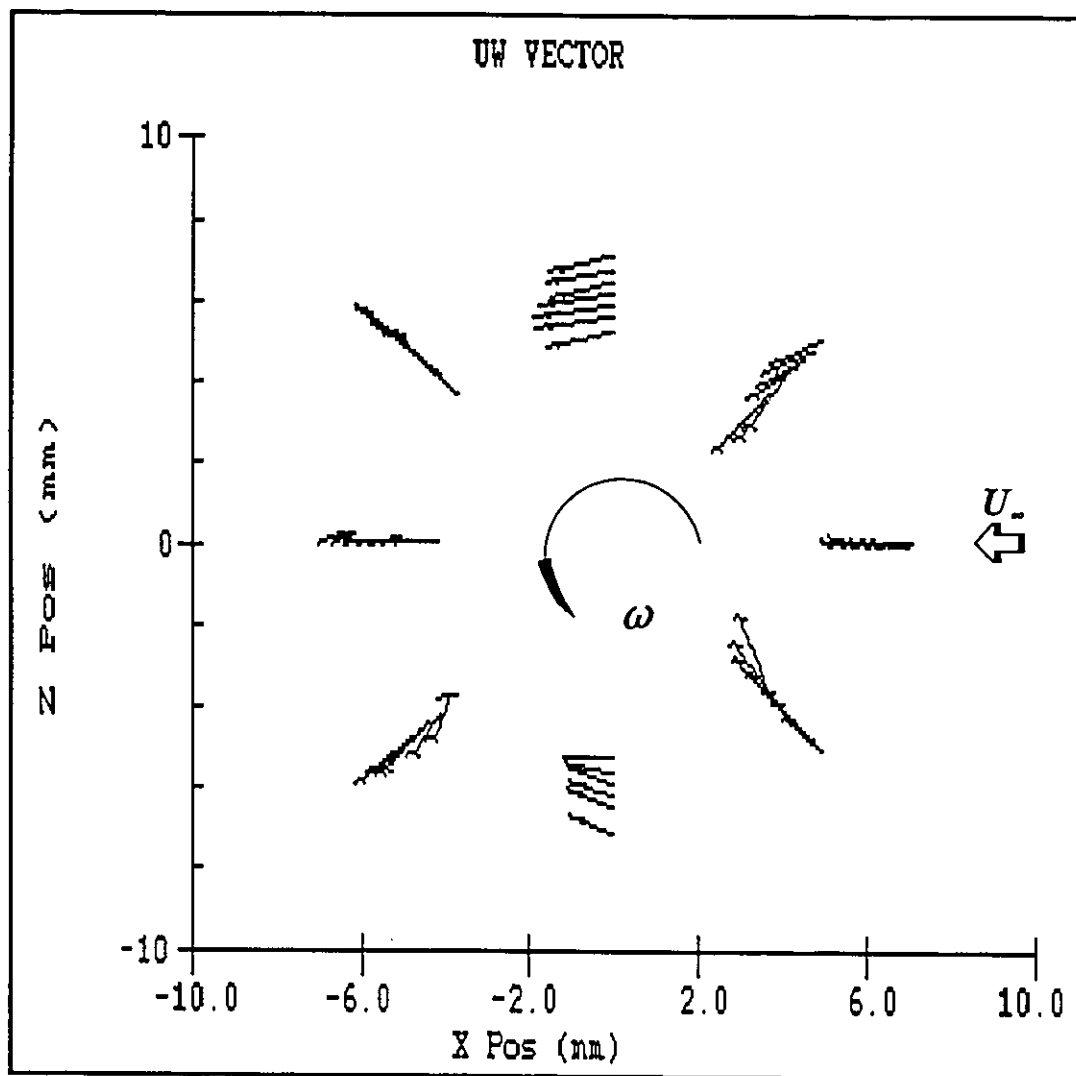
Figure 6.5 Vectors in radial directions of equatorial plane, $Re < 1 \times 10^5$, $U\infty = 11.4$ m/s, $Ta/Re^2 < 1$
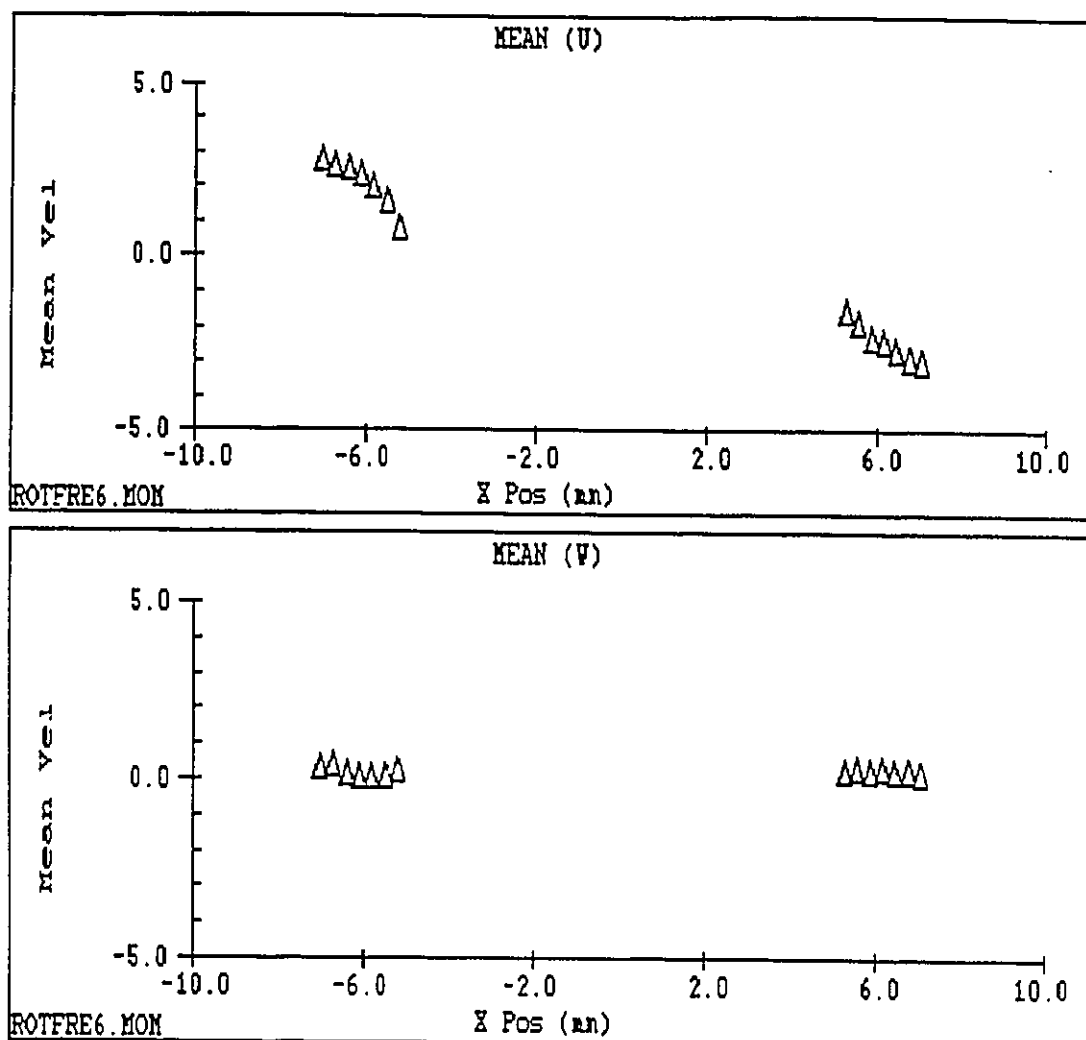
Figure 6.6a   Mean velocities in horizontal radial
directions of equatorial plane
Re < 1×10⁵, U∞ = 11.4 m/s, Ta/Re² < 1
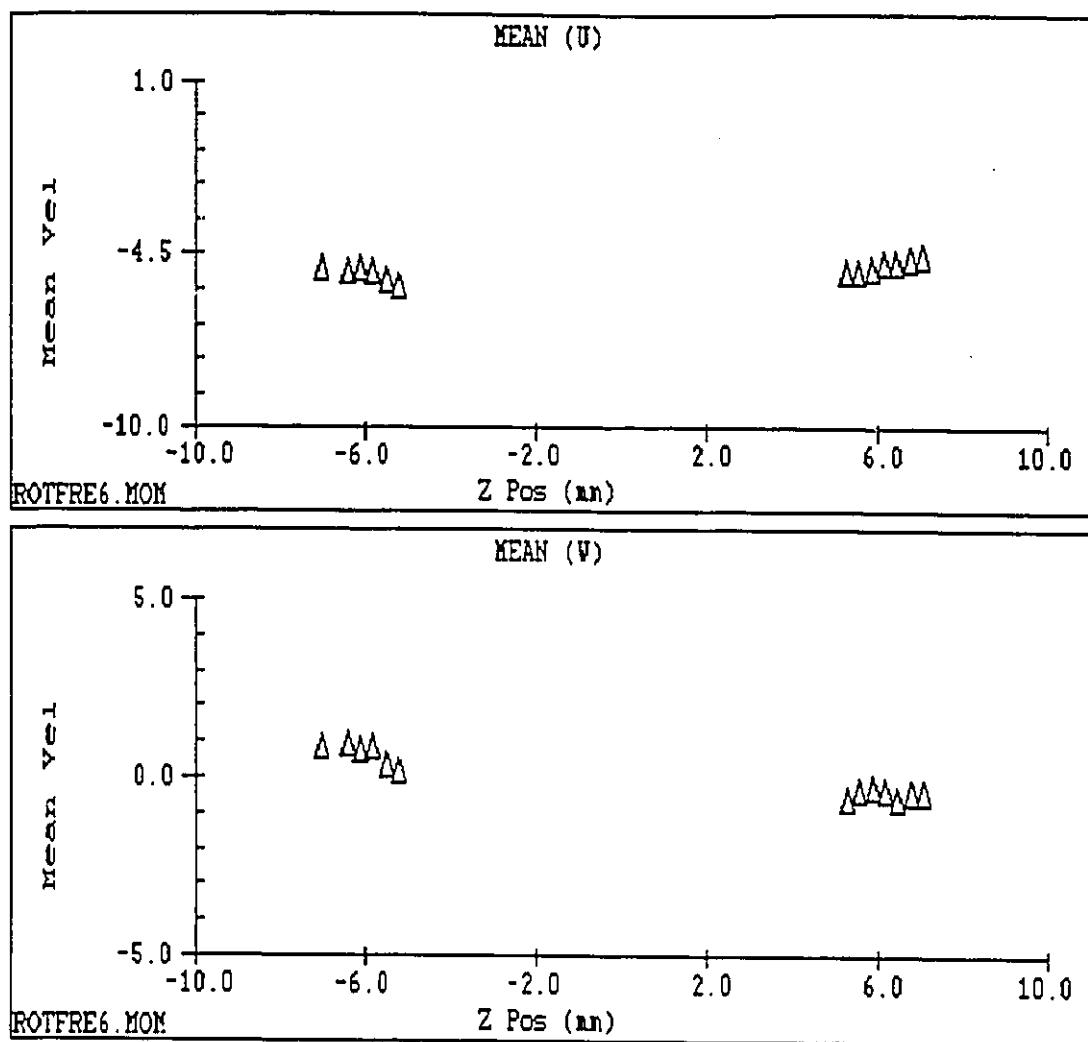
Figure 6.6b Mean velocities in vertical radial
directions of equatorial plane
$Re < 1 \times 10^5$, $U\infty = 11.4 \, m/s$, $Ta/Re^2 < 1$
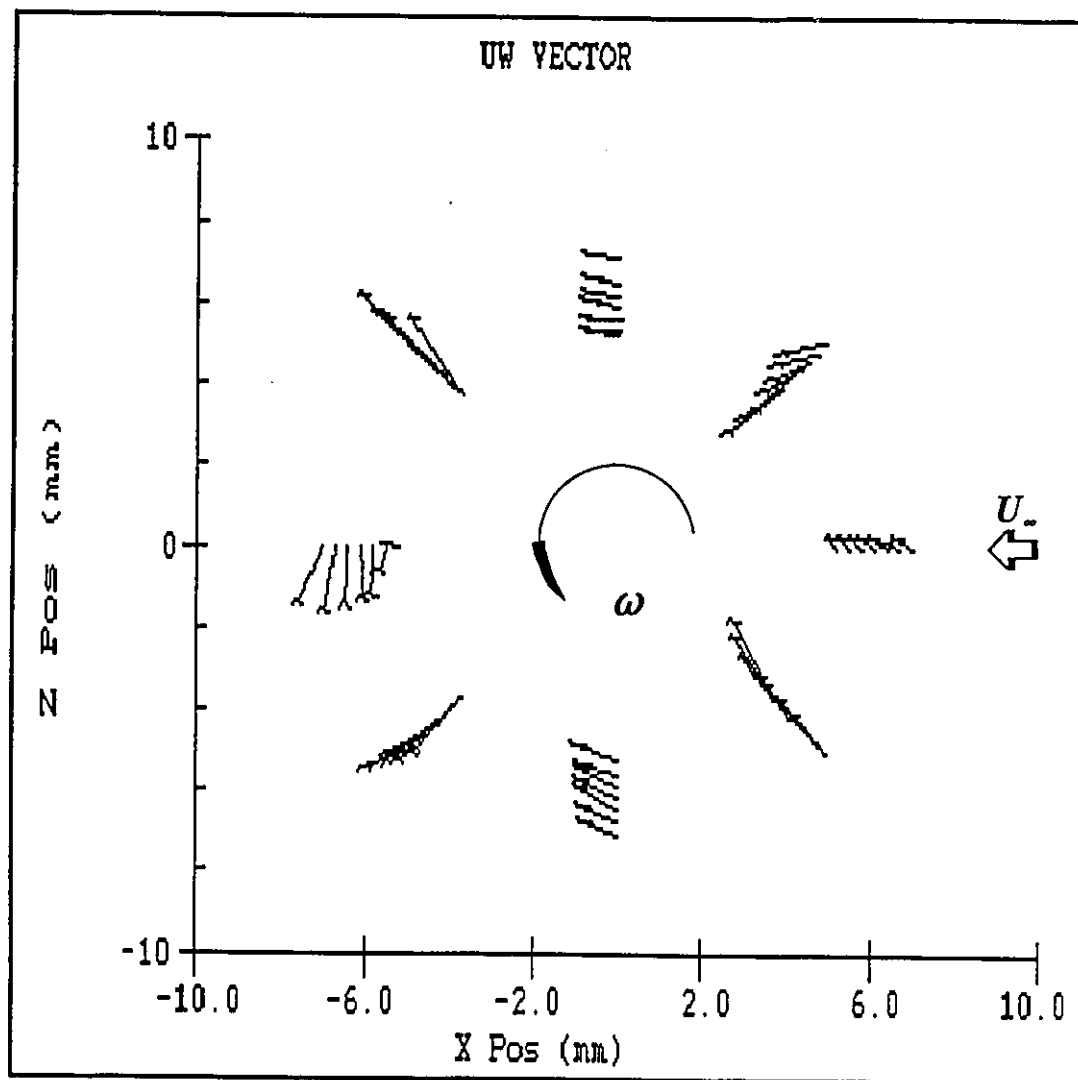
Figure 6.7 Vectors in radial directions of equatorial plane, $Re < 2 \times 10^5$, $U\infty = 23$ m/s, $Ta/Re^2 < 1$
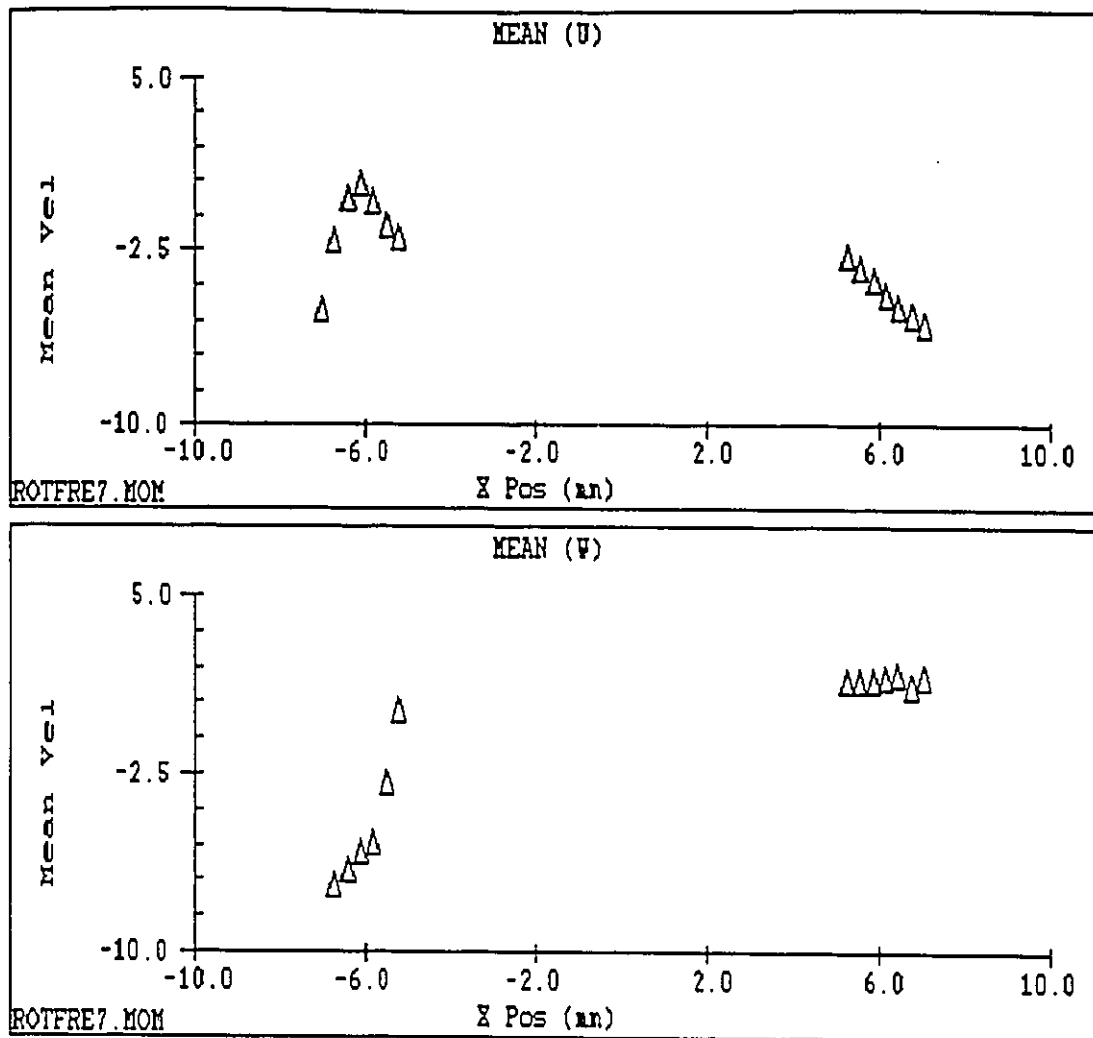
Figure 6.8a   Mean velocities in horizontal radial
directions of equatorial plane
$Re < 2 \times 10^5$, $U\infty = 23$ m/s, $Ta/Re^2 < 1$
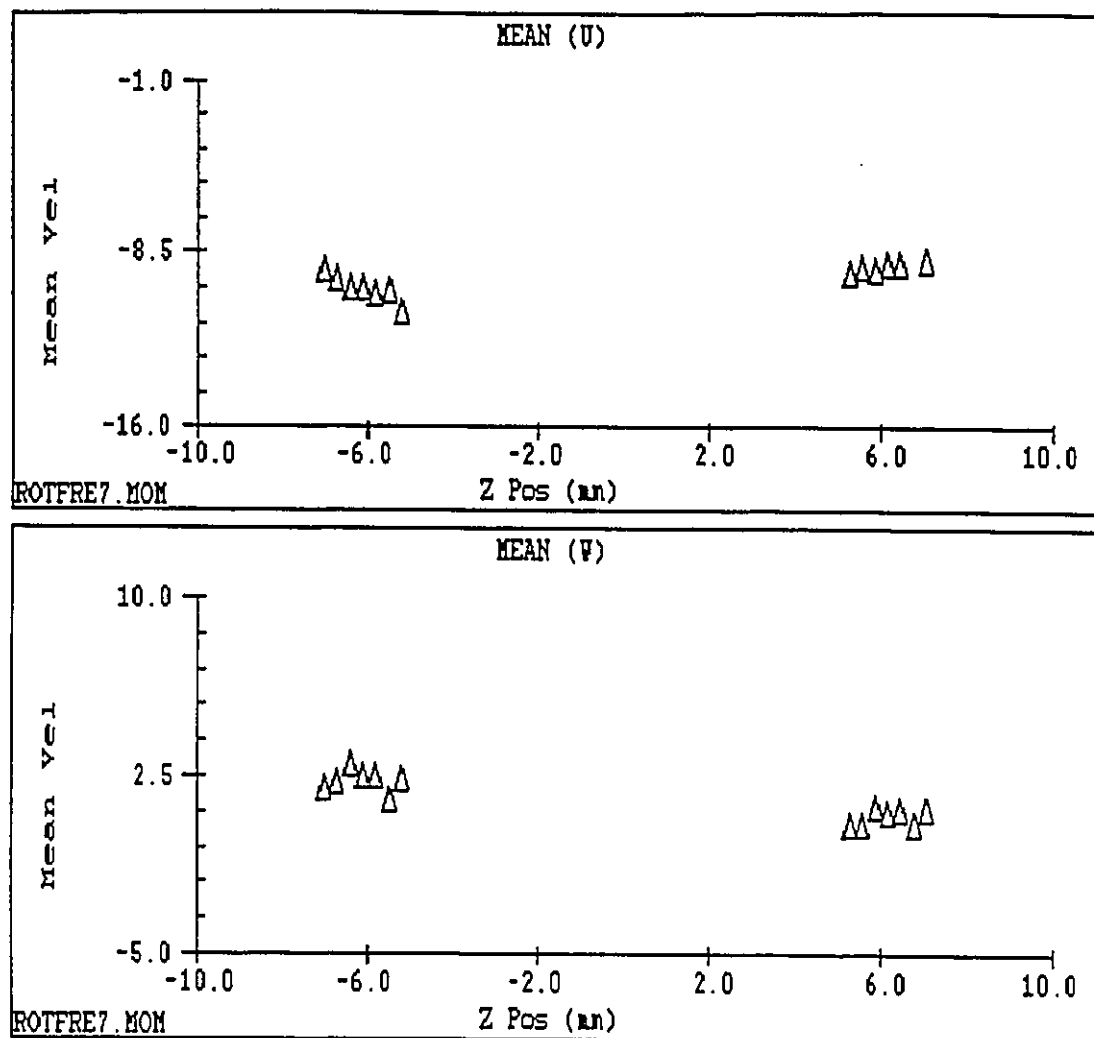
Figure 6.8b Mean velocities in vertical radial
directions of equatorial plane
Re < 2×10⁵, U∞ = 23 m/s, Ta/Re² < 1

SPECTRUM (a)

15.3k

S(f)

7.6k

0.0k
3RDS.000   0.00 0.10 0.20 0.30 0.40 0.50
                    Freq (KHz)

SPECTRUM (b)

15.3k

S(f)

7.7k

0.0k
3RDS.001   0.00 0.10 0.20 0.30 0.40 0.50
                    Freq (KHz)

SPECTRUM (c)

15.3k

S(f)

7.7k

0.0k
3RDS.002   0.00 0.10 0.20 0.30 0.40 0.50
                    Freq (KHz)

SPECTRUM (d)

15.3k

S(f)

7.7k

0.0k
3RDS.003   0.00 0.10 0.20 0.30 0.40 0.50
                    Freq (KHz)
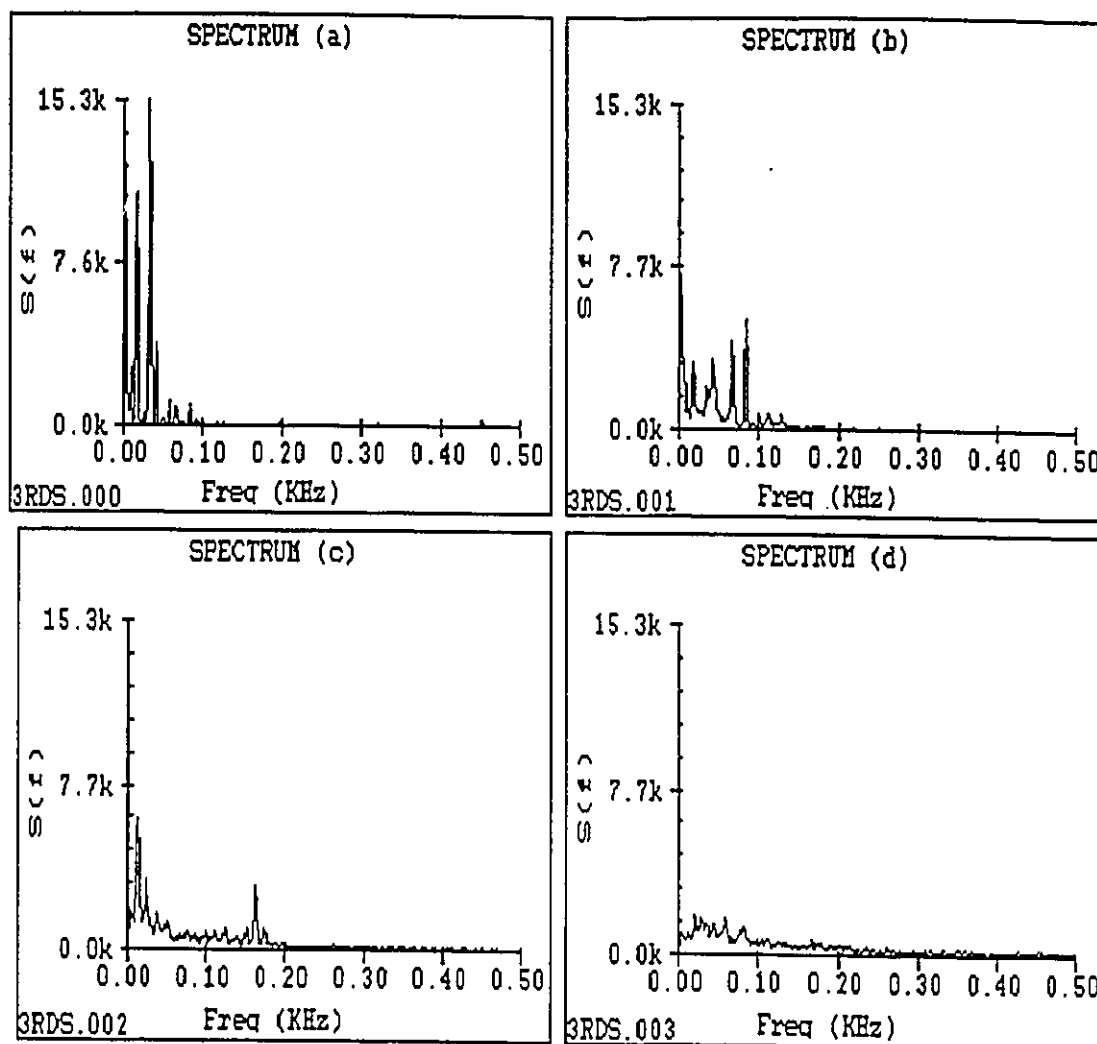
Figure 6.9   Spectra vs. frequency at a point
a: $\omega = 500\ rpm$;   b: $\omega = 1000\ rpm$;
c: $\omega = 1500\ rpm$; d: $\omega = 2000\ rpm$.
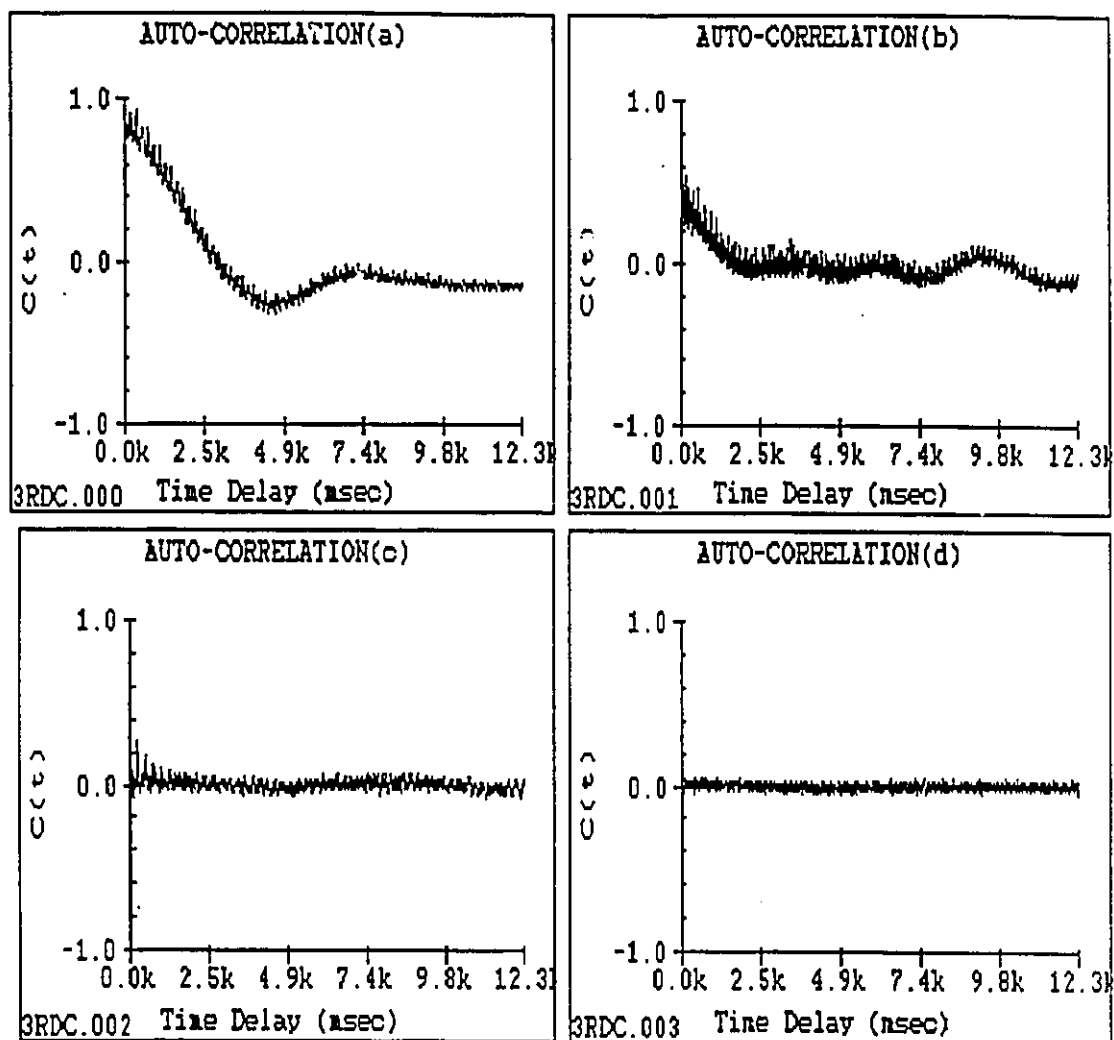
Figure 6.10a Auto-correlation vs. time delay *(U)*
a: *ω = 500 rpm*; b: *ω = 1000 rpm*;
c: *ω = 1500 rpm*; d: *ω = 2000 rpm*.
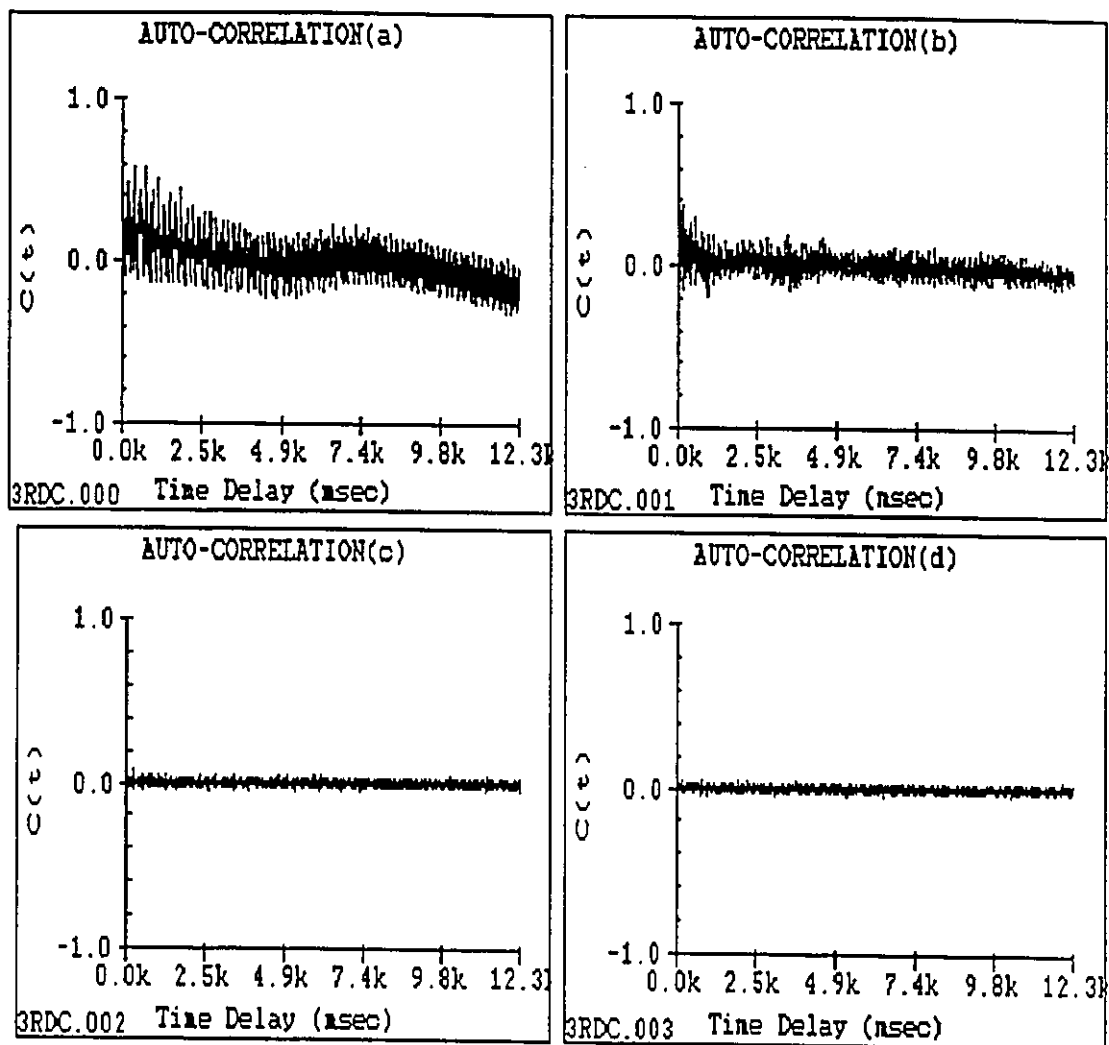
Figure 6.10b Auto-correlation vs. time delay *(V)*
a: $\omega = 500 \ rpm$; b: $\omega = 1000 \ rpm$;
c: $\omega = 1500 \ rpm$; d: $\omega = 2000 \ rpm$.
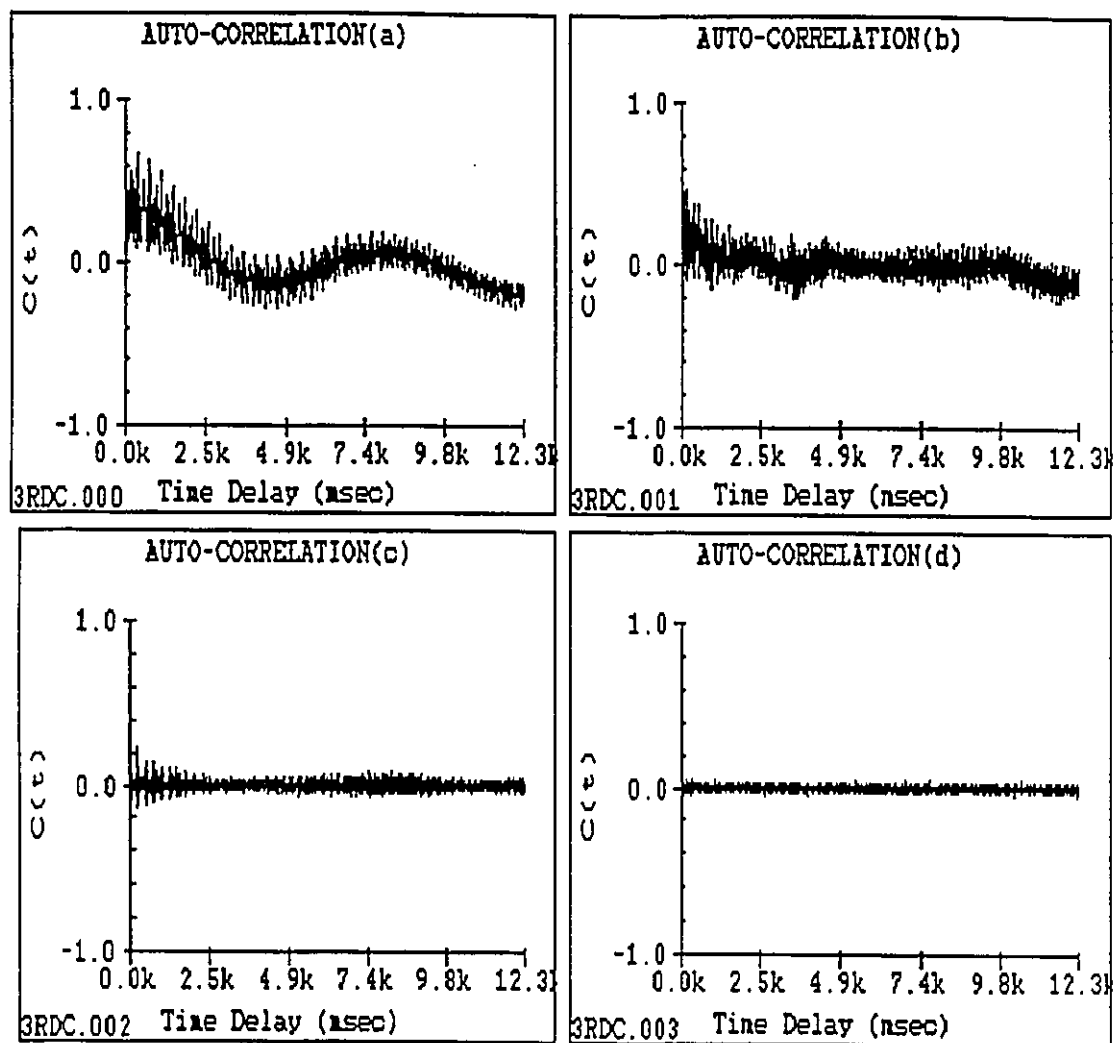
Figure 6.10c Auto-correlation vs. time delay *(W)*
a: *ω = 500 rpm*; b: *ω = 1000 rpm*;
c: *ω = 1500 rpm*; d: *ω = 2000 rpm*.
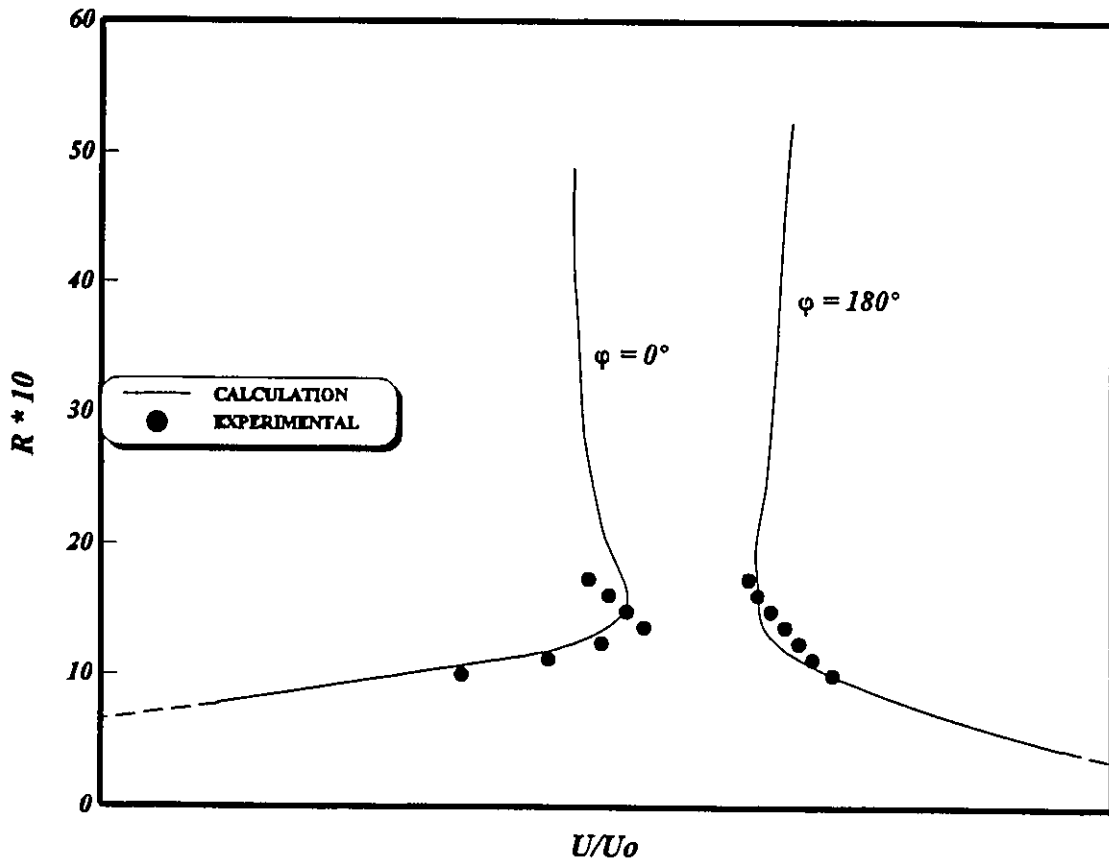
Figure 6.11a Comparisons of nondimensional velocity on equatorial plane (free stream direction)
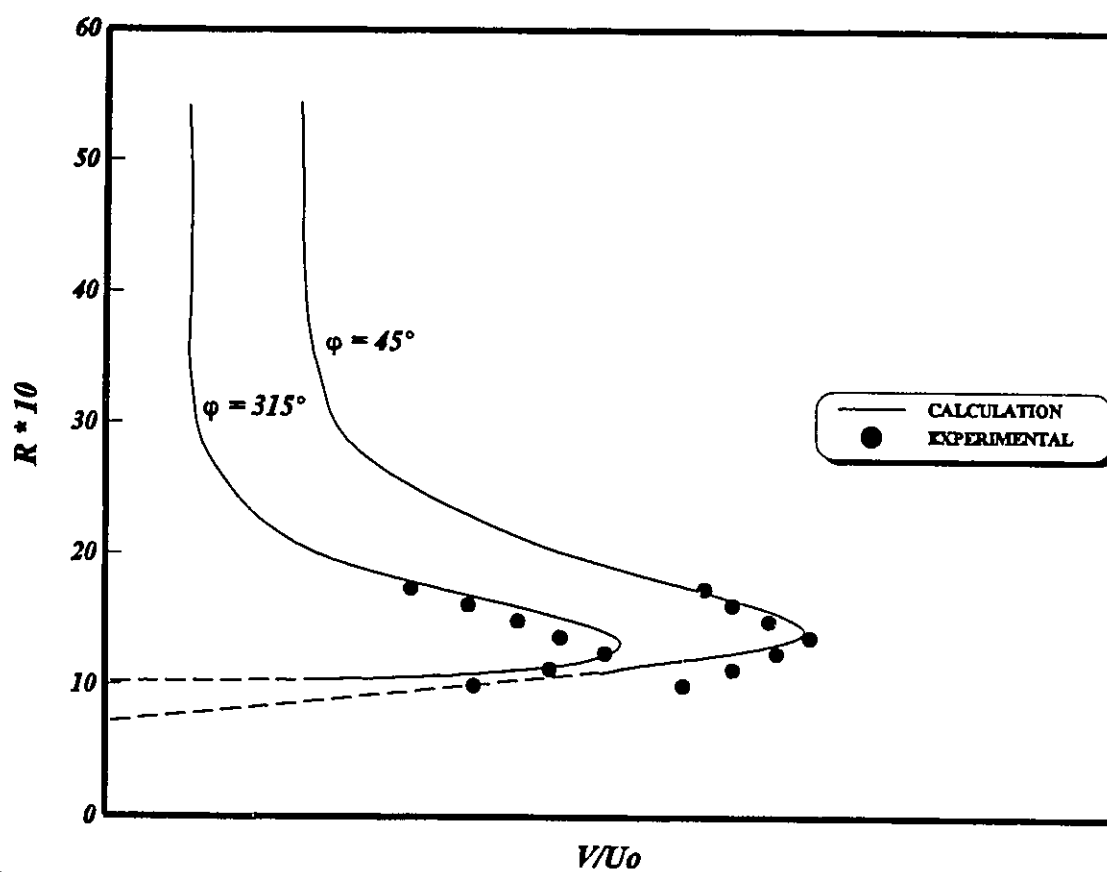
Figure 6.11b Comparisons of nondimensional
velocity on equatorial plane
(vertical direction)
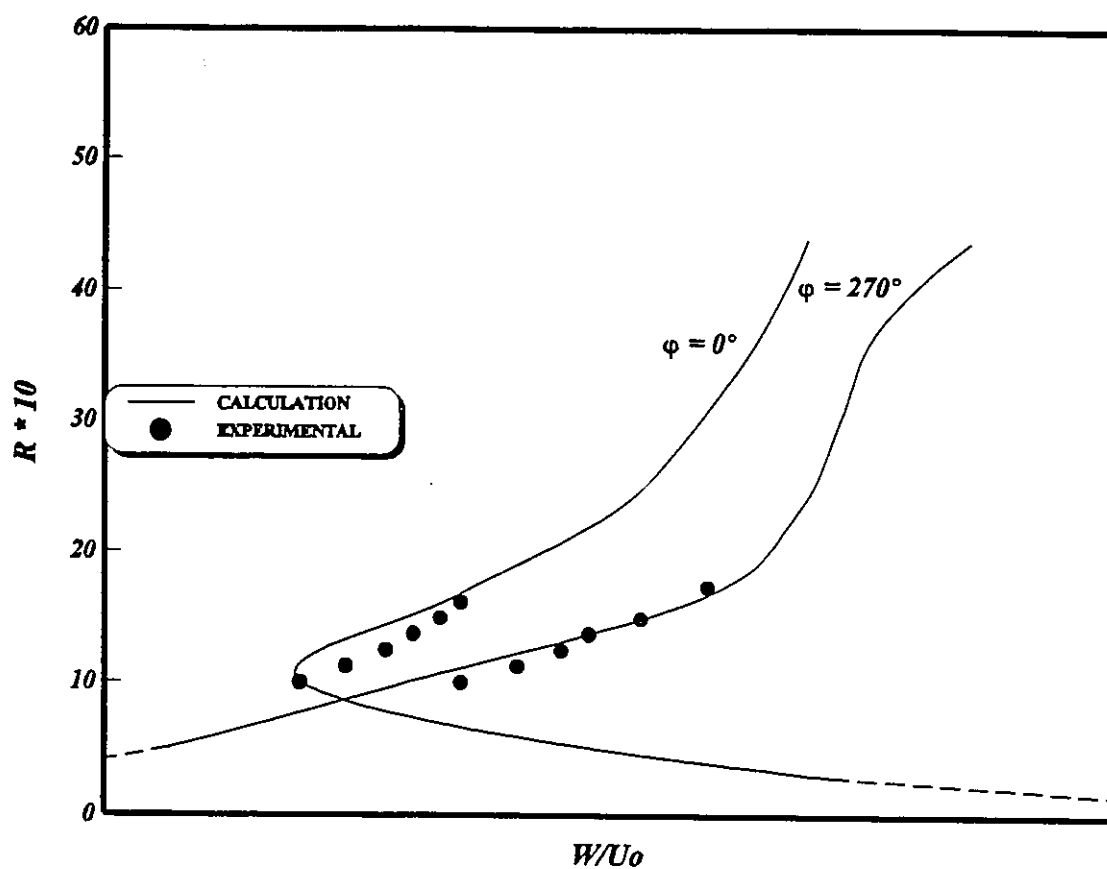
Figure 6.11c Comparisons of nondimensional
velocity on equatorial plane
(cross flow direction)

CHAPTER 7

CONCLUSIONS AND RECOMMENDATIONS

7.1   Conclusions

This thesis is concerned with the flow fields around a rotating sphere in both aspects numerical prediction and experimental measurement.

The boundary - layer equations and corresponding boundary conditions derived are suitable for a rotating sphere whose axis is perpendicular to free stream direction. The important parameters are the Reynolds number and the spin parameter. Both decide the rotation behavior of a rotating sphere.

For the flow fields around a stationary sphere, the numerical prediction results are in good agreement with other researcher's results. At lower Reynolds number, the flow corresponds to potential flow and became vortex flow when the Reynolds number increased to a certain value that is dependent on the diameter of the sphere and the free stream velocity.

For a steady flow due to a rotating sphere, the numerical prediction results indicate there is an inflow near the polar area, and an outflow near the equatorial plane. No separation occurs in this kind of flow.

The numerical prediction results obtained for the flow field around a rotating sphere whose axis is parallel to the free stream direction are reasonable. On the back half sphere, the flow field is severely disturbed, separation and vortex flow appeared.

The numerical prediction results obtained for the flow fields around a rotating sphere whose axis is perpendicular to the free stream direction are in good agreement with the available experimental data. If the Reynolds number is smaller than the critical Reynolds number and the spin parameter is equal to or larger than 1, the rotation altitude is large enough to overcome the free stream. Otherwise, if the rotation and free stream behavior are in the same range, the free stream has the same influence as rotation velocity and a zero velocity point occurs somewhere. The position of this point depends on the relation between the velocities of free stream and rotation.

All numerical predictions were made by using PHOENICS code with a FORTRAN code developed by the author. This code is very powerful and can handle the complex three-dimensional flow problems.

The experimental results show that a three-dimensional flow field can be measured by using a triple-sensor probe with the designed experimental device. The experimental measurements were not as complete as the numerical predictions due to the limitation of the test section size of the wind tunnel. Results of mean velocities agree with the calculated results and the vector distributions from both results are matched. With the rotation velocity increase the turbulence influence became smaller.

7.2 Recommendations for Future Work

The results obtained from the present calculations and experimental studies on the flow fields around a rotating sphere whose axis is perpendicular to the free stream are fairly comprehensive. But, this situation is a special case and is the first step in the solution of this type of problem. More general situations, such as arbitrary rotation angles and nonspherical particles, should be considered for engineering applications. Accordingly, suggestions for further research on the process are as follows:

Numerical predictions

A good point to start is from the present program. Using the same package, PHOENICS, which has a facility of choosing the rotation axis of a rotating body, calculate the flow field with variable angles between the rotating axis and free stream direction and change the

boundary conditions for different angles correspondingly.

Consideration of other kinds of rotation bodies, such as cubes and ellipses with body-fitted-coordinate. For these kinds of body, the difficulties are to decide the boundary conditions.

Experimental measurement

Consideration should be given to vary the angle between the rotation axis and free stream direction, adding an additional device that includes a one-dimensional movement and a 90° degree rotation movement at the bottom of the sphere support mechanism. In these circumstances, the rotating axis can be easily modified to change the angle.

For arbitrary rotating angle case, the problem is not symmetric. The measurement domain is the whole surface of a sphere. The probe positioning device needs to have the possibility of being fixed at the top and bottom of the wind tunnel to satisfy this requirement.

REFERENCES

Andreopoulos, J., 1983, "Improvement of the Performance of Triple Hot Wire Probe," *Res. Sci. Instrum*, vol. 54, pp. 733-740.

Banks, W.H.H., 1976, "The Laminar Boundary Layer on a Rotating Sphere," *Acta Mechanica*, vol. 24, pp. 273-287.

Beale, S.B., 1993, Fluid Flow and Heat Transfer in Tube Banks, *Ph. D. Thesis*, Imperial College, University of London.

Bearman, P.W., 1971, "Corrections for the Effect of Ambient Temperature Drift on Hot-wire Measurements in Incompressible Flow," *DISA Information*, No. 11, pp. 25-30.

Burgers, J.M., 1941, "Some Considerations on the Development of Boundary Layers in the Case of Flows Having a Rotational Component," *Kon. Akad. Von Wetenschappen*, Amsterdam 44, pp. 13-25.

Chen, T. S., and Mucoglu, A., 1977, "Analysis of Mixed Forced and Free Convection about a Sphere," *Int. J. Heat Mass Transfer*, vol. 20, pp. 867-875.

Chew, Y.T. and Simpson, R.L., 1988, "An Explicit Non-Real Time Data Reduction Method of Triple Sensors Hot-wire Anemometer in Three-dimensional Flow," *J. of Fluid*

Eng., Transaction of the ASME, vol. 110, No. 2, pp. 110-119.

Dennis, S.C.R. and Walker, J.D.A., 1971, "Calculation of the Steady Flow Past a Sphere at Low and Moderate Reynolds Numbers," *J.Fluid Mech.*, vol. 48, pt.4, pp. 771-789.

Dennis, S.C.R., Ingham, D.B. and Cook, R.N., 1979, "Finite-Difference Methods for Calculating Steady Incompressible Flows in Three Dimensions," *J. Computational Phys.*, vol. 33, pp. 325-339.

Dennis, S.C.D. and Ingham, D.B., 1982, "The Boundary Layer on a Fixed Sphere on the Axis of an Unbounded Rotating Fluid," *J. Fluid Mech.*, vol. 123, pp. 219-236.

Dennis, S.C.R., Singh, S.N. and Ingham, D.B., 1980, "The Steady Flow Due to a Rotating Sphere at Low and Moderate Reynolds Numbers," J. *of Fluid Mech.*, vol. 101, pp. 257-279.

Dennis, S.C.R., Ingham, D.B.and Singh, S.N., 1981, "The Steady Flow of a Viscous Fluid Due to a Rotating Sphere," *Q. J. Mech. Appl. Math.*, vol. 34, pt. 3, pp. 361-381.

El-Shaarawi, M.A.I., El-Refaie, M.F. and El-Bedeawi, S.A., 1985, "Numerical Solution of Laminar Boundary Layer Flow about a Rotating Sphere in an Axial Stream," *J. of Fluids Eng.*, vol. 107, pp. 97-104.

El-Shaarawi, M.A.I., Kemry, M.M. and El-Bedeawi, S.A., 1987, "Experiments on Laminar Flow about a Rotating Sphere in an Air Stream," *J. of Mech. Eng. Science*, vol. 201, iss. 6, pp. 427-438.

El-Shaarawi, M.A.I., Kemry, M.M. and El-Bedeawi, S.A., 1987, "Further Studies on Laminar Flow about a Rotating Sphere in an Axial Stream," *J. of Fluids Eng.*, vol. 109, pp. 75-77.

El-Shaarawi, M.A.I., Ahmad, N.T. and Kodah, Z., 1990, "Mixed Convection about a Rotating Sphere in an Axial Stream," *Numerical Heat Transfer*, pt. a, vol. 18, pp. 71-93.

El-Shaarawi, M.A.I. and Al-Jamal, K., 1992, "Forced Convection about a Rotating Sphere," *Applied Energy*, vol. 43, pp. 221-238.

El-Shaarawi, M.A.I., El-Refare, M.E., Kemry, M.M. and El-Bedeawi, S.A., 1993, "Induced Laminar Flow Due to a Rotating Sphere," *JSME International Journal*, Series B, vol. 36, No. 4, pp. 553-559.

Face, A., 1936, "Experiments on a Sphere at Critical Reynolds Numbers," *Aeronautical Research Council technical report*, Report and Memoranda 1766.

Fletcher, C.A.J., 1988, Computational Techniques for Fluid Dynamics, Volume I, II, *Springer-Verlag*, New York.

Fornberg, B., 1988, "Steady Viscous Flow Past a Sphere at High Reynolds Numbers," *J. Fluid Mech.*, vol. 190, pp. 471-489.

Furuta, T., Jimbo, T., Okazaki, M. and Toei, R., 1975, "Mass Transfer to a Rotating Sphere in an Axial Stream," *J. Chemical Eng. of Japan*, vol. 8, No. 6, pp. 456-462.

Furuta, T., Okazaki, M. and Toei, R., 1977, "Mass Transfer to a Rotating Sphere in a Stream," *J. Chemical Eng. of Japan*, vol. 10, No. 4, pp. 286-292.

Gorlin, S.M. and Slezinger, I.I., 1966, <u>Wind Tunnels and Their Strumentation</u>, *Israel Program for Scientific Translations*, Jerusalem.

Gosman, A.D. and Spalding D.B., 1970, "Computation of Laminar Flow between Shrouded Rotating Discs," *HTS/70/8*, Imperial College University of London.

Hamielec, A.E., Hoffman, T.W. and Ross, L.L., 1967, "Numerical Solution of the Navier-Stokes Equation for Flow Past Spheres: Part I. Viscous Flow Around Spheres with and without Radial Mass Efflux," *A. I. Ch. E.Journal*, vol. 13, No. 2, pp. 212-219.

Hamielec, A.E., Johnson, A.I. and Houghton, W.T., 1967, "Numerical Solution of the Navier-Stokes Equation for Flow Past Spheres: Part II. Viscous Flow Around Circulating Sphere of Low Viscosity," *A. I. Ch. E. Journal*, vol.13, No. 2, pp. 220-224.

Hinze, J.O., 1959, <u>Turbulence</u>, *McGraw-Hill Book Co.*, New York.

Honkan, A. and Andreopoulos, J., 1993, "Direct Calculation Mapping and Data Analysis in Triple Hot-wire Anemometry," *Thermal Anemometry ASME*, Vol. 167, pp. 67-77.

Howarth, L., 1951, "Note on the Boundary Layer on a Rotating Sphere," *Philos. Mag.*, ser. 42, pp. 1308-1315.

Ilyin, A. A., 1994, "Navier-Stokes Equations on the Rotating Sphere. A Simple Proof of

the Attractor Dimension Estimate," *Nonlinearity*, vol. 7, iss. 1, pp. 31-39.

Inchul Kin and Arne J. Pearlstein, 1990, "Stability of the Flow Past a Sphere," *J. Fluid Mech.*, vol. 211, pp. 73-93.

Janna, W.S., 1987, Introduction to Fluid Mechanics, *PWS-Kent Publishing Co.*, Boston.

Kobashi, Y., 1956, "Measurements of Boundary Layer of Rotating Sphere," *J. of Science*, Hiroshima University, ser. A., vol. 20, pp. 149-156.

Kohama, Y. and Kobayashi, R., 1983, "Boundary-Layer Transition and the Behavior of Spiral Vortices on Rotating Sphere," *J. Fluid Mech.*, vol. 137, pp. 153-164.

Lomas, C.G., 1986, Fundamentals of Hot Wire Anemometry, *Cambridge University Press*, Cambridge.

Malin, M.R., Rosten, H.I., Spalding, D.B., and Tatchell, D.G., 1985, "Application of PHOENICS to Flow around Ship' Hulls," *2nd International Symposium on Ship Viscous Resistance*, Goteborg.

Mihai S., Mihai M. and Vasile G., 1985, "Simulation of Slow Flow of a Fluid Past a Solid Sphere," *Annual Review in Automatic Programming*, vol. 12, pt. 2, pp. 364-366.

Milne-Thomson, L.M., 1968, Theoretical Hydrodynamics, *McGray-Hill Publishing Co.*.

Moghadam, A. and Squire, L. C., 1989, "The Mixing of three-dimensional Turbulent Wakes and Boundary Layers," *Aeronautical J.*, pp. 153-161.

Nigam, S. D., 1974, "Note on the Boundary Layer on a Rotating Sphere," *Z. angew. Math. Phys.*, vol. 5, pp. 151-155.

Oesterle, B., Tri, B. Dinh and Vial, J.L., 1991, "Measurements of Lift and Torque on a Rotating Sphere at Intermediate Reynolds Numbers," *Mechanics Research Communications*, vol. 18, (2/3), pp. 145-150.

Palec, G. Le and Daguenet, M., 1984, "Analysis of Free Convective Effects about a Rotating Sphere in Forced Flow," *Int. Comm. Heat Mass Transfer*, vol. 11, pp. 409-416.

Palec, G. Le and Daguenet, M., 1987, "Laminar Three - dimensional Mixed Convection about a Rotating Sphere in a Stream," *Int. J. Heat Mass Transfer*, vol. 30, No. 7, pp. 1511-1523.

Parr, O., 1964, "Flow in the Three-dimensional Boundary Layer on a Spinning Body of Revolution," *AIAA J.*, vol. 2, No. 2, pp. 361-363.

Patankar, S. V., 1980, Numerical Heat Transfer and Fluid Flow, *Hemisphere Publishing Co.*, New York.

Patankar, S. V. and Spalding, D.B., 1972, "A Calculation Procedure for Heat, Mass, and Momentum Transfer in Three-dimensional Parabolic Flows," *International Journal of Heat and Mass Transfer*, vol. 15, pp. 1787-1806.

Peter P. Wegener and Harry Ashkenas, 1961, "Wind Tunnel Measurements of Sphere Drag at Supersonic Speeds and Low Reynolds Number," *J. Fluid Mech.*, vol. 10, pt. 4, pp. 550-560.

Rajasekaran, R. and Palekar, M. G., 1985, "Mixed Convection about a Rotating Sphere," *Int. J. Heat Mass Transfer*, vol. 28, No. 5, pp. 959-968.

Rimon, Y. and Cheng, S.I., 1969, "Numerical Solution of a Uniform Flow over a Sphere at Intermediate Reynolds Numbers," *The physics of Fluids*, vol. 12, No. 5, pp. 949-959.

Round, G.F. and Garg, V.K., 1986, Applications of Fluid Dynamics, *Edward Arnold Ltd.*.

Sawatzki, O., 1971, "Measurements in the Disturbed Laminar Boundary Layer of a Special Three-dimensional Flow Field," *DISA Information*, No. 11, pp. 5-24.

Schlichting, H., 1953, "Laminar Flow about a Rotating Body of Revolution in an Axial Airstream," *National Advisory Committee for Aeronautics*, TM 1415.

Schlichting, H., 1979, Boundary-Layer Theory, *McGraw - Hill Publishing Co.*, New York.

Singh, S.N., 1970, "Laminar Boundary Layer on a Rotating Sphere," *The Physics of Fluid*, vol. 13, No. 10, pp. 2452-2454.

Spalding, D.B., 1980, "Mathematical Modelling of Fluid-mechanics, Heat-transfer and Chemical-reaction Processes," *A Lecture Course. HTS/80/1, Computational Fluid Dynamics Unit*, Imperial College, University of London.

Spalding, D.D., Rosten, H.I., Glynn, D.R., Malin, M.R. and Edwards, D.R., 1986, "Lecture Panels for Use of the Body-fitted Coordinates in PHOENICS," *TR/126*, Concentration Heat and Momentum Ltd., London.

Tomotika, S., 1935, "The Laminar Boundary Layer on the Surface of a Sphere in a Uniform Stream," *Aeronautical Research Committee,* Reports and Memoranda, 1678, London.

Tomotika, S. and Imai, I., 1938, "On the Transition from Laminar to Turbulent Flow in the Boundary Layer of a Sphere," *Tokyo Imp. Univ. Aeronaut. Res. Inst. Rep.,* vol. 13, pp. 339-423.

Warsi, Z.U.A., 1993, Fluid Dynamics Theoretical and Computational Approaches, *CRC Press Inc.,* Boca Raton.

Yeung, C.P. and Squire, L.C., 1993, "Numerical Calibration and Verification Test of an Orthogonal Triple-hot-wire Probe," *Meas. Science & Tech.,* vol. 4, No. 12, pp.1446-1456.

Yoden, S. and Yamada, M., 1993, "A Numerical Experiment on Two-Dimensional Decaying Turbulence on a Rotating Sphere," *J. of the Atmospheric Sciences,* vol. 50, No. 4, pp. 631-643.

APPENDIX I

TRANSFORMATION OF

BOUNDARY CONDITIONS

Using the coordinate system show in Figure A1.1, the velocity components of the potential

flow for the rotating sphere whose axis is parallel to the free-stream are given as equations

(A1.1) and (A1.2) (Milne-Thomson, 1968)
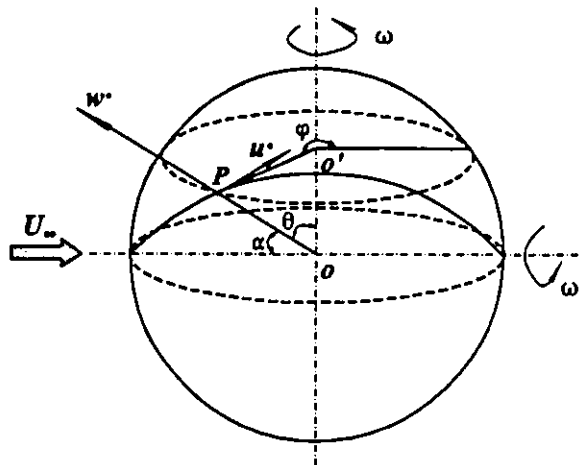
Figure A1.1   Original coordinates

$$u^{\cdot} = - U_{\infty} [1 + a^3 / 2 (a + z)^3] \sin \alpha \qquad (A1.1)$$

$$w^{\cdot} = U_{\infty} [1 - a^3 / (a + z)^3] \cos \alpha \qquad (A1.2)$$

116

These velocity components may be transformed to the vertically rotating spherical coordinate system step by step as follows:

i.   First, u^* is projected to the radial direction of the sphere, w_*', and the horizontal plane, u_1^*, Figure A1.2.
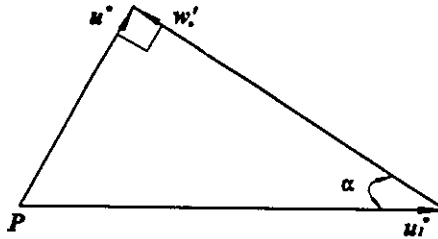
Figure A1.2   Vertical projected plane

Here, the projected velocity components are written as

$$u_1^* = u^* / \sin \alpha \qquad (A1.3)$$

$$w_*' = u^* \cot \alpha \qquad (A1.4)$$

ii.   Then u_1^* is divided into tangential and radial components, v_* and u_2^*, on the horizontal plane, Figure A1.3.
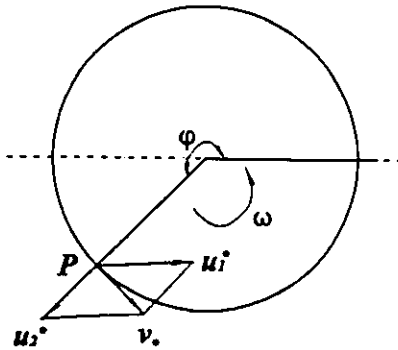
Figure A1.3   Horizontal projected plane

The tangential and radial components on the horizontal plane can express as

$$v_. = - u_1^. \sin \varphi \qquad (A1.5)$$

$$u_2^. = u_1^. \cos \varphi \qquad (A1.6)$$

iii.   Furthermore, $u_2^.$ is divided into radial and tangential components on the sphere, $w_."$ and $u_.$, Figure A1.4.
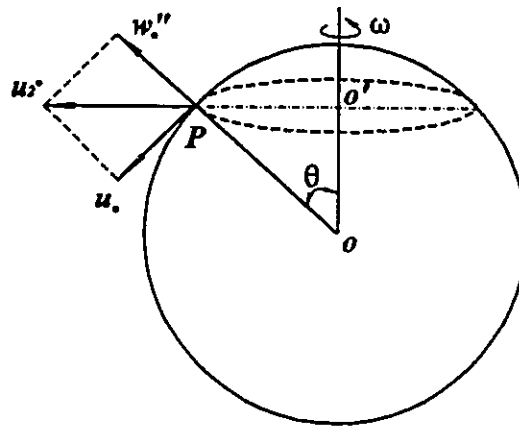
Figure A1.4   Components on sphere

The two components are given as:

$$u_. = u_2^. \cos \theta \qquad (A1.7)$$

$$w_."= u_2^. \sin \theta \qquad (A1.8)$$

iv.   The total components of $u_.$, $w_.$ in the tangential and radial directions of the sphere, and $v_.$ in the tangential direction of the horizontal plane are shown in Figure A1.5.
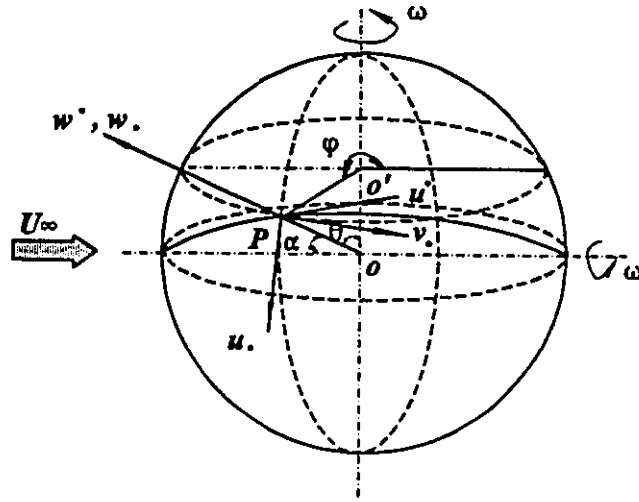
Figure A1.5 Velocity components

Finally, the velocities in the radial direction and tangential directions of the horizontal and vertical planes are expressed

$$
\begin{aligned}
u_{\bullet} &= u_2^{\bullet}\ \cos\theta = (\ u_1^{\bullet}\ \cos\varphi\ )\ \cos\theta \\
&= (\ u^{\bullet}\ /\ \sin\alpha\ )\ \cos\varphi\cos\theta \\
&= U_{\infty}\ [\ 1 + a^3\ /\ 2\ (a + z)^3\ ]\ \cos\varphi\cos\theta
\end{aligned}
\tag{A1.9}
$$

$$
\begin{aligned}
v_{\bullet} &= -\ u_1^{\bullet}\ \sin\varphi = -(\ u^{\bullet}\ /\ \sin\alpha\ )\ \sin\varphi \\
&= U_{\infty}\ [\ 1 + a^3\ /\ 2\ (a + z)^3\ ]\ \sin\varphi
\end{aligned}
\tag{A1.10}
$$

$$
\begin{aligned}
w_{\bullet} &= w^{\bullet} + w_{\bullet}^{\prime} + w_{\bullet}^{\prime\prime} \\
&= w^{\bullet} + u^{\bullet}\ \cot\alpha + (\ u^{\bullet}\ /\ \sin\alpha\ )\ \cos\varphi\sin\theta \\
&= 3\ U_{\infty}\ a^3\ \cos\alpha\ /\ 2\ (a + z)^3 \\
&\quad + U_{\infty}\ [\ 1 + a^3\ /\ 2\ (a + z)^3\ ]\ \cos\varphi\sin\theta
\end{aligned}
\tag{A1.11}
$$

v.   Transferring triangle relations according to the geometrical relation, Figure A1.6.
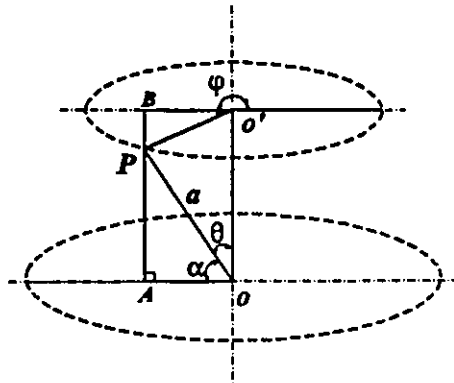
Figure A1.6   Triangle relation

$OA = O'B$, $OA = a\,Cos\,\alpha$ and $O'B = -\,O'P\,Cos\,\varphi = -\,a\,Sin\,\theta\,Cos\,\varphi$. So

$$\cos\alpha \;=\; -\;\sin\theta\cos\varphi \tag{A1.12}$$

Substituting equation A1.12 into equation A1.11, then we may write the velocity components of potential flow for a rotating sphere whose axis is perpendicular to the free-stream in the following way:

$$u_\bullet \;=\; U_\infty\,[\;1 + a^3\,/\,2\,(a+z)^3\;]\;\cos\varphi\cos\theta \tag{A1.13}$$

$$v_\bullet \;=\; U_\infty\,[\;1 + a^3\,/\,2\,(a+z)^3\;]\;\sin\varphi \tag{A1.14}$$

$$w_\bullet \;=\; -\,U_\infty\,[\;1 + a^3\,/\,(a+z)^3\;]\;\cos\varphi\sin\theta \tag{A1.15}$$

APPENDIX II

COMPUTER PROGRAMS

A2.1 Potential Flow

Q1 File

TALK=F; RUN(1,1)

GROUP 1. Run title and other preliminaries
═══════════════════════════════════════

TEXT(POTENTIAL FLOW)

GROUP 6. Body-fitted coordinates or grid distortion
═══════════════════════════════════════

```
BFC=T; NONORT=T
GSET(D,10,20,30,1.0,2.0,3.0)
GSET(P,P1,0,0,0)
GSET(P,P2,10,0,0)
GSET(P,P3,10,0,10)
GSET(P,P4,10,0,20)
GSET(P,P5,10,0,30)
GSET(P,P6,0,0,30)
GSET(L,L1,P1,P2,10,1.0)
GSET(L,L2,P2,P3,10,1.0)
GSET(L,L3,P3,P4,10,1.0,ARC,5,0,15)
GSET(L,L4,P4,P5,10,1.0)
GSET(L,L5,P5,P6,10,1.0)
GSET(P,P7,0,0,20)
GSET(P,P8,0,0,10)
GSET(L,L8,P8,P1,10,1.0)
GSET(L,L6,P6,P7,10,1.0)
GSET(L,L7,P7,P8,10,1.0)
GSET(F,F1,P1,-,P2,P3.P4,P5,-,P6,P7.P8)
```

```
GSET(M,F1,+I+K,1,1,1,LAP10.TFFFFF)
GSET(C,J21,F,J1,RZ,-6.2832,10,0.0,INC,1.0)
```

GROUP 7. Variables stored, solve & named

```
SOLUTN(P1,Y,Y,Y,N,N,N)
ISOLZ=1
```

GROUP 9. Properties of the medium (or media)

```
RHO1=1.17736; ENUL=1.6E-5
```

GROUP 11. Initialization of variable or porosity fields

```
FIINIT(W1)=1.0
```

GROUP 13. Boundary conditions and special sources

```
INLET(INLET,HIGH,1,NX,1,NY,NZ,NZ,1,1)
VALUE(INLET,P1,1.0)
VALUE(INLET,W1,1.0)

PATCH(OUTLET,LOW,1,NX,1,NY,1,1,1,1)
COVAL(OUTLET,P1,FIXP,0.0)
COVAL(OUTLET,V1,ONLYMS,0.0)
COVAL(OUTLET,W1,ONLYMS,0.0)

DARCY=T
```

GROUP 15. Termination of sweeps

```
LSWEEP=20
```

GROUP 22. Spot-value print-out

```
ECHO=T; IYMON=3; IZMON=10

TSTSWP=-1
STOP
```

A2.2 Vortex Flow

Q1 File

TALK=F; RUN(1, 1)

GROUP 1. RUN title and other preliminaries
==

TEXT(VORTEX FLOW)

GROUP 6. Body-fitted coordinates or grid distortion
==

```
BFC=T; NONORT=T
GSET(D,10,20,30,1,1,1)
GSET(P,P1,0,0,0)
GSET(P,P2,10,0,0)
GSET(P,P3,10,0,10)
GSET(P,P4,10,0,20)
GSET(P,P5,10,0,30)
GSET(P,P6,0,0,30)
GSET(L,L1,P1,P2,10,1.0)
GSET(L,L2,P2,P3,10,1.0)
GSET(L,L3,P3,P4,10,1.0,ARC,5,0,15)
GSET(L,L4,P4,P5,10,1.0)
GSET(L,L5,P5,P6,10,1.0)
GSET(P,P7,0,0,20)
GSET(P,P8,0,0,10)
GSET(L,L8,P8,P1,10,1.0)
GSET(L,L6,P6,P7,10,1.0)
GSET(L,L7,P7,P8,10,1.0)
GSET(F,F1,P1,-,P2,P3.P4,P5,-,P6,P7.P8)
GSET(M,F1,+I+K,1,1,1,LAP10.TFFFFF)
GSET(C,J21,F,J1,RZ,-6.2832,10,0.0,INC,1.0)
```

GROUP 7. Variables stored, solve & named
==

```
SOLVE(U1,V1,W1,P1)
SOLUTN(P1,Y,Y,Y,N,N,N)
ISOLZ=1
```

GROUP 9. Properties of the medium (or media)
==

RHO1=1.17736; ENUL=1.6E-5

GROUP 11. Initialization of variable or porosity fields
===

FIINIT(W1)=0.0

GROUP 13. Boundary conditions and special sources
===

OUTLET(INLET,LOW,1,NX,1,NY,1,1,1,1)
VALUE(INLET,P1,0.0)
VALUE(INLET,U1,0.0)
VALUE(INLET,V1,0.0)
VALUE(INLET,W1,60.0)

PATCH(OUTLET,HIGH,1,NX,1,NY,NZ,NZ,1,1)
COVAL(OUTLET,P1,FIXP,10.0)
COVAL(OUTLET,U1,ONLYMS,0.0)
COVAL(OUTLET,V1,ONLYMS,0.0)
COVAL(OUTLET,W1,ONLYMS,0.0)

GROUP 15. Termination of sweeps

LSWEEP=20

GROUP 22. Spot-value print-out
===

ECHO=T; IYMON=3; IZMON=10

TSTSWP=-1
STOP

A2.3 Steady Flow due to a Rotating Sphere

Q1 File

TALK=F; RUN(1,1)
TSTSWP=-1

```
******************************************************************
*
* GROUP 1. Run title and other preliminaries.
*
******************************************************************
TEXT(ROTATING SPHERE)
REAL(OMEGA,PI,RSPH,UPOT,RENO,FI,THI,DELTA,SNFI,SNTHI,CS,COTHI)
RSPH=6.5; DELTA=30.0; UPOT=0.0; OMEGA=10.0; PI=3.14159
*
******************************************************************
*
* GROUP 3. X-direction grid specification.
*
******************************************************************
* Body Fitted Coordinates Grid Selected
* Number of Cells in the X-Direction
NX=31
*
******************************************************************
*
* GROUP 4. Y-direction grid specification.
*
******************************************************************
* Number of Cells in the Y-Direction
NY=15
* Equal Grid Spacing in the Y-Direction
*
******************************************************************
*
* GROUP 5. Z-direction grid specification.
*
******************************************************************
* Number of Cells in the Z-Direction
NZ=11
* Equal Grid Spacing in the Z-Direction
*
******************************************************************
*
* GROUP 6. Body-fitted coordinates or grid distortion.
*
******************************************************************
BFC=T; NONORT=T
DOMAIN(1,NX+1,1,NY+1,1,NZ+1)
SETLIN(XC,(RSPH+DELTA*LNJ)*COS(PI*LNK/2)*CSI)
SETLIN(YC,(RSPH+DELTA*LNJ)*SIN(PI*LNK/2))
SETLIN(ZC,(RSPH+DELTA*LNJ)*COS(PI*LNK/2)*SNI)
*
******************************************************************
*
* GROUP 7. Variables stored, solved & named.
*
```

```
*****************************************************************
 * Solve for the Pressure & X,Y,Z-Direction Velocity Components
SOLVE(P1,U,V,W)
SOLUTN(P1,Y,Y,Y,N,N,N)
  *
 *****************************************************************
  *
 * GROUP 9. Properties of the medium (or media).
  *
 *****************************************************************
 * Material is : AIR (300K AND 1 ATMOSPHERE)
 * Density Value: 1.177360E+00 (kg/cu.m)
RHO1= 1.177360E+00
 * Laminar Kinematic Viscosity: 1.568200E-05 (sq.m/s)
ENUL= 1.568200E-05
 * K-E Turbulence Model
 * ENUT = CMU * (Mixing-Length) * K**0.5
 * EL1 = (CD * K**1.5)/E
TURMOD(KEMODL)
 * Automatically internally Solves for: Turbulent Kinetic Energy
 *                            Kinetic-Energy Dissipation Rate
 *
 *****************************************************************
 *
 * GROUP 11. Initialization of variable or porosity fields.
 *
 *****************************************************************
FI=2*PI/NX; THI=PI/(2*NZ)
 *
 *****************************************************************
 *
 * GROUP 13. Boundary conditions and special sources.
 *
 *****************************************************************
 * Inlet Boundary Condition(outside surface)
PATCH(BFCINLET,NORTH,1,NX,NY,NY,1,NZ-1,1,1)
COVAL(BFCINLET,P1,1.0,GRND1)
COVAL(BFCINLET,UCRT,0.0,0.0)

RSG13=1.177360E+00

WALL(SURF1,SOUTH,31,31,1,1,1,1,1,1)
VALUE(SURF1,P1,1.0)

DO II=1,NZ
COTHI=THI*II
PATCH(SURF,SWALL,1,NX,1,1,II,II,1,1)
COVAL(SURF,U1,FIXVAL,OMEGA*RSPH*COS(COTHI))
ENDDO
```

* Rotational Boundary Condition
RSG25=0.0; RSG26=0.0; RSG27=0.0
RSG28=0.0; RSG29=-1.0; RSG30=0.0
RSG21=OMEGA; ISG18=0
PATCH(ROTA,PHASEM,1,NX,1,1,1,NZ,1,1)
COVAL(ROTA,V1,FIXFLU,GRND1)
COVAL(ROTA,U1,FIXFLU,GRND1)
COVAL(ROTA,W1,FIXFLU,GRND1)

* Cyclic Boundary Condition
XCYIZ(1,NZ,T)
  *
  ****
  *
* GROUP 15. Termination of sweeps.
  *
  ****
* Number of Iterative Sweeps (Outer Iterations)
LSWEEP=200
  * Automatic Reference Residual for the Pressure
RESREF(P1)=-GRND1
  * Automatic Reference Residual for the X-Direction Velocity Component
RESREF(U1)=-GRND1
  * Automatic Reference Residual for the Y-Direction Velocity Component
RESREF(V1)=-GRND1
  * Automatic Reference Residual for the Z-Direction Velocity Component
RESREF(W1)=-GRND1
  * Reference Residual for the Turbulent Kinetic Energy
RESREF(KE)= 1.000000E-10
  * Reference Residual for the Kinetic-Energy Dissipation Rate
RESREF(EP)= 1.000000E-10
  *
  ****
  *
* GROUP 16. Termination of iterations.
  *
  ****
* Linear-Iterations and Termination Criterion for P1
LITER(P1)=20; ENDIT(P1)= 1.000000E-08
  * Linear-Iterations and Termination Criterion for U1
LITER(U1)=20; ENDIT(U1)= 1.000000E-08
  * Linear-Iterations and Termination Criterion for V1
LITER(V1)=20; ENDIT(V1)= 1.000000E-08
  * Linear-Iterations and Termination Criterion for W1
LITER(W1)=20; ENDIT(W1)= 1.000000E-08
  * Linear-Iterations and Termination Criterion for KE
LITER(KE)=20; ENDIT(KE)= 1.000000E-08
  * Linear-Iterations and Termination Criterion for EP
LITER(EP)=20; ENDIT(EP)= 1.000000E-08
  *

```
************************************************************
*
*  GROUP 17. Under-relaxation devices.
*
************************************************************
* Linear Relaxation Applied to P1
RELAX(P1,LINRLX, 1.000000E+00)
  * Smallest Cell Size { SCALEL }: 1.250000E-01 (m)
  * Maximum Velocity { SCALEU }: 4.000000E+00 (m/s)
REAL(SCALEL,SCALEU); SCALEL= 1.250000E-01; SCALEU= 4.000000E+00
  * Automatic False-Time-Step Relaxation Applied to U1
RELAX(U1,FALSDT, 1.000000E+00*SCALEL/SCALEU)
  * Automatic False-Time-Step Relaxation Applied to V1
RELAX(V1,FALSDT, 1.000000E+00*SCALEL/SCALEU)
  * Automatic False-Time-Step Relaxation Applied to W1
RELAX(W1,FALSDT, 1.000000E+00*SCALEL/SCALEU)
  * Automatic False-Time-Step Relaxation Applied to KE
RELAX(KE,FALSDT, 1.000000E+00*SCALEL/SCALEU)
  * Automatic False-Time-Step Relaxation Applied to EP
RELAX(EP,FALSDT, 1.000000E+00*SCALEL/SCALEU)
  *
************************************************************
*
*  GROUP 19. Data communicated by SATELLITE to GROUND.
*
************************************************************
* Graphical Convergence Monitoring Active
LSG6=T
  *
************************************************************
*
*  GROUP 20. Preliminary print-out.
*
************************************************************
* Activate Printout of SATELLITE Data.
ECHO=T
  *
************************************************************
*
*  GROUP 21. Print-out of variables.
*
************************************************************
* Printout for the Pressure
OUTPUT(P1,Y,N,N,Y,Y,Y)
  * Printout for the X-Direction Velocity Component
OUTPUT(U1,Y,N,N,Y,Y,Y)
  * Printout for the Y-Direction Velocity Component
OUTPUT(V1,Y,N,N,Y,Y,Y)
  * Printout for the Z-Direction Velocity Component
OUTPUT(W1,Y,N,N,Y,Y,Y)
  * Printout for the Turbulent Kinetic Energy
```

```
OUTPUT(KE,Y,N,N,Y,Y,Y)
 * Printout for the Kinetic-Energy Dissipation Rate
OUTPUT(EP,Y,N,N,Y,Y,Y)
 *
 *****************************************************************
 *
 *  GROUP 22. Spot-value print-out.
 *
 *****************************************************************
 * X,Y,Z-Direction Index of Spot-Value
IXMON=17; IYMON=3; IZMON=6
 *
 *****************************************************************
 *
 *  GROUP 23. Field print-out and plot control.
 *
 *****************************************************************
 * Frequency of tabulation/plots of Spot/Residuals Values
 * (DO NOT Reset)
NPLT=1
 * Print TABLES AND PLOTS of Spot-Values and Residuals
ITABL=3
 *
 *****************************************************************
 *
 *  GROUP 24. Preparations for continuation runs.
 *
 *****************************************************************
 *
 *****************************************************************
STOP
 *****************************************************************
```

A2.4 Rotating Sphere whose Axis is Parallel to Free Stream

Q1 File

```
TALK=F; RUN(1,1)


    GROUP 1.Run title and other preliminaries
    ==============================


TEXT(ROTATING SPHERE WHOSE AXIS IS PARALLEL TO FREE STREAM )
REAL(TT1,TT2,TV1,TV2,OMEGA,RSPH)

    GROUP 6. Body-fitted coordinates or grid distortion
    ==============================
```

```
BFC=T; NONORT=T
GSET(D,20,10,30,1,1,1)
GSET(P,P1,0,0,0)
GSET(P,P2,0,10,0)
GSET(P,P3,0,10,10)
GSET(P,P4,0,10,20)
GSET(P,P5,0,10,30)
GSET(P,P6,0,0,30)
GSET(L,L1,P1,P2,10,1.0)
GSET(L,L2,P2,P3,10,1.0)
GSET(L,L3,P3,P4,10,1.0,ARC,0.0,5.0,15)
GSET(L,L4,P4,P5,10,1.0)
GSET(L,L5,P5,P6,10,1.0)
GSET(P,P7,0,0,20)
GSET(P,P8,0,0,10)
GSET(L,L8,P8,P1,10,1.0)
GSET(L,L6,P6,P7,10,1.0)
GSET(L,L7,P7,P8,10,1.0)
GSET(F,F1,P1,-,P2,P3.P4,P5,-,P6,P7.P8)
GSET(M,F1,+J+K,1,1,1,LAP10.TFFFFF)
GSET(C,I21,F,I1,RZ,-6.2832,0.0,10.0,INC,1.0)
```

GROUP 7. Variables stored, solve & named
================================

```
SOLVE(U1,V1,W1,P1)
SOLUTN(P1,Y,Y,Y,N,N,N)
ISOLZ=1
```

GROUP 9. Properties of the medium (or media)
================================

```
RHO1=1.17736; ENUL=1.6E-5
TURMOD(KEMODL)
```

GROUP 11. Initialization of variable or porosity fields
================================

```
FIINIT(W1)=0.0; OMEGA=1.0; RSPH=5.0
```

GROUP 13. Boundary conditions and special sources
================================

```
OUTLET(INLET,LOW,1,NX,1,NY,1,1,1,1)
VALUE(INLET,P1,0.0)
VALUE(INLET,U1,0.0)
VALUE(INLET,V1,0.0)
```

```
VALUE(INLET,W1,-10.0)

PATCH(OUTLET,HIGH,1,NX,1,NY,NZ,NZ,1,1)
COVAL(OUTLET,P1,FIXP,10.0)
COVAL(OUTLET,U1,ONLYMS,0.0)
COVAL(OUTLET,V1,ONLYMS,0.0)
COVAL(OUTLET,W1,ONLYMS,0.0)

DO II=1,5

TT1=RSPH*RSPH-((RSPH*(5-II)/5)*(RSPH*(5-II)/5))
TT2=RSPH*RSPH-((RSPH*II/5)*(RSPH*II/5))
TV1=SQRT(TT1)
TV2=SQRT(TT2)
PATCH(INWALL1,NWALL,1,NX,NY,NY,II+10,II+10,1,1)
COVAL(INWALL1,U1,FIXVAL,OMEGA*TV1)
PATCH(INWALL2,NWALL,1,NX,NY,NY,II+15,II+15,1,1)
COVAL(INWALL2,U1,FIXVAL,OMEGA*TV2)

ENDDO

ROTAXA=0.0; ROTAYA=1.0; ROTAZA=0.0
ROTAXB=0.0; ROTAYB=1.0; ROTAZB=3.0
ANGVEL=OMEGA; IROTAA=1.0; BFCA=1.17736
PATCH(ROTA,PHASEM,1,NX,NY,NY,1,NZ,1,1)
COVAL(ROTA,U1,FIXFLU,GRND1)
COVAL(ROTA,V1,FIXFLU,GRND1)
COVAL(ROTA,W1,FIXFLU,GRND1)

XCYIZ(1,NZ,T)
```

GROUP 15. Termination of sweeps

```
LSWEEP=100
```

GROUP 22. Spot-value print-out

```
ECHO=T; NPLT=1; IYMON=3; IZMON=10


TSTSWP=-1
STOP
```

A2.5 Rotating Sphere Whose Axis is Perpendicular to Free Stream

Q1 File

```
TALK=F; RUN(1,1)
TSTSWP=-1
 ****************************************************************
 *
 * GROUP 1. Run title and other preliminaries.
 *
 ****************************************************************
TEXT(ROTATING SPHERE WHOSE AXIS IS NORMAL TO FREE STREAM )
REAL(OMEGA,PI,RSPH,UPOT,RENO,FI,THI,DELTA,SNFI,SNTHI,CS,COTHI)
RSPH=6.5; DELTA=35; UPOT=5.7; OMEGA=0.88; PI=3.14159
 *
 ****************************************************************
 *
 * GROUP 3. X-direction grid specification.
 *
 ****************************************************************
 * Body Fitted Coordinates Grid Selected
 * Number of Cells in the X-Direction
NX=31; NXPRIN=2
INTEGER(NXF01,NXL01); NXF01=1; NXL01=8
INTEGER(NXF02,NXL02); NXF02=9; NXL02=16
INTEGER(NXF03,NXL03); NXF03=17; NXL03=24
INTEGER(NXF04,NXL04); NXF04=25; NXL04=31
 *
 ****************************************************************
 *
 * GROUP 4. Y-direction grid specification.
 *
 ****************************************************************
 * Number of Cells in the Y-Direction
NY=15; NYPRIN=2
 * Equal Grid Spacing in the Y-Direction
INTEGER(NYF01,NYL01); NYF01=1; NYL01=NY
 *
 ****************************************************************
 *
 * GROUP 5. Z-direction grid specification.
 *
 ****************************************************************
 * Number of Cells in the Z-Direction
NZ=11; NZPRIN=2
 * Equal Grid Spacing in the Z-Direction
INTEGER(NZF01,NZL01); NZF01=1; NZL01=NZ
 *
```

```
*****************************************************************
*
*  GROUP 6. Body-fitted coordinates or grid distortion.
*
*****************************************************************
BFC=T; NONORT=T
DOMAIN(1,NX+1,1,NY+1,1,NZ+1)
SETLIN(XC,(RSPH+DELTA*LNJ)*COS(PI*LNK/2)*CSI)
SETLIN(YC,(RSPH+DELTA*LNJ)*SIN(PI*LNK/2))
SETLIN(ZC,(RSPH+DELTA*LNJ)*COS(PI*LNK/2)*SNI)
  *
*****************************************************************
  *
*  GROUP 7. Variables stored, solved & named.
  *
*****************************************************************
*  Solve for the Pressure and X, Y and Z-Direction Velocity Components
SOLVE(P1,U1,V1,W1)
SOLUTN(P1,Y,Y,Y,N,N,N)
  *
*****************************************************************
  *
*  GROUP 9. Properties of the medium (or media).
  *
*****************************************************************
*  Material is : AIR (300K AND 1 ATMOSPHERE)
*  Density Value: 1.177360E+00 (kg/cu.m)
RHO1= 1.177360E+00
*  Laminar Kinematic Viscosity: 1.568200E-05 (sq.m/s)
ENUL= 1.568200E-05
 *  K-E Turbulence Model
 *  ENUT = CMU * (Mixing-Length) * K**0.5
 *  EL1 = (CD * K**1.5)/E
TURMOD(KEMODL)
 *  Automatically internally Solves for: Turbulent Kinetic Energy
 *                      Kinetic-Energy Dissipation Rate
 *
*****************************************************************
 *
*  GROUP 11. Initialization of variable or porosity fields.
 *
*****************************************************************
FI=2*PI/NX; THI=PI/(2*NZ)
  *
*****************************************************************
  *
*  GROUP 13. Boundary conditions and special sources.
  *
*****************************************************************
*  Inlet Boundary Condition(outside surface)
PATCH(BFCINLET,NORTH,1,NX,NY,NY,1,NZ,1,1)
```

```
COVAL(BFCINLET,P1,1.0,GRND1)
COVAL(BFCINLET,UCRT,0.0,5.7)

RSG13=1.177360E+00

WALL(SURF1,SOUTH,31,31,1,1,1,1,1,1)
VALUE(SURF1,P1,1.0)

DO II=1,NZ

COTHI=THI*II
PATCH(SURF,SWALL,1,NX,1,1,II,II,1,1)
COVAL(SURF,U1,FIXVAL,OMEGA*RSPH*COS(COTHI))

ENDDO

 * Rotational Boundary Condition
RSG25=0.0; RSG26=0.0; RSG27=0.0
RSG28=0.0; RSG29=-1.0; RSG30=0.0
RSG21=OMEGA; ISG18=0
PATCH(ROTA,PHASEM,1,NX,1,1,1,NZ,1,1)
COVAL(ROTA,V1,FIXFLU,GRND1)
COVAL(ROTA,U1,FIXFLU,GRND1)
COVAL(ROTA,W1,FIXFLU,GRND1)

 * Cyclic Boundary Condition
XCYIZ(1,NZ,T)
 *
 **************************************************************
 *
 * GROUP 15. Termination of sweeps.
 *
 **************************************************************
 * Number of Iterative Sweeps (Outer Iterations)
LSWEEP=190
 * Automatic Reference Residual for the Pressure
RESREF(P1)=-GRND1
 * Automatic Reference Residual for the X-Direction Velocity Component
RESREF(U1)=-GRND1
 * Automatic Reference Residual for the Y-Direction Velocity Component
RESREF(V1)=-GRND1
 * Automatic Reference Residual for the Z-Direction Velocity Component
RESREF(W1)=-GRND1
 * Reference Residual for the Turbulent Kinetic Energy
RESREF(KE)= 1.000000E-10
 * Reference Residual for the Kinetic-Energy Dissipation Rate
RESREF(EP)= 1.000000E-10
 *
```

```
************************************************************
*
* GROUP 16. Termination of iterations.
*
************************************************************
* Linear-Iterations and Termination Criterion for P1
LITER(P1)=20; ENDIT(P1)= 1.000000E-08
* Linear-Iterations and Termination Criterion for U1
LITER(U1)=20; ENDIT(U1)= 1.000000E-08
* Linear-Iterations and Termination Criterion for V1
LITER(V1)=20; ENDIT(V1)= 1.000000E-08
* Linear-Iterations and Termination Criterion for W1
LITER(W1)=20; ENDIT(W1)= 1.000000E-08
* Linear-Iterations and Termination Criterion for KE
LITER(KE)=20; ENDIT(KE)= 1.000000E-08
* Linear-Iterations and Termination Criterion for EP
LITER(EP)=20; ENDIT(EP)= 1.000000E-08
*
************************************************************
*
* GROUP 17. Under-relaxation devices.
*
************************************************************
* Linear Relaxation Applied to P1
RELAX(P1,LINRLX, 1.000000E+00)
 * Smallest Cell Size { SCALEL }: 1.250000E-01 (m)
 * Maximum Velocity { SCALEU }: 4.000000E+00 (m/s)
REAL(SCALEL,SCALEU); SCALEL= 1.250000E-01; SCALEU= 4.000000E+00
 * Automatic False-Time-Step Relaxation Applied to U1
RELAX(U1,FALSDT, 1.000000E+00*SCALEL/SCALEU)
 * Automatic False-Time-Step Relaxation Applied to V1
RELAX(V1,FALSDT, 1.000000E+00*SCALEL/SCALEU)
 * Automatic False-Time-Step Relaxation Applied to W1
RELAX(W1,FALSDT, 1.000000E+00*SCALEL/SCALEU)
 * Automatic False-Time-Step Relaxation Applied to KE
RELAX(KE,FALSDT, 1.000000E+00*SCALEL/SCALEU)
 * Automatic False-Time-Step Relaxation Applied to EP
RELAX(EP,FALSDT, 1.000000E+00*SCALEL/SCALEU)
*
************************************************************
*
* GROUP 19. Data communicated by SATELLITE to GROUND.
*
************************************************************
* Graphical Convergence Monitoring Active
   LSG6=T
*
************************************************************
*
* GROUP 20. Preliminary print-out.
*
```

```
*****************************************************************
* Activate Printout of SATELLITE Data.
ECHO=T
 *
*****************************************************************
 *
* GROUP 21. Print-out of variables.
 *
*****************************************************************
* Printout for the Pressure
OUTPUT(P1,Y,N,N,Y,Y,Y)
 * Printout for the X-Direction Velocity Component
OUTPUT(U1,Y,N,N,Y,Y,Y)
 * Printout for the Y-Direction Velocity Component
OUTPUT(V1,Y,N,N,Y,Y,Y)
 * Printout for the Z-Direction Velocity Component
OUTPUT(W1,Y,N,N,Y,Y,Y)
 * Printout for the Turbulent Kinetic Energy
OUTPUT(KE,Y,N,N,Y,Y,Y)
 * Printout for the Kinetic-Energy Dissipation Rate
OUTPUT(EP,Y,N,N,Y,Y,Y)
 *
*****************************************************************
 *
* GROUP 22. Spot-value print-out.
 *
*****************************************************************
* X-Direction Index of Spot-Value
IXMON=17
 * Y-Direction Index of Spot-Value
IYMON=3
 * Z-Direction Index of Spot-Value
IZMON=6
 *
*****************************************************************
 *
* GROUP 23. Field print-out and plot control.
 *
*****************************************************************
* Frequency of tabulation/plots of Spot/Residuals Values
* (DO NOT Reset)
NPLT=1
 * Print TABLES AND PLOTS of Spot-Values and Residuals
ITABL=3
 *
*****************************************************************
 *
* GROUP 24. Preparations for continuation runs.
 *
```

```
******************************************************************
*
STOP
*
******************************************************************
```

Ground File

```
C FILE NAME GROUND.FTN-------------------------------011093
      SUBROUTINE GROUND
      INCLUDE 'lp2/d_includ/satear'
      INCLUDE 'lp2/d_includ/grdloc'
      INCLUDE 'lp2/d_includ/grdear'
      INCLUDE 'lp2/d_includ/grdbfc'
CXXXXXXXXXXXXXXXXXXXXXXXXXXXXXXXXXXXXXXXXXXXXX USER SECTION STARTS:
C
C 1  Set dimensions of data-for-GROUND arrays here. WARNING: the
C    corresponding arrays in the MAIN program of the satellite
C    and EARTH must have the same dimensions.
      PARAMETER (NLG=100, NIG=200, NRG=200, NCG=100)
C
      COMMON/LGRND/LG(NLG)/IGRND/IG(NIG)/RGRND/RG(NRG)/CGRND/CG(NCG)
      LOGICAL LG
      CHARACTER*4 CG
C
C 2  User dimensions own arrays here, for example:
C    DIMENSION GUH(10,10),GUC(10,10),GUX(10,10),GUZ(10)
      DIMENSION GX2(35,20),GY2(35,20),GZ2(35,20)
      DIMENSION GINFL(11),UIN(11),VIN(11),WIN(11),A(3),B(3),C(3),D(3)
      REAL UPOT
      INTEGER I1,K1
C
C 3  User places his data statements here, for example:
C    DATA NXDIM,NYDIM/10,10/
      DATA NXD,NYD,NZD/35,20,15/
      PARAMETER (NFDIM=900000)
C
C 4  Insert own coding below as desired, guided by GREX examples.
C    Note that the satellite-to-GREX special data in the labelled
C    COMMONs /RSG/, /ISG/, /LSG/ and /CSG/ can be included and
C    used below but the user must check GREX for any conflicting
C    uses. The same comment applies to the EARTH-spare working
C    arrays EASP1, EASP2,....EASP20. In addition to the EASPs,
C    there are 10 GRound-earth SPare arrays, GRSP1,...,GRSP10,
C    supplied solely for the user, which are not used by GREX. If
C    the call to GREX has been deactivated then all of the arrays
C    may be used without reservation.
C
```

```
C*********************************************************************
C
      IXL=IABS(IXL)
C     UPOT=15.0
      IF(IGR.EQ.13) GO TO 13
      IF(IGR.EQ.19) GO TO 19
      GO TO (1,2,3,4,5,6,25,8,9,10,11,12,13,14,25,25,25,25,19,20,25,
     125,23,24),IGR
   25 CONTINUE
      RETURN
C*********************************************************************
C
C--- GROUP 1. Run title and other preliminaries
C
    1 GO TO (1001,1002),ISC
 1001 CONTINUE
C
C   User may here change message transmitted to the VDU screen
      IF(IGR.EQ.1.AND.ISC.EQ.1.AND..NOT.NULLPR)
     1 CALL WRYT40('GROUND file is GROUND.F  of:   011093 ')
C
      RETURN
 1002 CONTINUE
      RETURN
C*********************************************************************
C
C--- GROUP 2. Transience; time-step specification
C
    2 CONTINUE
      RETURN
C*********************************************************************
C
C--- GROUP 3. X-direction grid specification
C
    3 CONTINUE
      RETURN
C*********************************************************************
C
C--- GROUP 4. Y-direction grid specification
C
    4 CONTINUE
      RETURN
C*********************************************************************
C
C--- GROUP 5. Z-direction grid specification
C
    5 CONTINUE
      RETURN
C*********************************************************************
C
C--- GROUP 6. Body-fitted coordinates or grid distortion
```

```
C
  6 CONTINUE
    RETURN
C******************************************************************
C  * Make changes for this group only in group 19.
C--- GROUP 7. Variables stored, solved & named
C******************************************************************
C
C--- GROUP 8. Terms (in differential equations) & devices
C
  8 GO TO (81,82,83,84,85,86,87,88,89,810,811,812,813,814,815)
   1,ISC
 81 CONTINUE
C  *------------------ SECTION  1 ------------------------
C  For U1AD.LE.GRND--- phase 1 additional velocity. Index VELAD
    RETURN
 82 CONTINUE
C  *------------------ SECTION  2 ------------------------
C  For U2AD.LE.GRND--- phase 2 additional velocity. Index VELAD
    RETURN
 83 CONTINUE
C  *------------------ SECTION  3 ------------------------
C  For V1AD.LE.GRND--- phase 1 additional velocity. Index VELAD
    RETURN
 84 CONTINUE
C  *------------------ SECTION  4 ------------------------
C  For V2AD.LE.GRND--- phase 2 additional velocity. Index VELAD
    RETURN
 85 CONTINUE
C  *------------------ SECTION  5 ------------------------
C  For W1AD.LE.GRND--- phase 1 additional velocity. Index VELAD
    RETURN
 86 CONTINUE
C  *------------------ SECTION  6 ------------------------
C  For W2AD.LE.GRND--- phase 2 additional velocity. Index VELAD
    RETURN
 87 CONTINUE
C  *------------------ SECTION 7 ---- Volumetric source for gala
    RETURN
 88 CONTINUE
C  *------------------ SECTION 8 ---- Convection fluxes
    RETURN
 89 CONTINUE
C  *------------------ SECTION 9 ---- Diffusion coefficients
C--- Entered when UDIFF =.TRUE.; block-location indices are LAE
C  for east, LAW for west, LAN for north, LAS for
C  south, LD11 for high, and LD11 for low.
C  User should provide INDVAR and NDIREC IF's as above.
C  EARTH will apply the DIFCUT and GP12 modifications after the user
C  has made his settings.
C
```

```
      RETURN
  810 CONTINUE
C  *------------------ SECTION 10 --- Convection neighbours
      RETURN
  811 CONTINUE
C  *------------------ SECTION 11 --- Diffusion neighbours
      RETURN
  812 CONTINUE
C  *------------------ SECTION 12 --- Linearised sources
      RETURN
  813 CONTINUE
C  *------------------ SECTION 13 --- Correction coefficients
      RETURN
  814 CONTINUE
C  *------------------ SECTION 14 --- User's own solver
      RETURN
  815 CONTINUE
C  *------------------ SECTION 15 --- Change solution
      RETURN
C
C  * See the equivalent section in GREX for the indices to be
C    used in sections 7 - 15
C
C  * Make all other group-8 changes in GROUP 19.
C****************************************************************
C
C--- GROUP 9. Properties of the medium (or media)
C
C  The sections in this group are arranged sequentially in their
C  order of calling from EARTH. Thus, as can be seen from below,
C  the temperature sections (10 and 11) precede the density
C  sections (1 and 3); so, density formulae can refer to
C  temperature stores already set.
    9 GO TO (91,92,93,94,95,96,97,98,99,900,901,902,903,904,905),ISC
C****************************************************************
  900 CONTINUE
C  *------------------ SECTION 10 --------------------------
C   For TMP1.LE.GRND--------- phase-1 temperature Index TEMP1
      RETURN
  901 CONTINUE
C  *------------------ SECTION 11 --------------------------
C   For TMP2.LE.GRND--------- phase-2 temperature Index TEMP2
      RETURN
  902 CONTINUE
C  *------------------ SECTION 12 --------------------------
C   For EL1.LE.GRND--------- phase-1 length scale Index LEN1
      RETURN
  903 CONTINUE
C  *------------------ SECTION 13 --------------------------
C   For EL2.LE.GRND--------- phase-2 length scale Index LEN2
      RETURN
```

```
      904 CONTINUE
C  *------------------ SECTION 14 ------------------------
C   For SOLVE(TEMP1)------------------------- phase-1 specic heat
      RETURN
      905 CONTINUE
C  *------------------ SECTION 15 ------------------------
C   For SOLVE(TEMP2)------------------------- phase-2 specic heat
      RETURN
      91 CONTINUE
C  *------------------ SECTION  1 ------------------------
C   For RHO1.LE.GRND--- density for phase 1     Index DEN1
      RETURN
      92 CONTINUE
C  *------------------ SECTION  2 ------------------------
C   For DRH1DP.LE.GRND--- D(LN(DEN))/DP for phase 1
C                              Index D1DP
      RETURN
      93 CONTINUE
C  *------------------ SECTION  3 ------------------------
C   For RHO2.LE.GRND--- density for phase 2     Index DEN2
      RETURN
      94 CONTINUE
C  *------------------ SECTION  4 ------------------------
C   For DRH2DP.LE.GRND--- D(LN(DEN))/DP for phase 2
C                              Index D2DP
      RETURN
      95 CONTINUE
C  *------------------ SECTION  5 ------------------------
C   For ENUT.LE.GRND--- reference turbulent kinematic viscosity
C                              Index VIST
      RETURN
      96 CONTINUE
C  *------------------ SECTION  6 ------------------------
C   For ENUL.LE.GRND--- reference laminar kinematic viscosity
C                              Index VISL
      RETURN
      97 CONTINUE
C  *------------------ SECTION  7 ------------------------
C   For PRNDTL( ).LE.GRND--- laminar PRANDTL nos., or diffusivity
C                              Index LAMPR
      RETURN
      98 CONTINUE
C  *------------------ SECTION  8 ------------------------
C   For PHINT( ).LE.GRND--- interface value of first phase
C                              Index FII1
      RETURN
      99 CONTINUE
C  *------------------ SECTION  9  ------------------------
C   For PHINT( ).LE.GRND--- interface value of second phase
C                              Index FII2
      RETURN
```

```
C*********************************************************************
C
C--- GROUP 10. Inter-phase-transfer processes and properties
C
   10 GO TO (101,102,103,104),ISC
  101 CONTINUE
C  *----------------- SECTION  1 ------------------------
C  For CFIPS.LE.GRND--- inter-phase friction coeff.
C                            Index INTFRC
     RETURN
  102 CONTINUE
C  *----------------- SECTION  2 ------------------------
C  For CMDOT.EQ.GRND- inter-phase mass transfer  Index INTMDT
     RETURN
  103 CONTINUE
C  *----------------- SECTION  3 ------------------------
C  For CINT( ).EQ.GRND--- phase1-to-interface transfer coefficients
C                            Index COI1
     RETURN
  104 CONTINUE
C  *----------------- SECTION  4 ------------------------
C  For CINT( ).EQ.GRND--- phase2-to-interface transfer coefficients
C                            Index COI2
     RETURN
C*********************************************************************
C
C--- GROUP 11. Initialization of variable or porosity fields
C                            Index VAL
   11 CONTINUE
     RETURN
C*********************************************************************
C
C--- GROUP 12. Convection and diffusion adjustments
C
   12 CONTINUE
     RETURN
C*********************************************************************
C
C--- GROUP 13. Boundary conditions and special sources
C                       Index for Coefficient - CO
C                       Index for Value    - VAL
   13 CONTINUE
     GO TO (130,131,132,133,134,135,136,137,138,139,1310,
    11311,1312,1313,1314,1315,1316,1317,1318,1319,1320,1321),ISC
  130 CONTINUE
C----------------- SECTION  1 ------------- coefficient = GRND
     RETURN
  131 CONTINUE
C----------------- SECTION  2 ------------- coefficient = GRND1
     RETURN
  132 CONTINUE
```

```fortran
C------------------ SECTION 3 ------------ coefficient = GRND2
      RETURN
  133 CONTINUE
C------------------ SECTION 4 ------------ coefficient = GRND3
      RETURN
  134 CONTINUE
C------------------ SECTION 5 ------------ coefficient = GRND4
      RETURN
  135 CONTINUE
C------------------ SECTION 6 ------------ coefficient = GRND5
      RETURN
  136 CONTINUE
C------------------ SECTION 7 ------------ coefficient = GRND6
      RETURN
  137 CONTINUE
C------------------ SECTION 8 ------------ coefficient = GRND7
      RETURN
  138 CONTINUE
C------------------ SECTION 9 ------------ coefficient = GRND8
      RETURN
  139 CONTINUE
C------------------ SECTION 10 ------------ coefficient = GRND9
      RETURN
 1310 CONTINUE
C------------------ SECTION 11 ------------ coefficient = GRND10
      RETURN
 1311 CONTINUE
C------------------ SECTION 12 ------------------ value = GRND
      RETURN
 1312 CONTINUE
C------------------ SECTION 13 ------------------ value = GRND1
      RETURN
 1313 CONTINUE
C------------------ SECTION 14 ------------------ value = GRND2

C$$$$$$$$$$$$$$$$$$$$$$$$$$$$$$$$$$$$$$$$$$$$$$$$$$$$$$$$$$$$$$$$$$$$$$$$$$$$$$$$$$


C    DO 8800 K1 = 1, 10
      DO 8000 I1 = 1, 30

C---Mass flux inlet boundary condition at IY=NY North face.
      CALL ONLYIF(P1,P1,'INLET')
      IF(ISWEEP.EQ.1) THEN
C---Get corner coordinates of the 4 corners at the North boundary of
C   the domain, at the current salb. These corners are labelled A, B,
C   C and D, and the Cartesian coordinates XC, YC, ZC for each corner
C   are stored in the arrays A(3), B(3), C(3) and D(3). The labels are
C   attached in the sense of a right-hand screw out the domain, so as
C   to give the outward normal
      CALL SUB3(I,I1,NJ,NY+1,K,IZSTEP)
```

```
      CALL GETPT(I1,NJ,K,A(1),A(2),A(3))
      CALL GETPT(I1,NJ,K+1,B(1),B(2),B(3))
      CALL GETPT(I1+1,NJ,K+1,C(1),C(2),C(3))
      CALL GETPT(I1+1,NJ,K,D(1),D(2),D(3))
C---Construction outward normal
      CALL NORML(A,B,C,D,EV)
C---Re-set external flow direction unit vector
      CALL VECTOR(QV,1.,0.,0.)
C---Calculate mass inflow, reversing sign to get inward normal.
C---UPOT = external flow total velocity
      GINFL(IZSTEP)=-UPOT*RHO1*DOT(EV,QV)
C---Calculate U,V and W resolutes convected into domain at the north
C  boundary
C---Get arrays for vectors in the U-resolute direction.
      CALL GTIZYX(80,IZSTEP,GX2,NYD,NXD)
      CALL GTIZYX(81,IZSTEP,GY2,NYD,NXD)
      CALL GTIZYX(82,IZSTEP,GZ2,NYD,NXD)
      IX=1
      IY=NY
C---Set east face unit vector for U-resolute direction.
      CALL VECTOR(EV,GX2(IY,IX),GY2(IY,IX),GZ2(IY,IX))
C---Calculate U-resolute.
      UIN(IZSTEP)=UPOT*DOT(EV,QV)
C---Get arrays for vections in V-resolute direction.
      CALL GTIZYX(83,IZSTEP,GX2,NYD,NXD)
      CALL GTIZYX(84,IZSTEP,GY2,NYD,NXD)
      CALL GTIZYX(85,IZSTEP,GZ2,NYD,NXD)
      IX=1
      IYM=NY-1
C---Set north face unit vector in V-resolute direction.
      CALL VECTOR(EV,GX2(IYM,IX),GY2(IYM,IX),GZ2(IYM,IX))
C---Calculate V-resolute.
      VIN(IZSTEP)=UPOT*DOT(EV,QV)
C---Get arrays for vectors in W-resolute direction.
      CALL GTIZYX(86,IZSTEP,GX2,NYD,NXD)
      CALL GTIZYX(87,IZSTEP,GY2,NYD,NXD)
      CALL GTIZYX(88,IZSTEP,GZ2,NYD,NXD)
      IX=1
      IY=NY
C---Set high face unit vector for W-resolute direction
      CALL VECTOR(EV,GX2(IY,IX),GY2(IY,IX),GZ2(IY,IX))
C---Calculate W-resolute.
      WIN(IZSTEP)=UPOT*DOT(EV,QV)
      ENDIF
C---Set mass inflow boundary condition.
      CALL FN1(VAL,GINFL(IZSTEP))
C---Set U-resolute at inlet boundary.
      CALL ONLYIF(U1,U1,'INLET')
      CALL FN1(VAL,UIN(IZSTEP))
C---Set V-resolute at inlet boundary.
      CALL ONLYIF(V1,V1,'INLET')
```

```
      CALL FN1(VAL,VIN(IZSTEP))
C---Set W-resolute at inlet boundary.
      CALL ONLYIF(W1,W1,'INLET')
      CALL FN1(VAL,WIN(IZSTEP))


 8000 CONTINUE
C8800 CONTINUE
CC    NPAT=NPATCH(1:4)
CC    IF(NPAT.EQ.'KESO') THEN
CC      CALL GXKESO(VIST,LEN1,VISL,FIXVAL)
CC    ELSEIF(NPAT.EQ.'KEBU') THEN
CC      CALL GXKEGB
CC    IF(NPAT(1:3).EQ.'BFC') THEN
CC      CALL GXBFC(NX,NY,NZ)
CC    ENDIF
C$$$$$$$$$$$$$$$$$$$$$$$$$$$$$$$$$$$$$$$$$$$$$$$$$$$$$$$$$$$$$$$$$$$$$$


      RETURN
 1314 CONTINUE
C------------------ SECTION 15 ----------------- value = GRND3
      RETURN
 1315 CONTINUE
C------------------ SECTION 16 ----------------- value = GRND4
      RETURN
 1316 CONTINUE
C------------------ SECTION 17 ----------------- value = GRND5
      RETURN
 1317 CONTINUE
C------------------ SECTION 18 ----------------- value = GRND6
      RETURN
 1318 CONTINUE
C------------------ SECTION 19 ----------------- value = GRND7
      RETURN
 1319 CONTINUE
C------------------ SECTION 20 ----------------- value = GRND8
      RETURN
 1320 CONTINUE
C------------------ SECTION 21 ----------------- value = GRND9
      RETURN
 1321 CONTINUE
C------------------ SECTION 22 ----------------- value = GRND10
      RETURN
C**************************************************************
C
C--- GROUP 14. Downstream pressure for PARAB=.TRUE.
C
   14 CONTINUE
      RETURN
C**************************************************************
C* Make changes to data for GROUPS 15, 16, 17, 18  GROUP 19.
C**************************************************************
```

```
C
C--- GROUP 19. Special calls to GROUND from EARTH
C
   19 GO TO (191,192,193,194,195,196,197,198,199,1910),ISC
  191 CONTINUE
C  *------------------- SECTION 1 ---- Start of time step.
      RETURN
  192 CONTINUE
C  *------------------- SECTION 2 ---- Start of sweep.
      UPOT=RG(1)
      RETURN
  193 CONTINUE
C  *------------------- SECTION 3 ---- Start of iz slab.
      RETURN
  194 CONTINUE
C  *------------------- SECTION 4 ---- Start of iterations over slab.
      RETURN
  199 CONTINUE
C  *------------------- SECTION 9 ---- Start of solution sequence for
C                                     a variable
      RETURN
 1910 CONTINUE
C  *------------------- SECTION 10---- Finish of solution sequence for
C                                     a variable
      RETURN
  195 CONTINUE
C  *------------------- SECTION 5 ---- Finish of iterations over slab.
      RETURN
  196 CONTINUE
C  *------------------- SECTION 6 ---- Finish of iz slab.
      RETURN
  197 CONTINUE
C  *------------------- SECTION 7 ---- Finish of sweep.
      RETURN
  198 CONTINUE
C  *------------------- SECTION 8 ---- Finish of time step.
C
      RETURN
C***************************************************************
C
C--- GROUP 20. Preliminary print-out
C
   20 CONTINUE
      RETURN
C***************************************************************
C* Make changes to data for GROUPS 21 and 22 only in GROUP 19.
C***************************************************************
C
C--- GROUP 23. Field print-out and plot control
   23 CONTINUE
      RETURN
```

```
C********************************************************************
C
C--- GROUP 24. Dumps for restarts
C
  24 CONTINUE
    END
```

APPENDIX III

MEASURING TECHNIQUE

Because of the fact that the thickness of the boundary layer of a sphere is very thin, and that the flow in the thin layer is three-dimensional, a fine wire triple sensor probe, which has the advantages of high sensitivity, compactness and capability of detecting the direction of flow, was used. The principle of the method can be described as follows: when a fine wire is heated by an electric current and mounted in a three-dimensional flow field, the voltage across the wire is a function of flow velocity and its direction.

It is helpful to define two distinct coordinate systems: the wire coordinate system and the laboratory coordinate system. The wire coordinate system is defined relative to the axes of the sensors by the orthogonal unit vectors $(\vec{i}_1, \vec{i}_2, \vec{i}_3)$, each hot wire defines one axis of the coordinate system. A fluid velocity vector, $\vec{U}$, in wire coordinates is described by:

$$\vec{U} = \psi_1 \vec{i}_1 + \psi_2 \vec{i}_2 + \psi_3 \vec{i}_3 \qquad (A3.1)$$

where ψ_1, ψ_2, ψ_3 are components of $\vec{U}$ in the directions $\vec{i}_1$, $\vec{i}_2$, $\vec{i}_3$, respectively.

The axes of the laboratory coordinate system are defined relative to the experimental facility by the orthogonal unit vectors $(\vec{i}_x, \vec{i}_y, \vec{i}_z)$. A fluid velocity vector, $\vec{U}$, in laboratory coordinates is described by:

$$\vec{U} = U\vec{i}_x + V\vec{i}_y + W\vec{i}_z \tag{A3.2}$$

where U, V and W are components of $\vec{U}$ in the directions x, y, z, respectively.

The thermal sensor is cooled by velocity components in all directions. Neither a single component nor the magnitude of the velocity vector alone cools the heated sensor, but rather an effective cooling velocity, U_{eff}, which is related to the magnitude of the velocity vector, and includes different effects from different velocity components in the wire coordinate system. Using an improved model of the Cosine Law, Joergensen's equations, for wires along axis 1, 2 and 3, with the planes of the supports defined by $(\vec{i}_1, \vec{i}_2)$, $(\vec{i}_2, \vec{i}_3)$ and $(\vec{i}_3, \vec{i}_1)$, respectively are:

$$U^2_{eff1} = k_t^2\psi_1^2 + \psi_2^2 + k_n^2\psi_3^2 \tag{A3.3}$$

$$U^2_{eff2} = k_n^2\psi_1^2 + k_t^2\psi_2^2 + \psi_3^2 \tag{A3.4}$$

$$U^2_{eff3} = \psi_1^2 + k_n^2\psi_2^2 + k_t^2\psi_3^2 \tag{A3.5}$$

where k_t is the yaw factor, $k_t = 0.2$, and k_n is the pitch factor, $k_n = 1.02$.

Equations (A3.3) - (A3.5) may be written as

$$
\begin{bmatrix} U^2_{\mathit{eff1}} \\ U^2_{\mathit{eff2}} \\ U^2_{\mathit{eff3}} \end{bmatrix} = \begin{bmatrix} k_t^2 & 1 & k_n^2 \\ k_n^2 & k_t^2 & 1 \\ 1 & k_n^2 & k_t^2 \end{bmatrix} \begin{bmatrix} \psi_1^2 \\ \psi_2^2 \\ \psi_3^2 \end{bmatrix}
\tag{A3.6}
$$

Solving for the components in wire coordinates, yields

$$
\begin{bmatrix} \psi_1^2 \\ \psi_2^2 \\ \psi_3^2 \end{bmatrix} = \begin{bmatrix} k_t^2 & 1 & k_n^2 \\ k_n^2 & k_t^2 & 1 \\ 1 & k_n^2 & k_t^2 \end{bmatrix}^{-1} \begin{bmatrix} U^2_{\mathit{eff1}} \\ U^2_{\mathit{eff2}} \\ U^2_{\mathit{eff3}} \end{bmatrix}
\tag{A3.7}
$$

Transposing the velocities from wire coordinate system to the laboratory coordinate system by multiplying the components of the vector in one coordinate system by the direction cosines of the solid angle subtending the unit vector of the two coordinate system results in:

$$
\begin{bmatrix} U \\ V \\ W \end{bmatrix} = \cos y_{ij} \begin{bmatrix} \psi_1 \\ \psi_2 \\ \psi_3 \end{bmatrix}
\tag{A3.8}
$$

where y_{ij} is the solid angle subtended by the unit vectors ($\vec{i}_i$, $\vec{i}_j$), $i = 1, 2, 3, j = x, y, z$.

In Figure A3.1, all solid angles labeled are in the plane (x, z), wire 1, 2 and line EF are in plane $ABCD$ which has 35 degrees with respect to horizontal plane (x, y), the probe stem

is horizontal and defines the x-direction, the vertical direction defines the z-direction, wire 3

is in the vertical plane. Then the Dantec triple sensor probe is gives:

$$
\cos y_{ij} = \begin{bmatrix} \cos 45^{\circ} \cos 35^{\circ} & \cos 45^{\circ} \cos 35^{\circ} & \cos 55^{\circ} \\ -\cos 45^{\circ} & \cos 45^{\circ} & 0 \\ -\cos 45^{\circ} \sin 35^{\circ} & -\cos 45^{\circ} \sin 35^{\circ} & \cos 35^{\circ} \end{bmatrix} \qquad (A3.9)
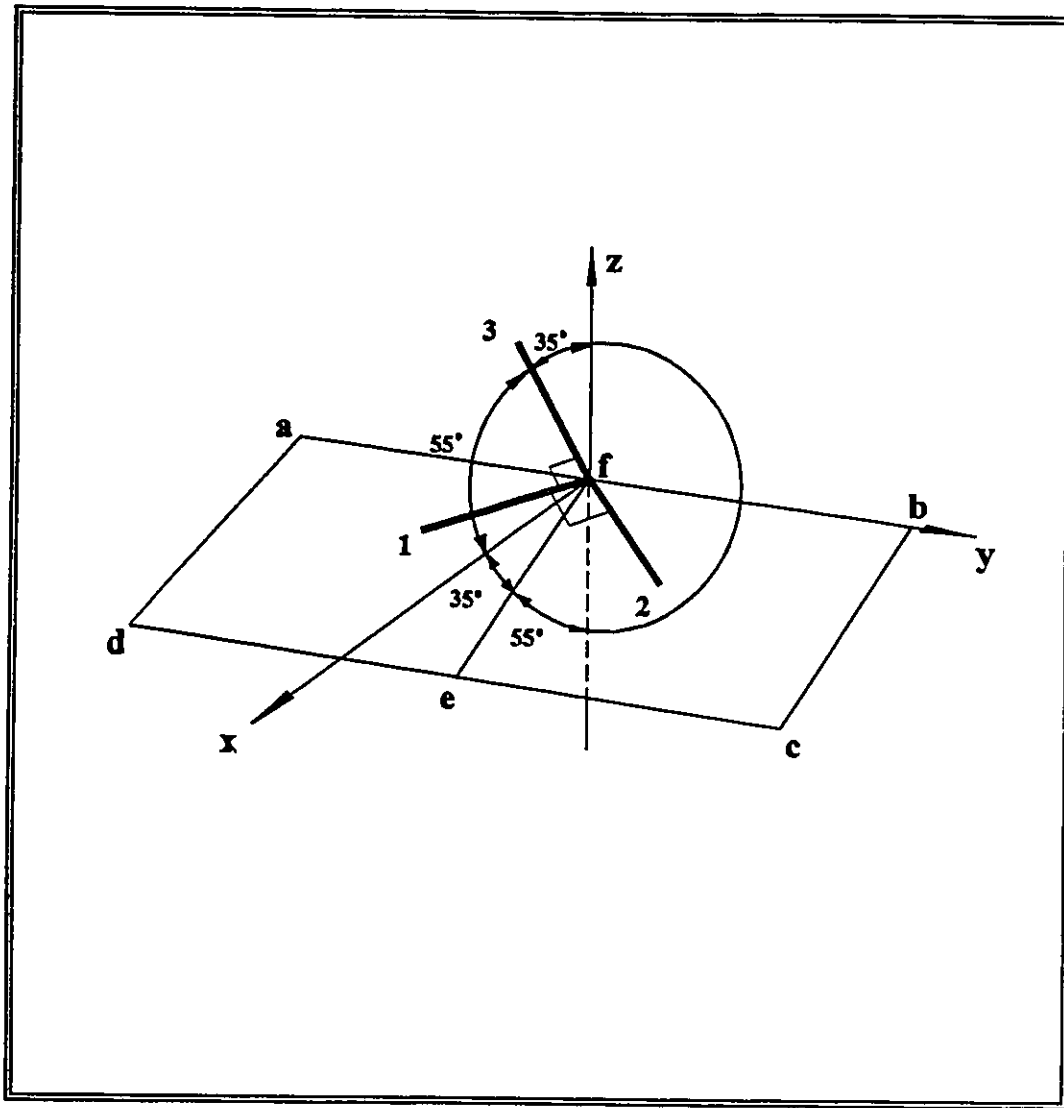$$

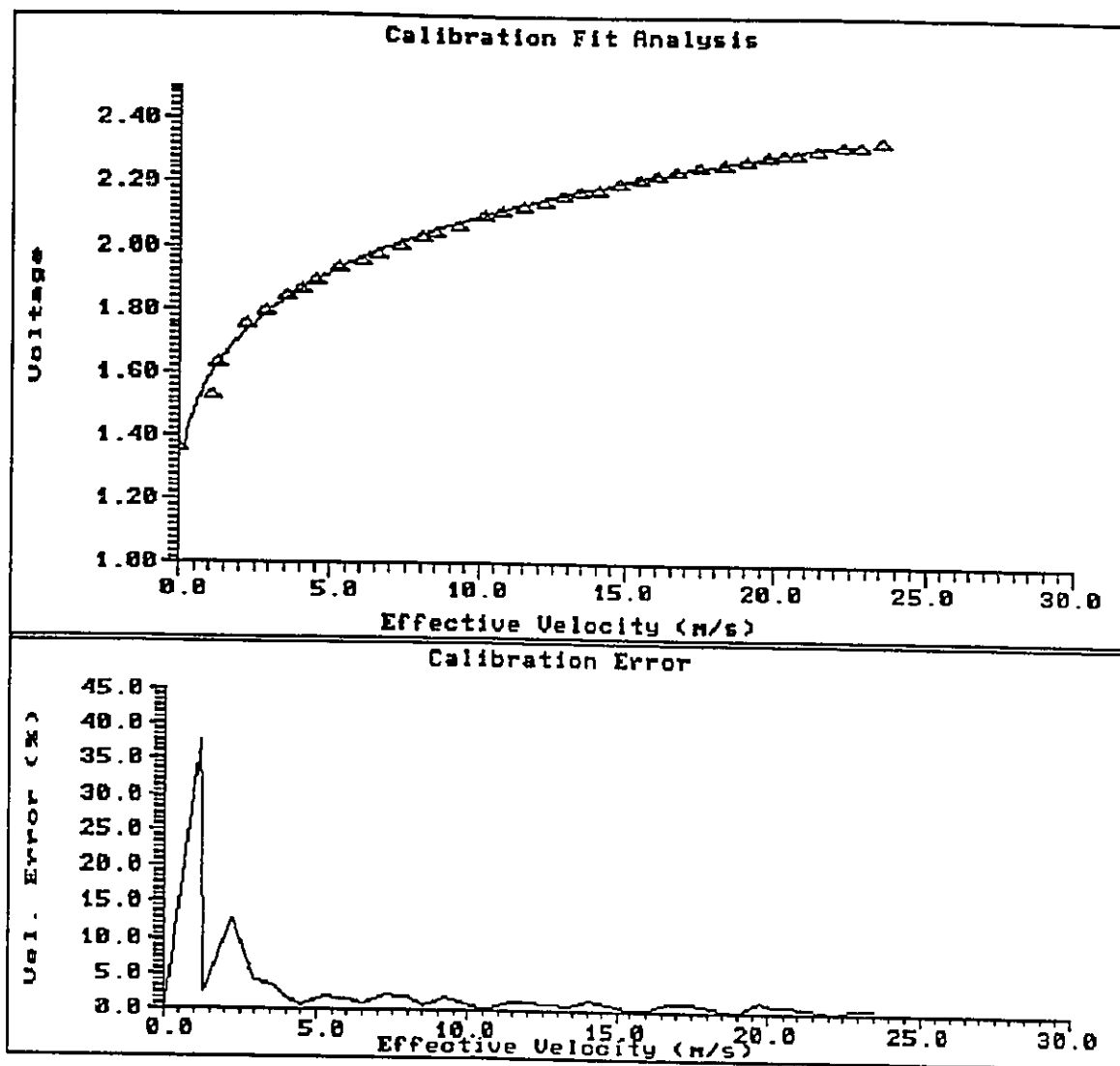**Figure A3.1** Orientation of the triple sensor probe

Figure A3.2a   Calibration curve and percentage error for triple sensor probe (wire 1)
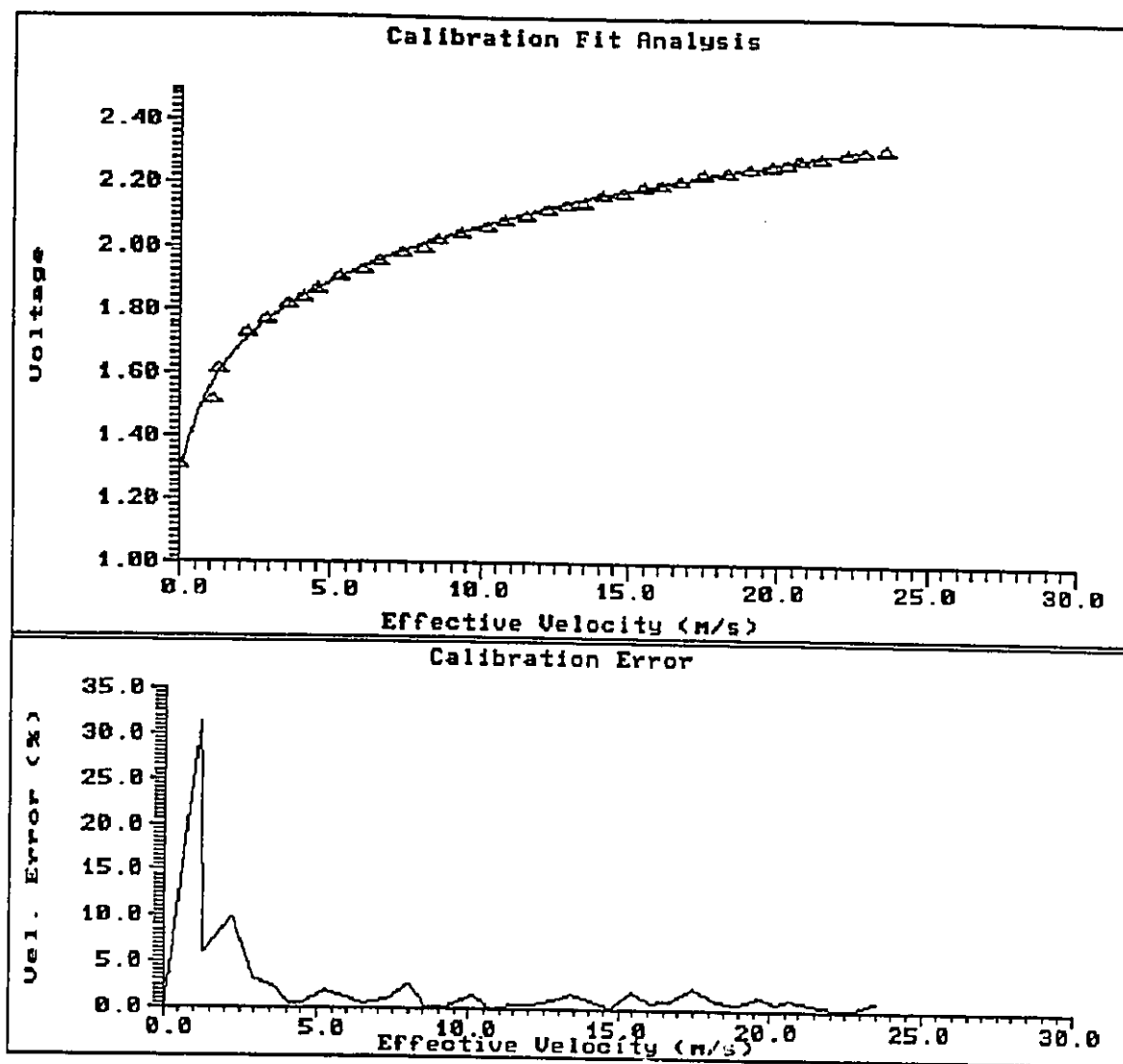
Figure A3.2b Calibration curve and percentage error for triple sensor probe (wire 2)
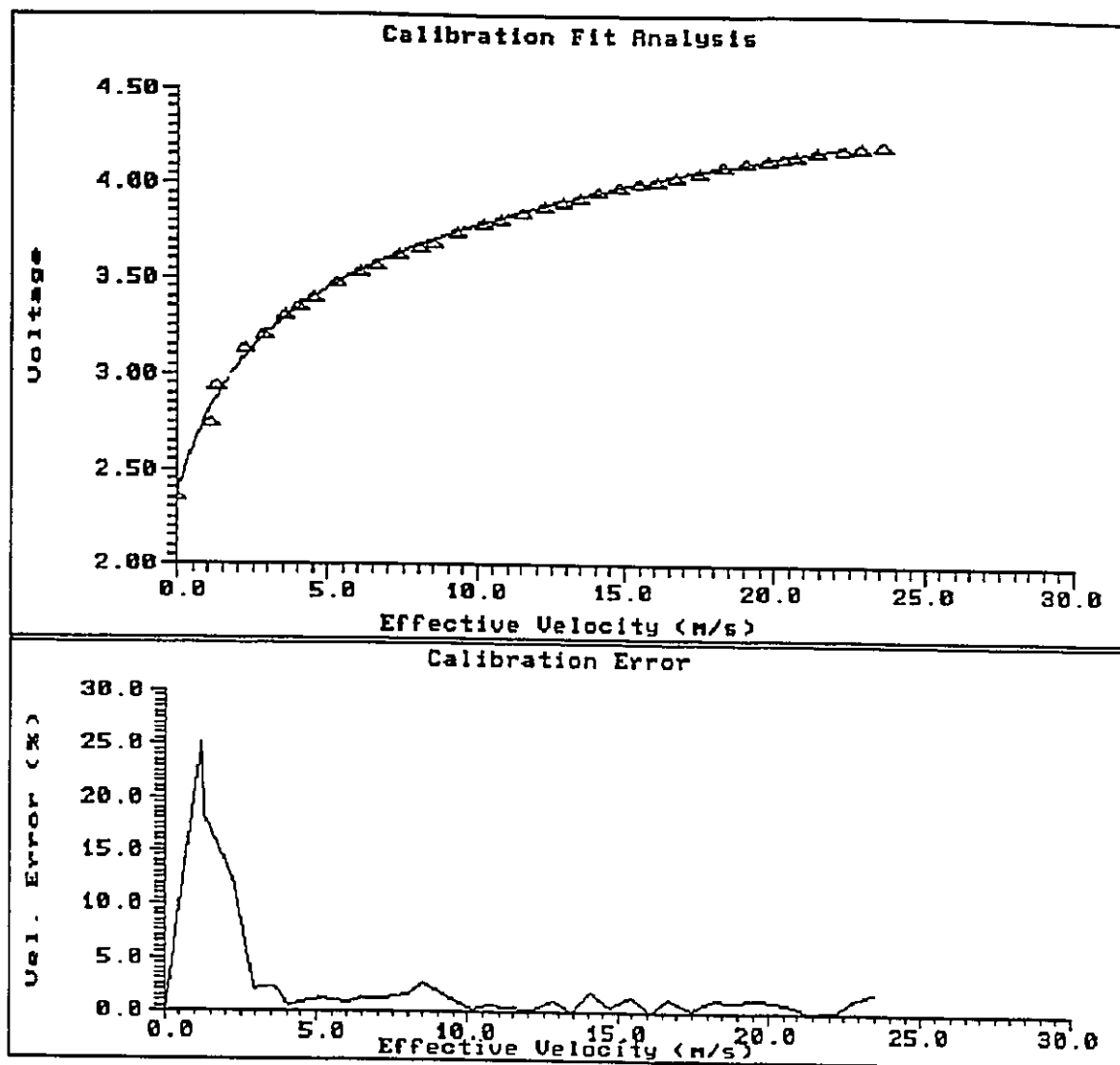
Figure A3.2c Calibration curve and percentage error for triple sensor probe (wire 3)